THE OXYSTEROL BINDING PROTEIN GENE FAMILY:

Protein Interactions and Functional Characterization

By

Jessica P. Wyles

Submitted in partial fulfillment of the requirements for the degree of Doctor of Philosophy at Dalhousie University

Halifax, Nova Scotia

June, 2003

Your file Votre référence
ISBN: 0-612-83716-5
Our file Notre référence
ISBN: 0-612-83716-5

DALHOUSIE UNIVERSITY

DEPARTMENT OF BIOCHEMISTRY AND MOLECULAR BIOLOGY

The undersigned hereby certify that they have read and recommend to the Faculty of Graduate Studies for acceptance a thesis entitled "THE OXYSTEROL BINDING PROTEIN GENE FAMILY: Protein Interactions and Functional Characterization" by Jessica P. Wyles in partial fulfillment for the degree of Doctor of Philosophy.

Dated: June 16, 2003

External Examiner:

Research Supervisor:

Examining Committee:

Departmental Representative:

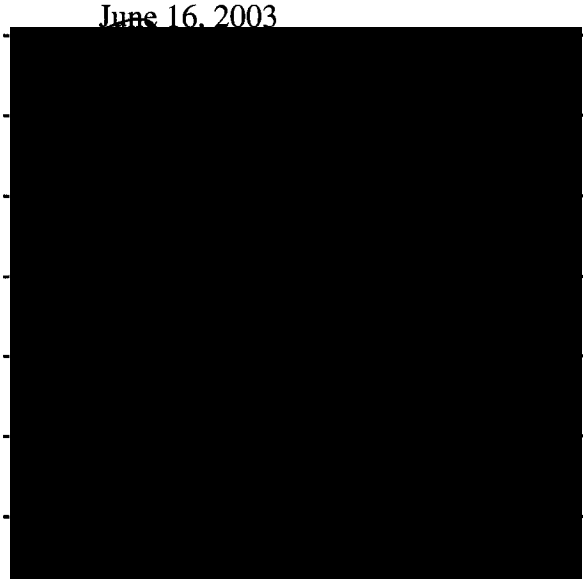

DALHOUSIE UNIVERSITY

DATE: June 16, 2003

AUTHOR: Jessica P. Wyles

TITLE: THE OXYSTEROL BINDING PROTEIN GENE FAMILY:
Protein Interactions and Functional Characterization

Department: Biochemistry and Molecular Biology

Degree: Ph. D. Convocation: October, 2003

Permission is herewith granted to Dalhousie University to circulate and to have copied for non-commercial purposes, at its discretion, the above title upon the request of individuals or institutions.

[redacted]

Jessica P. Wyles

Dedicated to my family

Table of Contents

List of Tables

List of Figures

Abstract

Oxysterol binding protein (OSBP) and eleven OSBP-related proteins (ORPs) constitute a highly conserved protein family characterized by N-terminal pleckstrin homology (PH) and C-terminal OSBP homology domains (OHD)s. OSBP and ORPs are implicated in the regulation of vesicle trafficking, cell signalling and lipid metabolism, but their precise roles are poorly understood. To gain insight into the function of this gene family, yeast two-hybrid analysis was used to clone the OSBP-interacting protein vesicle-associated membrane protein (VAMP)-associated protein (VAP)-A, an ER-localized protein implicated in vesicle transport. Further yeast two-hybrid analysis determined that VAP-A interacted with both ORP9 variants, ORP9S and ORP9L. Furthermore, GST-VAP-A pulldown assays showed that ORP1L, ORP3(1d) and ORP4L also interacted with VAP-A, defining it as a central and functional regulator of the ORP family. The role of VAP-A/OSBP and VAP-A/ORP9 complex(es) in ER structure and export was characterized by inducible overexpression in CHO cells. Overexpressed OSBP was localized in a Golgi/vesicular compartment similar to endogenous OSBP. Overexpressed OSBP W174A, in which the conserved PH domain tryptophan was mutated, displayed enhanced interaction with VAP-A and caused the formation of irregular ER-derived vesicular structures to which VAP and OSBP W174A localized. We demonstrated that these ER-derived structures are involved at an early stage of ceramide and protein export from the ER. Similar to OSBP W174A, overexpression of both ORP9 variants caused dramatic changes in the structure of the ER, ERGIC (ER/Golgi intermediate compartment) and nucleus. This was accompanied by reduced cell growth, and in the case of ORP9S, cell death by a non-apoptotic mechanism. In summary, we have identified protein-protein interactions between VAP-A, OSBP and several ORPs, and implicated this network in an early stage of protein and ceramide export from the ER, as well as the regulation of ER membrane structure.

List of Abbreviations

25OH	25-hydroxycholesterol
ACAT	acyl-CoA:cholesterol acyltransferase
ADP	adenosine diphosphate
ARF	ADP ribosylation factor
β-ARK	β-adrenergic receptor kinase
β-COP	β-coatomer protein
BFA	brefeldin A
bp	base pair
BSA	bovine serum albumin
C_5-DMB-ceramide	*N*-(4,4-difluoro-5-(2-thienyl)-4-boro-3α,4α-diaza-*s*-indacene-3-pentanoyl)sphingosine
CK	casein kinase
cDNA	complementary DNA
CPY	carboxypeptidase Y
CSN	COP9 signalosome
CHO	Chinese hamster ovary
DABCO	2.5% (w/v)1,4-diazadicyclo[2.2.2]octane in 50 mM Tris-HCl and 90% (v/v) glycerol
DAG	diacylglycerol
DIGs	detergent-insoluble, glycosphingolipid-rich domains
DMEM	Dulbecco's modified Eagle's medium
DMSO	dimethyl sulfoxide
DNA	deoxyribonucleic acid
dNTP	deoxynucleotide triphosphate
EDTA	ethylene-diaminetetra-acetic acid
EGTA	ethylene-glycol-(*bis*)(β-aminoethyl ether)-N,N,N',N'-tetra-acetic acid

ER	endoplasmic reticulum
ERG30	ER/Golgi 30 kDa protein
ERGIC	ER/Golgi intermediate compartment
EST	expressed sequence tag
FCS	fetal calf serum
FFAT	two phenylalanines in an acidic tract
FITC	fluorescein isothiocyanate
GAL	galactose
GAP	GTPase activating protein
GAR	goat anti-rabbit
GAM	goat anti-mouse
GAP	GTPase activating protein
GEF	guanine nucleotide exchange factor
GFP	green fluorescent protein
GOLD	Golgi dynamics
G-PEM	PEM buffer with GTP
GRP78/BiP	glucose-regulated protein (78 kDa)/immunoglobulin binding protein
GRP94	glucose-regulated protein (94 kDa)
GST	glutathione *S*-transferase
GTP	guanosine triphosphate
h	hour
HBS	Hepes-buffered saline
HEK	human embryonic kidney
HEPES	4-(2-hydroxyethyl)-2-piperazine-N-[2-ethanaesulfonic acid]
HLA	human leukocyte antigen
HMG-CoA	3-hydroxy-3-methylgluataryl-coenzyme A
IPTG	isopropyl-1-thio-β-D-galactopyranoside

kDa	kilodalton
LB	Luria Bertani
LDL	low density lipoprotein
LiAc	lithium acetate
LXR	liver X receptor
MAP	microtubule-associated protein
MARK	microtubule affinity-regulating kinase
min	minute
mRNA	messenger ribonucleic acid
NA	no addition
NPC	Niemann-Pick C
NSF	N-ethylmaleimide-sensitive factor
NV	nucleus-vacuole
OD	optical density
OHD	OSBP homology domain
ORP	OSBP-related protein
OSBP	oxysterol binding protein
PA28	proteasome activator 28
PAGE	polyacrylamide gel electrophoresis
PARP	poly(ADP-ribose) polymerase
PBS	phosphate-buffered saline
PBS-IF	PBS immunofluorescence buffer
PC	phosphatidylcholine
PCI	proteasome/COP9 signalosome/initiation factor
PCR	polymerase chain reaction
PDI	protein disulfide isomerase
PEG	polyethylene glycol
PEM	Pipes/EDTA/magnesium

PH	pleckstrin homology
PI	phosphatidylinositol
PI-3-P	phosphatidylinositol-3-phosphate
PI-4-P	phosphatidylinositol-4-phosphate
PI-4,5-P_2	phosphatidylinositol-4,5-bisphosphate
PI-3,4-P_2	phosphatidylinositol-3,4-bisphosphate
PI-3,4,5-P_3	phosphatidylinositol-3,4,5-trisphosphate
PKA	protein kinase A
PKC	protein kinase C
PM	plasma membrane
PP2A	protein phosphatase 2A
PS	phosphatidylserine
RACK	receptor for activated C kinase
s	seconds
SDS	sodium dodecyl sulfate
SM	sphingomyelin
SMase	sphingomyelinase
SNAP	soluble NSF attachment protein
SNARE	soluble NSF attachment protein receptor
SRE	sterol response element
SREBP	sterol regulatory element binding protein
SRD	sterol regulatory defective
TBS	Tris-buffered saline
TE	Tris-EDTA buffer
TM	transmembrane domain
TPA	12-*O*-tetradecanoylphorbol-13-acetate
Tris	Tris (hydroxymethyl)aminomethane
TX100	Triton X-100

TXR	Texas Red
U18666A	3-β-(2-diethylaminoethoxy)androst-5-en-17-one
UPR	unfolded protein response
v/v	volume per volume
VAP	VAMP-associated protein
VAMP	vesicle-associated membrane protein
VSVG	ts045 vesicular stomatitis virus protein G
w/w	weight per weight
YPD	yeast rich medium

Acknowledgements

First and foremost I would like to thank Neale for putting up with me for the last six years, even when the going got tough I enjoyed working with him a great deal and will always remember my grad school days with great fondness (even if sometimes the cell lines were a little "wacky"...). I would also like to thank the members of my supervisory committee, Dr. Melanie Dobson, Dr. Roger McLeod and Dr. Chris McMaster for helpful suggestions and support. As well, I would like to thank Bob Zwicker and Gladys Keddy for the hours of tissue culture work that they did on my behalf (I think Bob earned this degree as much as I did!), Dr. Abbas Mohammadi for making the two OSBP cell lines, Cheng Wang for cloning ORP9 as well as preparing the ORP9 antibody, and Stephen Whitefield for help with confocal microscopy. As well, thanks to Debbie Hayes and Allison Drysdale for all their hard work, and to Tom Lagace, Ryan Perry, Cheng Wang, Ada Poranek and Kerry Hewitt, as well as past members of the Ridgway lab, for being great people to work with. Thanks also to the rest of the ARC. Finally, I would like to thank CIHR, the IWK Hospital and the Sumner Foundation for financial support.

My family and friends were a great source of support for me throughout my time in Halifax. While I enjoyed my studies and working in the lab a great deal, I also enjoyed living in Halifax, and will miss it and all the wonderful people I met. Thanks especially to Laura, Leticia, Janet, and Micheline for being fantastic friends (even if they dyed my hair blonde), to Eileen and Tom F. for supporting me when I really needed it, to Tom and Diane for always being there for me (thanks for the bag of food just before the thesis was due!) and for getting me started in curling (even if I was just one big bruise at the beginning – who knew you could break your nose by going curling...), to Pete and Bob and the rest of the curling gang for making me laugh at myself (and them) (don't worry guys, Tom has a new assistant to help with the radioactive crickets), and finally to Tanya and Ning for teaching me how to throw a frisbee properly and being a great source of stress relief over the last year.

Thank-you everyone, I couldn't have done it without you!

1. Introduction

The proliferation of genomic and expressed sequence tag (EST) databases has enabled the identification of the oxysterol binding protein (OSBP) related protein (ORP) family of proteins based on sequence identity to OSBP, the founding member. The human ORP family, which consists of OSBP plus eleven related proteins (ORP1-11), is identified by two conserved protein motifs: an N-terminal pleckstrin homology (PH) domain and an OSBP homology domain (OHD) (Fig. 1). The 350 amino acid OHD is exclusive to members of the ORP family and contains the absolutely conserved sequence 'EQVSHHPP', which has been designated the OSBP fingerprint. All but one of the ORPs contain both an OHD and a PH domain, although alternate promoters and splicing produce variants that lack PH domains [1-5]. The ORP family can be divided into five or six subfamilies based on sequence identity in the OHD (Fig. 1) [2,4,6,7]. Members of the human ORP family exhibit complex mRNA expression patterns: some display ubiquitous and invariant expression, while others are expressed in a tissue-specific manner. Splice variants for several members of the ORP family have been identified that have tissue distribution patterns distinct from the corresponding full-length mRNA [1-5].

Orthologues of human ORPs have been identified in a wide range of species from several phyla, including *Saccharomyces cerevisiae, Schizosaccharomyces pombe, Candida albicans, Dictyostelium discoidium, Caenorhabditis elegans, Arabidopsis thaliana, Drosophila melanogaster, Mus musculus, Mesocricetus auratus* (hamster), *Oryctolagus cuniculus* and *Macaca mulatta* (rhesus monkey), [8-18] implying an evolutionarily conserved function.

Figure 1. Structural organization of human ORP family. Sequences are aligned by the conserved EQVSHHPP motif, and proteins are subdivided into families by the grouping suggested by Lehto *et al* [6]. Short variants for ORP1, ORP4 and ORP9 are shown. Where there are known to be splice variants that truncate an ORP, full-length forms are designated Long (L) and truncated forms are designated Short (S).

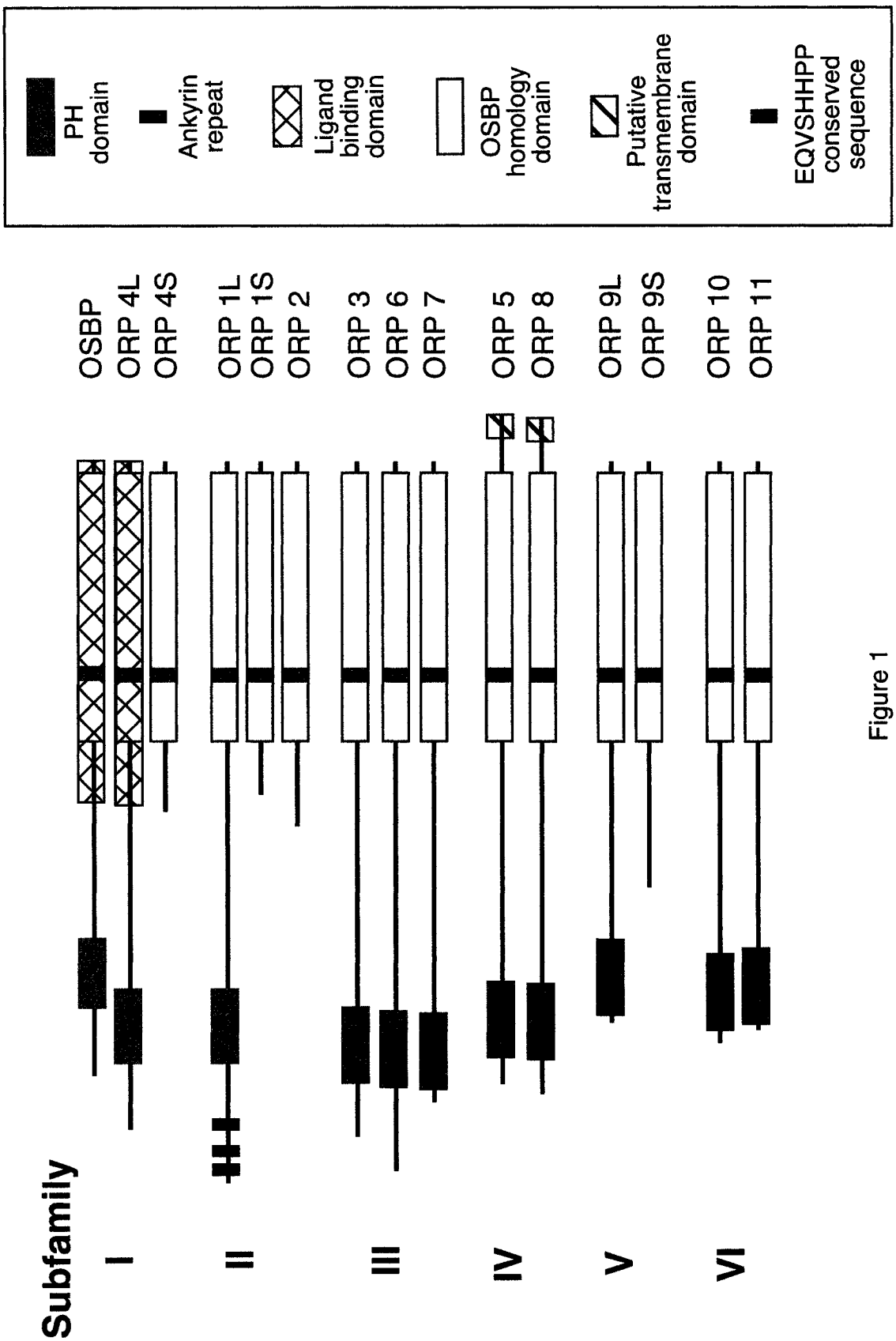
PH domain
Ankyrin repeat
Ligand binding domain
OSBP homology domain
Putative transmembrane domain
EQVSHHPP conserved sequence
Subfamily
I
II
III
IV
V
VI
OSBP
ORP 4L
ORP 4S
ORP 1L
ORP 1S
ORP 2
ORP 3
ORP 6
ORP 7
ORP 5
ORP 8
ORP 9L
ORP 9S
ORP 10
ORP 11

Figure 1

OSBP was first identified based on 25-hydroxycholesterol (25OH) binding activity [19,20]. OSBP and the ORP family have been implicated in fundamental cellular functions such as lipid and sterol metabolism, cell signalling and vesicle trafficking, but their precise roles are not well defined. The existence of such a large gene family implies that their functions are overlapping but in different cellular compartments or tissues. Alternatively, they could have similar functions, but respond to different stimuli, such as oxysterol ligands. The concept of overlapping redundant functions among the ORPs appears to be true for the seven ORP orthologues in *S. cerevisiae*, designated Osh1-7p [8]. None of the *OSH* genes are essential, but deletion of all seven leads to dramatic increases in ergosterol content and death.

OSBP and ORP4 are the only members of the family that have been shown to bind oxysterols, while ligands for other members of the family are unknown [1,19], indicating that oxysterol binding may not be a universal property. The ability of OSBP to bind oxysterols, potent inhibitors of cholesterol synthesis, has led to the assumption that OSBP and, by extension, the ORP family, plays a pivotal role in cholesterol regulation. While overexpression of OSBP, ORP1, ORP2 or ORP4 causes changes in sterol homeostasis [1,3,21-23], it is unclear if other ORPs share this property. Similar to the ORP family, deletion of *OSH* genes has revealed roles in sterol synthesis or trafficking, as well as in vesicle biogenesis from the Golgi apparatus [8,9].

Cellular localization of several Osh proteins and OSBP is regulated by PH domain binding to phosphorylated phosphatidylinositols (PIs) [21,24-26], while OSBP localization is also regulated by sterol flux and oxysterol binding [22,27,28]. Cellular localization of these proteins is critical for their biological activity. By extrapolation,

other ORP family members could be dynamic receptors that translocate between cellular compartments in response to different signals or ligands.

Available evidence indicates that OSBP and ORPs are lipid sensors that transduce signals or regulate trafficking between cellular compartments. The goal of this project was to further define the role of OSBP and the ORP family in these processes by identifying their protein binding partners by yeast two-hybrid screening of human cDNA libraries. The characterization of these binding partners, both alone and in conjunction with OSBP or the appropriate ORP, will elucidate the role(s) of OSBP and the ORP family in the aforementioned processes.

1.1 OSBP

In 1977, Kandutsch and co-workers first identified and characterized OSBP in mouse fibroblast L-cells as a specific and reversible high affinity receptor for 25OH and other oxysterols [19]. Since 25OH showed the greatest affinity for OSBP and is one of the most potent inhibitors of cholesterol synthesis and uptake [19,29], it was widely assumed that OSBP was involved in sterol regulation. OSBP was purified to homogeneity from hamster liver [20] and mouse L cells [30]. The cDNAs were later cloned from rabbits and humans [17,31].

1.1.1 OSBP structural and functional domains

OSBP contains distinct protein domains with both defined and unknown functions (Fig. 2). The function of the N-terminal glycine/alanine (G/A) rich region has

Figure 2. Structural features of OSBP. Schematic representation of OSBP showing structural domains and interaction motifs. Abbreviations: *PH*, PH domain; *G/A*, glycine/alanine rich region; *LZ*, leucine zipper.

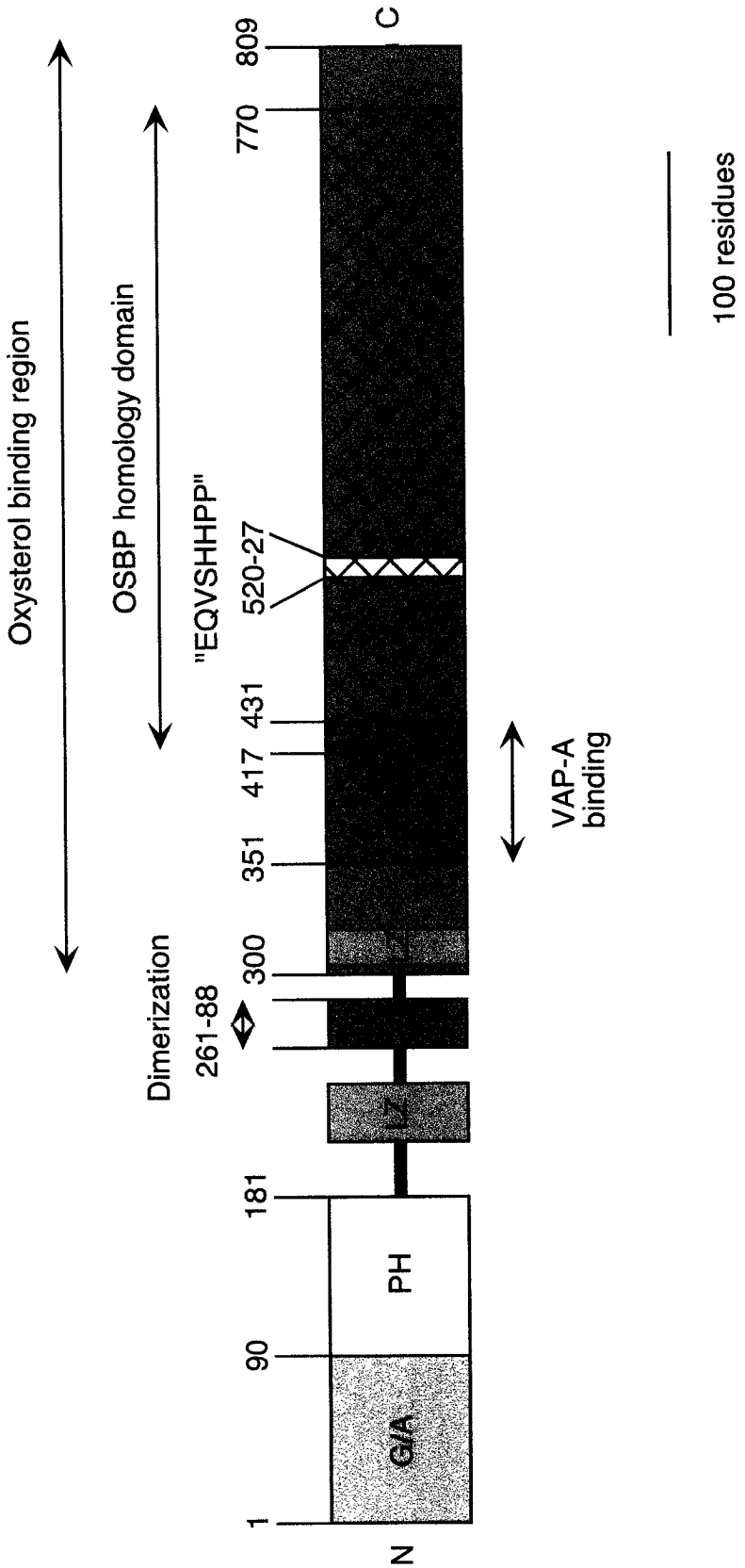
Oxysterol binding region
OSBP homology domain
"EQVSHHPP"
Dimerization
261-88
VAP-A
binding
100 residues
N
C
1
90
181
300
351
417
431
520-27
770
809
GA
PH
LZ

Figure 2

not been defined, but it is similar in amino acid composition to the amino terminus of a Ras (p21) guanosine triphosphate (GTP)ase activating protein (GAP) [32,33]. Immediately C-terminal of the G/A rich region is a PH domain, which binds phosphorylated PIs and mediates the interaction of OSBP with the Golgi apparatus (Section 1.1.2.2) [25,33]. C-terminal to the PH domain are two potential leucine zippers, the first of which may be involved in the binding of OSBP to the βγ subunit of heterotrimeric G-proteins (Section 1.1.2.4). The C-terminal half of the protein contains both the OHD and the oxysterol-binding region. The oxysterol-binding region of OSBP has been broadly defined by deletion mapping and its exact boundaries have not been determined [33]. Thus it is possible that the OSBP homology domain and the oxysterol-binding region do not entirely overlap. Indeed, comparison of 25OH binding activity and sequence data of OSBP, ORP4L, and its truncated splice variant, ORP4S, indicates that the ligand-binding domain may be situated nearer the N-terminus of OSBP than is shown in Figure 2 [1].

1.1.2 Role of the PH domain in OSBP localization

OSBP translocates between a cytosolic/vesicular compartment and the Golgi apparatus in response to alterations in sterol trafficking or ligand binding (Section 1.1.2.3). Unlike most PH domains that regulate localization primarily to the plasma membrane (PM) [34] (reviewed in [35]), the PH domain of OSBP mediates localization to the Golgi apparatus [21,24]. Since PH domains are found in almost all ORPs, as well as three Osh proteins, one of which is also targeted to the Golgi apparatus via its PH domain, membrane targeting by this domain is central to the function(s) of this family.

The PH domain of OSBP is both necessary and sufficient for localization to the Golgi apparatus (Section 1.1.2.2), where it has been shown to bind phosphatidylinositol-4,5-bisphosphate (PI-4,5-P_2), most likely in conjunction with a second Golgi-specific protein target that has not been clearly defined.

1.1.2.1 PH domain structure and function

PI can be phosphorylated on three of its five hydroxyl groups, giving rise to seven distinct phosphorylated PIs. Although these phospholipids are found in low abundance, they play key roles in the recruitment of proteins to membranes, thus contributing to the regulation of signalling processes, cytoskeletal organization and membrane trafficking. The regulation of PI phosphorylation can control the subcellular localization of proteins via binding to PH, PX, ENTH or FYVE domains (reviewed in [36]). PH domains are small modular domains of 100 to 120 amino acids that share limited primary sequence identity, but have highly conserved secondary and tertiary structure [37,38]. X-ray crystallographic and nuclear magnetic resonance (NMR) analysis of numerous PH domains has revealed a common structure consisting of seven β-strands that form a sandwich composed of two orthogonal β-sheets with a hydrophobic core. These sheets are capped at one end with a C-terminal α-helix [35,39-44], which stabilizes the β-sheets through a hydrophobic interaction between a conserved tryptophan at the C-terminus of the helix and the hydrophobic core of two β-sheets [45]. PH domains are electrostatically polarized, with three of the loops connecting the β-strands coinciding with the positively charged face, forming the phosphorylated PI-binding site [35,40,43].

The loops are variable with respect to length and sequence, allowing distinct binding specificities [35,37,46-48].

PH domains have a wide range of specificities and affinities for phosphorylated PIs, and have been extensively reviewed elsewhere [35,37-40,45,48-55]. The interaction of PH domains with PI-4,5-P_2 and phosphatidylinositol-4-phosphate (PI-4-P) have been the most widely investigated, but it was recently recognized that some PH domains also bind phosphatidylinositol-3,4-bisphosphate (PI-3,4-P_2) and phosphatidylinositol-3,4,5-trisphosphate (PI-3,4,5-P_3) [56-61]. While PI-4,5-P_2 and PI-4-P are constitutively present in cellular membranes, PI-3,4-P_2 and PI-3,4,5-P_3 are barely detectable under basal conditions and are induced by a number of stimuli, including insulin and growth factors [62-64]. This indicates that PI-4,5-P_2 and PI-4-P may be involved in constitutive membrane localization of PH domain containing proteins, while PI-3,4-P_2 and PI-3,4,5-P_3 regulate localization in response to transient stimuli.

However, only ~10% of PH domains have been shown to bind phosphorylated PIs with sufficient affinity and specificity to regulate membrane localization on their own [54]. In some instances, oligomerization of PH domains at membranes enhances their affinity for a specific phosphorylated PI or low affinity PH domains may dictate membrane localization in conjunction with other protein domains [25,54,55,65]. In a few cases, PH domains have been shown to bind to acidic residues in proteins rather than, or in conjunction with, phosphorylated PIs [55,66-69] (Section 1.1.2.4). Finally, studies involving Tiam1, a guanine nucleotide exchange factor (GEF), showed that initial membrane localization is PH domain-independent, but subsequent interaction of the

Tiam1-PH domain with phosphatidylinositol-3-phosphate (PI-3-P) regulates protein conformation and function [70].

1.1.2.2 Role of phosphorylated PIs in OSBP PH domain localization to the Golgi apparatus

The PH domain of OSBP, expressed as a green fluorescent protein (GFP) fusion (GFP-OSBP-PH), localized specifically to the Golgi apparatus *in vivo* and bound to PI-4,5-P_2 and PI-4-P *in vitro* [25]. Localization of GFP-OSBP-PH to the Golgi apparatus *in vivo* was studied using yeast strains carrying temperature-sensitive mutations in genes for the PI-4-P,5-P_2 kinase *MSS4*, the Golgi-localized PI-4-P kinase *PIK1* or the PM-localized PI-4-P kinase *STT1* [71]. GFP-OSBP-PH dissociated from the Golgi apparatus in response to inactivation of Pik1p, but not in response to inactivation of Stt1p or Mss4p, indicating that PI-4-P production in the Golgi apparatus is required for localization to that organelle.

However, both PI-4,5-P_2 and PI-4-P are found in membranes other than the Golgi apparatus, indicating that there could be a second Golgi-specific determinant of OSBP-PH localization. In support of this concept, dissociation of GFP-OSBP-PH from the Golgi apparatus in the *pik1*^{ts} yeast strain at the non-permissive temperature was not complete. As well, a mutant GFP-OSBP-PH that did not bind PI-4-P *in vitro* was still weakly localized to the Golgi apparatus *in vivo,* an effect that was enhanced by dimerization, and did not dissociate from the Golgi apparatus at the Pik1p^{ts} non-permissive temperature. The localization of both the wildtype and PI-4-P binding mutant OSBP PH domains was also shown to be dependent on Arf1p, a member of the ADP-

ribosylation factor (ARF) family of small GTPases involved in the recruitment of coat proteins to the Golgi apparatus for vesicle formation [71-73]. Thus the second Golgi-specific determinant responsible for OSBP-PH localization could be regulated by Arf1p activity [71].

1.1.2.3 Sterol- and oxysterol-mediated localization of OSBP to the Golgi apparatus

Although Golgi apparatus localization of OSBP is mediated via the PH domain, the signals that regulate this localization are sterol-derived [21,27,28,33]. OSBP is generally found in a cytoplasmic/vesicular compartment and translocates to the Golgi apparatus in response to 25OH binding [33]. This can be explained by a model in which the absence of an oxysterol ligand causes the ligand-binding region to obscure the PH domain, thereby preventing PH domain-mediated localization to the Golgi apparatus [21]. Ligand binding would induce a conformational change, expose the PH domain, and enable binding to lipid and/or protein targets on the Golgi apparatus. This model is supported by data from OSBP mutants that either (i) lacked a PH domain (OSBP ΔPH) and did not localize to the Golgi apparatus in response to 25OH treatment or (ii) lacked a complete ligand-binding domain or consisted solely of the PH domain and were constitutively localized to the Golgi apparatus [21,25,33]. Translocation of OSBP to the Golgi apparatus was necessary for effects on cholesterol synthesis and esterification. Cells overexpressing wildtype OSBP had increased cholesterol synthesis and reduced cholesterol esterification, while synthesis of cholesterol and cholesterol ester in cells overexpressing OSBP ΔPH was similar to that of mock-transfected controls (further discussed in Section 1.1.3) [21].

In addition to oxysterol-mediated translocation, OSBP localized to the Golgi apparatus in response to conditions that depleted cellular cholesterol or prevented cholesterol efflux from the lysosomal/endosomal system. An overview of the sterol-regulated translocation of OSBP between the Golgi apparatus and cytosolic/vesicular compartments is shown in Figure 3. In Chinese hamster ovary (CHO) cells cultured in low density lipoprotein (LDL) containing media, OSBP was found primarily in a cytosolic/vesicular compartment (Fig. 3, panel 1), while growth in delipidated serum caused localization to the Golgi apparatus [27], indicating that cholesterol efflux from the lysosomal/endosomal pathway was required for OSBP dissociation from the Golgi apparatus. This is supported by the localization of OSBP to the Golgi apparatus in Niemann-Pick C (NPC) cells [28], in which cholesterol efflux from the lysosomes/endosomes is blocked by a mutation in the NPC-1 protein [74-76] (Fig. 3, panel 2). OSBP also localized to the Golgi apparatus in response to other conditions that reduce the efflux of cholesterol from the lysosomal/endosomal pathway, such as depletion of cellular cholesterol by treatment with cyclodextrin, increased cholesterol influx from the PM in response to bacterial sphingomyelinase (SMase) or treatment with 3-β-(2-diethylaminoethoxy)androst-5-en-17-one (U18666A), a drug that reproduces the NPC cholesterol transport defect (Fig. 3, panel 2) [22,28]. As well, the addition of LDL to NPC or U18666A-treated cells failed to cause OSBP to dissociate from the Golgi apparatus, again implying that OSBP release from the Golgi apparatus is dependent on cholesterol trafficking out of the endosomal pathway [28]. Finally, OSBP localized to the Golgi apparatus in response to sterol starvation as indicated by enhanced localization in response to inhibition of cholesterol synthesis by lovastatin treatment (in the absence of

Figure 3. Regulation of OSBP localization by sterol transport and oxysterols. Panels display the localization of OSBP under conditions that alter cholesterol synthesis or transport. Panel 1 represents untreated (control) cells grown in the presence of LDL. Panel 2 represents cells that are defective in cholesterol synthesis, cholesterol transport or were treated to reduce cholesterol efflux from the lysosomal/endosomal pathway. Panel 3 represents the potential indirect effects of 25OH via suppression of cholesterol transport and synthesis. Panel 4 represents the response of OSBP to 25OH binding.

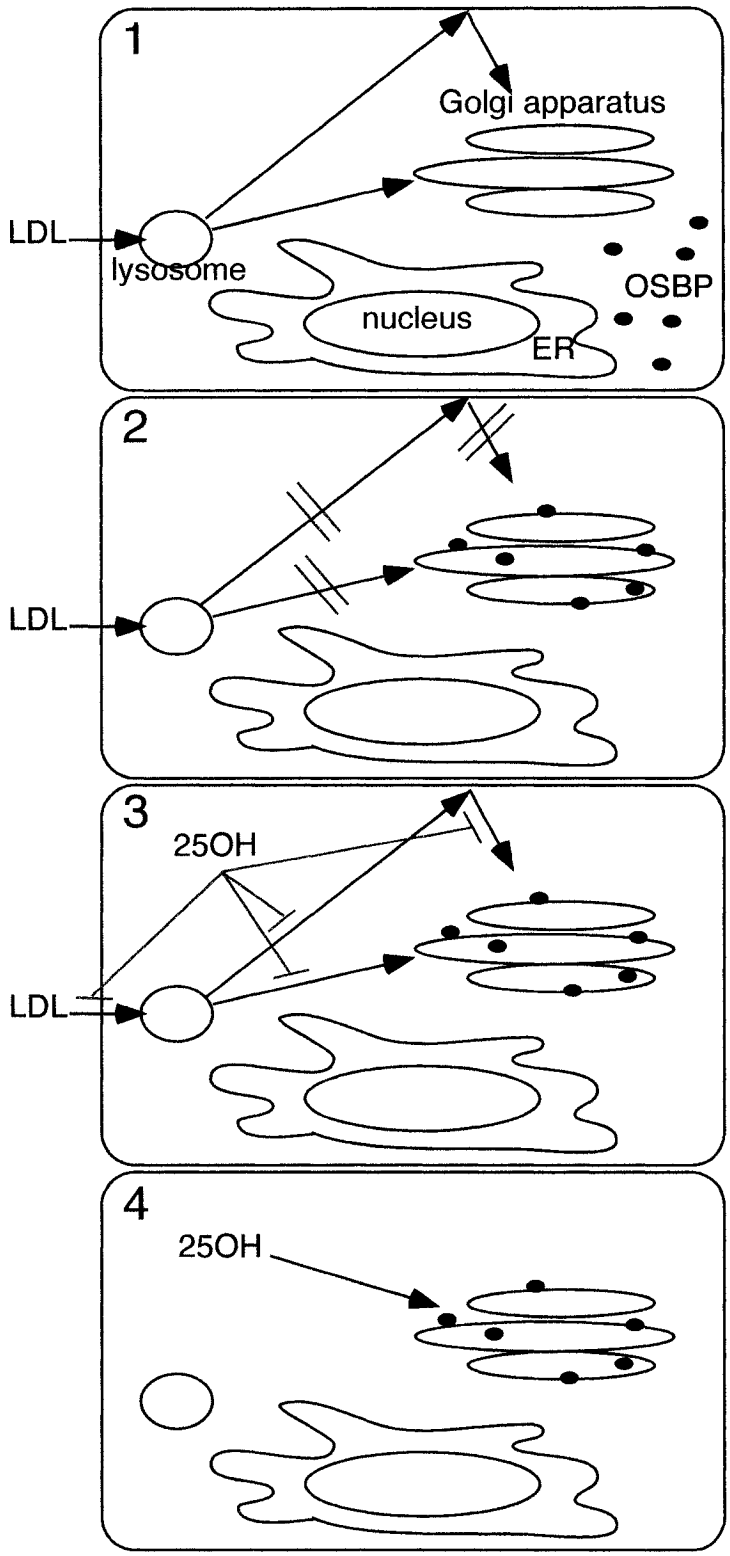
1
Golgi apparatus
LDL
lysosome
OSBP
nucleus
ER
2
LDL
3
25OH
LDL
4
25OH

Figure 3

LDL) or in cholesterol-starved sterol regulatory defective (SRD)6 cells, a CHO cell mutant unable to synthesize cholesterol or internalize LDL (Fig. 3, panel 2). When SRD6 cells were supplemented with cholesterol/cyclodextrin complexes, OSBP returned to a cytoplasmic/vesicular compartment [27]. Since treatment with LDL caused OSBP to dissociate from the Golgi apparatus except in NPC cells or U18666A treated cells, it seems that OSBP localization to the Golgi apparatus is primarily a response to reduced cholesterol transport from the lysosomes/endosomes.

Paradoxically, treatment of cells with 25OH (assumed to be a signal of cholesterol excess) also resulted in OSBP localization to the Golgi apparatus even in the presence of LDL (Fig. 3, panel 3) [33]. Since 25OH suppresses cholesterol synthesis, it is possible that 25OH regulates OSBP translocation to the Golgi apparatus on two levels: direct binding to OSBP (Fig. 3, panel 4) or creation of an OSBP binding site in the Golgi apparatus in response to reduced cholesterol levels or inhibition of lysosomal/endosomal transport. In support of the latter, 25OH treatment caused partial localization to the Golgi apparatus of a truncation mutant of OSBP expressing only amino residues 1-261. Since this mutant is truncated prior to the ligand-binding domain, its translocation is likely a result of 25OH-mediated changes in cholesterol homoeostasis rather than 25OH binding [33]. As well, this mutant lacks the dimerization domain, which may decrease its ability to interact with binding partners at the Golgi apparatus. An OSBP-PH domain that lacks phosphorylated PI binding activity localized more efficiently to the Golgi apparatus when expressed as a dimer (Section 1.1.2.2) [71]. As such, the weak Golgi apparatus localization of OSBP 1-261 in response to 25OH treatment could be due to its monomeric structure. Finally, we cannot discount the possibility that OSBP translocation in response

to 25OH is mediated by another ORP that interacts directly or indirectly with OSBP. The current data suggest that OSBP localization responds primarily to alterations in transport of cholesterol through the Golgi apparatus from the lysosomes/endosomes and to oxysterol binding.

1.1.2.4 Protein binding partners of the OSBP PH domain

The existence of a second Golgi-specific OSBP binding partner is also supported by *in vitro* results that have identified protein-protein interactions for the PH domain of OSBP. Several PH domains, including that of OSBP, bound the βγ subunit of heterotrimeric G proteins *in vitro*, an interaction that was inhibited by the addition of $G_0\alpha$ [68]. The PH domains tested in this study all had significant C-terminal extensions. In the case of OSBP, the construct contained an additional 40 amino acids that included a potential leucine zipper (Fig. 2). Since the C-terminal extension of one of the PH domains investigated in this study, guanine nucleotide releasing factor (GNRF)-PH, was shown to be required for the interaction of the PH domain with Gβγ, the PH domain was not the sole determinant of Gβγ binding [68]. It was subsequently shown that in addition to interaction with Gβγ, PI-4,5-P_2 was required for membrane localization of β-adrenergic receptor kinase (β-ARK), another protein investigated in this study [77].

The PH domain of OSBP has also been shown to bind to the receptor for activated C kinase (RACK)1 [78]. RACK1 anchors activated protein kinase C (PKC) to the membrane through its WD-40 motifs and could regulate the cellular localization of PKC in a lipid-independent manner. Interestingly, Gβ also contains WD-40 motifs. RACK1 can concomitantly bind PKC and a variety of PH domain containing proteins,

implying that it may enhance phosphorylation of PH domain containing proteins by bringing them into close proximity with PKC. Interestingly, the PKC activators TPA (12-*O*-tetradecanoylphorbol-13-acetate) and diacylglycerol (DAG) (produced by phospholipase C treatment) both caused localization of OSBP to the Golgi apparatus, but did not affect its phosphorylation [22]. It is unknown if this localization is mediated via the RACK1/PKC complex. Finally, the PH domain of OSBP has also been shown to bind to F-actin *in vitro* [79], although the significance of this finding is unclear.

1.1.3 Regulation of cholesterol and SM homeostasis by OSBP and oxysterols

The high-affinity binding of OSBP to 25OH, a potent inhibitor of cholesterol synthesis, led to the initial assumption that OSBP plays a pivotal role in cholesterol homeostasis. Indeed, overexpression of OSBP results in alterations in cholesterol synthesis and enhanced 25OH-mediated stimulation of SM synthesis [21,80]. Cholesterol and SM, essential components of eukaryotic membranes, are co-variant in a number of diseases and experimental models, interact physically in membranes and are metabolically co-regulated. These interactions play a role in the regulation of membrane structure, signal transduction, protein and lipid trafficking and cholesterol homeostasis (reviewed in [81]). The ratio of cholesterol, SM and phospholipids must be tightly regulated, as alterations could affect membrane fluidity, thereby affecting the activity of membrane-associated proteins and membrane permeability. Both cholesterol and SM are involved in the formation and maintenance of microdomains in the PM termed lipid rafts (also called detergent-insoluble, glycosphingolipid-rich domains (DIGs), detergent-

resistant membranes (DRMs) or caveolae) involved in signalling, transport and uptake (reviewed in [82-85].

OSBP and oxysterols could regulate cholesterol and SM synthesis by affecting lipid trafficking or by altering the activity of biosynthetic pathways in the endoplasmic reticulum (ER). Cholesterol and SM are synthesized in the ER and cis-medial elements of the Golgi apparatus, respectively, but the PM contains 60-90% of the total cellular content of both lipids [86-90]. Thus, the bulk of these lipids are physically separated from their sites of synthesis and regulation. Transport of newly synthesized cholesterol from the ER by caveolin, as well as transport of LDL-derived cholesterol from the lysosomal/endosomal pathway, has been shown to pass through the Golgi apparatus en route to the PM [91-94]. When the capacity of the PM to absorb cholesterol is reached, cholesterol is transported back to the ER where it is converted to cholesterol ester by acyl-CoA:cholesterol acyltransferase (ACAT). Elevated cholesterol content in the ER also inhibits the processing of sterol regulatory element binding protein (SREBP) [95], a membrane-bound transcription factor that is retained in the ER in cholesterol-replete conditions and is transported to the Golgi apparatus in response to cholesterol depletion [96]. Once in the Golgi apparatus, SREBP undergoes two proteolytic events, releasing a mature transcription factor that enters the nucleus and activates the transcription of numerous genes involved in cholesterol and fatty acid synthesis by binding to sterol response elements (SREs) in their promoters [95]. In this way, the cholesterol content of the ER regulates cholesterol synthesis.

Cholesterol homeostasis is also regulated by SM content, which determines the capacity of a membrane to absorb cholesterol [97] and regulates the transport of LDL-

derived cholesterol to the ER (reviewed in [81]). Elevation of cellular SM content by treatment with SM-containing liposomes increased cholesterol synthesis [98,99], while depletion of SM in the PM by bacterial SMase caused an influx of cholesterol to the ER, resulting in enhanced cholesterol esterification and down-regulation of cholesterol synthesis and uptake [88,97,100,101].

Synthesis of cholesterol and SM is also regulated by oxysterols, which have a number of protein targets in the cell, including OSBP and ORP4L, steroidogenic factor 1 and liver X receptor (LXR)α and LXRβ, all of which are involved in the regulation of lipid metabolism [102]. Oxysterols reduce cholesterol levels by enhancing influx of cholesterol from the PM to the ER, thereby inhibiting cholesterol synthesis and uptake, as well as suppressing the activity of 3-hydroxy-3-methylglutaryl (HMG)-CoA reductase activity [103] and stimulating bile acid synthesis [104,105].

In addition to regulating cholesterol metabolism, 25OH also increased SM synthesis in CHO-K1 cells, an effect that was enhanced in CHO-K1 cells stably overexpressing OSBP (CHO-OSBP) [106]. SM is synthesized in the Golgi apparatus from ceramide and phosphatidylcholine (PC) by SM synthase [107,108]. However, ceramide is synthesized in the ER and must be transported to the Golgi apparatus prior to conversion to SM. Since *in vitro* SM synthase activity was not increased by oxysterols, it appeared that SM synthesis was enhanced by transport of ceramide from the ER to the Golgi apparatus [106]. This implies that OSBP regulates a trafficking pathway rather than a biosynthetic reaction.

Cholesterol synthesis was also altered at the transcriptional and post-transcriptional levels in CHO-OSBP cells. In these cells, mRNA levels for three genes

involved in cholesterol synthesis (LDL receptor, HMG-CoA reductase and HMG-CoA synthase) increased by 50%, while ACAT mRNA decreased by 50%. As a result cholesterol synthesis increased by 80%, while cholesterol ester formation decreased by 50% compared to controls [21]. CHO-OSBP cells down-regulated cholesterol synthesis in response to 25OH treatment, but decreased cholesterol esterification rates in these cells could not be increased to control levels by 25OH or LDL treatment. The effects on cholesterol regulation are mediated by localization of OSBP to the Golgi apparatus (Section 1.1.2), as indicated by the lack of effect of OSBP ΔPH on cholesterol synthesis or esterification even though it bound 25OH with the same affinity as wildtype OSBP [21]. Since CHO-OSBP cells appear as if they were cholesterol depleted, but respond normally to 25OH, the unliganded form of OSBP is probably the primary mediator of enhanced cholesterol synthesis [21].

1.1.4 OSBP phosphorylation

OSBP is phosphorylated on five to six serine residues. Phosphorylation of serine 381 causes a size shift on SDS-polyacrylamide gel electrophoresis (PAGE), a property that was used to monitor the phosphorylation state of OSBP. OSBP phosphorylation is regulated by SM and cholesterol levels in the PM, as well as by alterations in cholesterol trafficking [27,28]. Cholesterol starvation as a result of inhibition of *de novo* cholesterol synthesis or inhibition of cholesterol transport from the lysosomal/endosomal system results in Golgi apparatus localization of OSBP and subsequent dephosphorylation of serines 381, 384 and 387 [28]. OSBP phosphorylation was not affected by oxysterol treatment, nor did the phosphorylation state alter ligand

binding or translocation to the Golgi apparatus in response to oxysterol treatment [109]. Depletion of SM in the PM by bacterial SMase also caused rapid dephosphorylation of OSBP and translocation to the Golgi apparatus. Following bacterial SMase treatment, OSBP was rephosphorylated coincident with SM resynthesis and down-regulation of cholesterol esterification, indicating that the phosphorylation state of OSBP plays an as yet undefined role in cholesterol and SM homeostasis [22]. Since inhibiting cholesterol transport out of the lysosomes or removing PM cholesterol with cyclodextrin did not inhibit bacterial SMase-induced dephosphorylation, OSBP dephosphorylation occurred as a result of SM hydrolysis rather than alterations in cholesterol trafficking [22]. However, translocation of OSBP to the Golgi apparatus in response to bacterial SMase was the result of alterations in sterol trafficking (Section 1.1.2.3). This data suggest that localization of OSBP to the Golgi apparatus and dephosphorylation of OSBP are two separate, albeit related, events. Inhibition of cholesterol trafficking or cholesterol starvation results in the localization of OSBP to the Golgi apparatus, where it becomes progressively dephosphorylated over several hours. Acute depletion of SM also results in rapid dephosphorylation, while the associated alterations in cholesterol trafficking cause the localization of OSBP to the Golgi apparatus.

OSBP was dephosphorylated in response to treatment of cells with brefeldin A (BFA), a fungal metabolite that causes the absorption of the cis, medial and trans elements of the Golgi apparatus into the ER by inhibiting anterograde transport to the Golgi apparatus, but not retrograde transport to the ER [110-112]. This indicates that an OSBP kinase(s) is localized to the Golgi apparatus or another BFA-sensitive compartment and is sequestered away from OSBP by relocalization to the ER. While it is

possible that the kinase(s) is directly inhibited by BFA, this is unlikely as BFA did not inhibit *in vitro* phosphorylation of OSBP by purified Golgi membranes [109].

Experiments using kinase inhibitors and activators, both in whole cells and *in vitro*, served to eliminate a number of potential OSBP kinases, such as protein kinase A (PKA), PKC and casein kinase (CK) II [109]. The phosphorylation of serine 381 is required for the subsequent phosphorylation on serines 384 and 387. Serines 384 and 387 become classical CKI substrates when serines 381 or 384 are phosphorylated three residues N-terminal of the target serine [113].

Since SM hydrolysis caused OSBP dephosphorylation, a ceramide-activated phosphatase such as protein phosphatase 2A (PP2A) could be involved [114-117]. Indeed, treatment with okadaic acid, an inhibitor of PP2A, enhanced OSBP phosphorylation [109]. However, since short-chain ceramides did not promote OSBP dephosphorylation, either a metabolite of SM other than ceramide is responsible for activating the phosphatase or short chain ceramides are not able to activate PP2A in CHO cells [22]. Although the role of OSBP phosphorylation has not yet been determined, identification of the kinase(s) and phosphatase(s) involved may give further clues as to the function of OSBP.

1.2 ORP1 (Subfamily II)

Two variants of ORP1, ORP1L and ORP1S, arise from alternate promoters and differential splicing [3,4] (Fig. 1). ORP1L contains an OHD, a PH domain and three ankyrin repeats. ORP1S lacks the PH domain and ankyrin repeats and consists almost exclusively of the OHD [2-4,6,118]. ORP1S was expressed primarily in skeletal muscle

and heart, while ORP1L was more abundant in macrophages, brain and lung tissue [3]. Both ORP1S and ORP1L were upregulated during the differentiation of monocytes to macrophages. However, ORP1S was only upregulated 2-4 fold compared to a 100-fold induction of ORP1L. ORP1L is the only member of the human ORP family with ankyrin repeats, which are found in a number of cytoskeletal proteins and transcription factors and are implicated in protein/protein interactions [119]. The ankyrin repeats, in conjunction with the PH domain, mediate the localization of ORP1L to late endosomal compartments. ORP1S was found in both the cytosol and the nucleus [3].

ORP1S was studied with respect to its ability to complement the function of Osh4/Kes1p, an *S. cerevisiae* orthologue of the ORP family that is a negative regulator of the *SEC14* pathway [120]. Sec14p is an essential PI/PC transfer protein involved in vesicle transport from the Golgi apparatus. Disruption of *OSH4/KES1* allowed a $sec14^{ts}$ strain to grow at the non-permissive temperature, indicating that Osh4/Kes1p and Sec14p have opposing functions [120]. Expression of ORP1S in $sec14^{ts}$/*osh4/kes1* yeast inhibited carboxypeptidase Y (CPY) processing at the non-permissive temperature, indicating that ORP1S complemented Osh4/Kes1p function with respect to vesicle transport from the Golgi apparatus [118]. ORP1S did not bind oxysterols, but exhibited strong binding to phosphatidic acid and weak binding to PI-3-P when these lipids were immobilized on nitrocellulose [118].

A recent study investigated the role of ORP1L with respect to cholesterol synthesis and esterification in mammalian cells [3]. A fragment of ORP1L containing only the ankyrin repeats and the PH domain showed enhanced localization to late endosomes relative to the entire protein [3]. This indicates that the C-terminal ligand-

binding region (or OHD) could inhibit endosome localization, analogous to inhibition of localization to the Golgi apparatus by the ligand-binding domain of OSBP [33]. The ORP1L ankyrin repeat/PH domain fragment also caused the late endosome compartment to aggregate and form unusual membranous structures [3]. One of the many functions of the lysosomal/endosomal pathway is the sorting and transport of LDL-derived cholesterol. The localization of ORP1L to the endosomes potentially implicates it in cholesterol and lipid uptake and transport, perhaps as a sensor of lipid or sterol content in this compartment. This is supported by the capacity of ORP1L, but not ORP1S, to increase the transcriptional activity of LXRs [3], oxysterol-binding nuclear hormone receptors that control expression of numerous genes involved in sterol and bile acid regulation [121]. The dramatic induction of ORP1L expression in macrophages, cells that are dependent on LXRs for regulation of lipid efflux pathways, also suggests that ORP1L and LXR regulation are connected via an unknown mechanism. As very little ORP1L was seen in the nucleus [3], its role in LXR activation is likely to be indirect, perhaps through the regulation of the production of LXR agonists such as polyunsaturated fatty acids [122], oxidized cholesterol 3-sulfate derivatives [123] or oxysterols. These data suggest that ORP1L may respond to increased sterol or lipid content of the endosomes by activating LXR and cholesterol efflux, potentially via the ATP-binding cassette transporter A1 (ABCA1) [124].

1.3 ORP2 (Subfamily II)

ORP2 is the only family member that consists solely of an OHD and, together with ORP1, constitutes Subfamily II. ORP2 mRNA is widely expressed in human tissues,

with the highest levels in the central nervous system (CNS), leucocytes, placenta and pancreas [23]. Two splice variants have been identified in mouse tissues, while a third was found only in CHO cells [23]. Another splice variant was identified in which exon 3 was omitted, leading to the in-frame deletion of 12 amino acids prior to the OHD [4]. The functional significance of these splice variants is unknown.

The ability of ORP2 to act as a suppressor of Sec14^{ts}p bypass mutant *osh4/kes1* was investigated in the same study as ORP1S [118] (Section 1.2). Although ORP1S and ORP2 are closely related, ORP2 was unable to complement the loss of Osh4/Kes1p [118] and was localized to the Golgi apparatus [23,118]. However, overexpression of ORP2 was toxic in *S. cerevisiae*, which made it difficult to draw conclusions about its function in this system.

Like OSBP and ORP1L, ORP2 has been shown to be involved in cellular cholesterol homeostasis. Cholesterol levels and ACAT activity were reduced in cells overexpressing ORP2 [23]. Cholesterol efflux to extracellular acceptors such as human serum, human apoA1 and palmitoyl-oleyl PC (POPC) vesicles was increased in ORP2 overexpressing cells, apparently due to an increase in the relative proportion of cholesterol caused by reduced ACAT activity.

Transport of vesicular stomatitis viral protein G fused to green fluorescent protein (VSVG-GFP) from the ER through the Golgi apparatus to the PM was examined using cells that were transiently transfected with both VSVG-GFP and ORP2 [23]. Cells expressing levels of ORP2 similar to the cell lines used for the cholesterol efflux experiments had normal VSVG-GFP transport. However, in cells expressing very high levels of ORP2, transport of VSVG-GFP to the Golgi apparatus was normal but

subsequent transport from the Golgi apparatus to the PM was inhibited. This suggests that ORP2 is involved in a late stage of the secretory pathway, possibly in the biogenesis of vesicles from the Golgi apparatus [23]. A role in the late secretory pathway is supported by the observation that transport of CPY to the vacuole was perturbed by expression of ORP2 in *S. cerevisiae* [118].

1.4 ORP3 (Subfamily III)

ORP3 was initially identified in an EST search for OSBP homologues [6,7] and was later cloned from hematopoietic cells using differential display PCR [125]. Less differentiated CD34+38- hematopoietic cells expressed up to twice as much ORP3 mRNA in relation to CD34+ cells, which in turn expressed 3-4 times more ORP3 mRNA compared to CD34- cells. Oxysterols inhibited proliferation of hematopoietic cells but since ORP3 did not bind 25OH (Wang and Ridgway, unpublished data), it is unlikely to be directly involved in this effect [125]. As many as 9 splice variants of ORP3 have been identified [4,125]. One study identified splice variants in which exons 9 and/or 12 were spliced out and/or exon 15 was extended. The extension of exon 15 caused a shift in the reading frame, resulting in premature truncation of the OHD [5]. This splicing pattern could lead to two distinct groups of ORP3 proteins: four that contain a complete OHD and four that are truncated in the OHD. mRNA for the truncated forms was expressed primarily in human brain, kidney, spleen, thymus and thyroid, while mRNA for complete OHD forms were found at variable levels in most other tissues. Another ORP3 splice variant in which exon 4 was deleted, removing a portion of the PH domain, was

identified in an earlier study [4]. The functional significance of these splice variants has not been defined.

1.5 ORP4 (Subfamily I)

An mRNA encoding a truncated form of ORP4, termed ORP4S, was identified by differential display as an upregulated transcript in metastatic tumours [126]. ORP4S is produced from an alternate promoter start site and differential splicing [1]. mRNA for both forms was expressed primarily in brain, although ORP4L mRNA was also expressed at lower levels in heart, skeletal muscle, kidney and spleen [1,6]. Additional splice variants missing exon 12 [4] and 14 (Ridgway, unpublished results) have been detected, but their functional significance is unknown.

ORP4 and OSBP have the greatest degree of similarity and constitute Subfamily I [1,6]. Although ORP4L possesses oxysterol-binding activity, its specificity is controversial. One report indicated that ORP4L from retinal tissue bound 7-ketocholesterol [15], while another report indicated high affinity (K_D=5-10 nM) 25OH binding but no 7-ketocholesterol binding activity [1]. The discrepancy is probably due to assay differences, as the ORP4L binding assay for 7-ketocholesterol used extracts from monkey retina [15], while 25OH binding was determined using extracts of COS cells transiently overexpressing ORP4L [1]. 25OH or 7-ketocholesterol treatment did not affect the localization of either form of ORP4 [1]. This study also showed that ORP4S did not bind 25OH and that oxysterol specificity of OSBP and ORP4L was similar.

Indirect immunofluorescence in CHO cells revealed that ORP4L was widely dispersed throughout the cell rather than localized to a specific organelle [1]. However,

subcellular fractionation of monkey retina cells indicated ORP4L was primarily membrane associated [15]. In contrast, ORP4S co-localized with vimentin filaments by indirect co-immunofluorescence [1]. Vimentin is a member of the intermediate filament family of proteins. These proteins form extensive networks that provide structural integrity to the cell and form a scaffold for binding of a number of proteins involved in metabolism, vesicle trafficking and signaling (reviewed in [127]). Overexpression of ORP4S in CHO cells re-organized vimentin from an extensive filamentous network to disorganized bundles surrounding the nucleus. The same phenotype was observed in control cells treated with nocodazole, a microtubule-disrupting agent. Thus, ORP4S may interfere with microtubule contacts, leading to disruption of the vimentin network. While ORP4L did not co-localize with vimentin, it altered the effect of nocodazole on vimentin localization. In control cells, nocodazole treatment caused vimentin to aggregate in bundles around the nucleus, while in cells expressing ORP4L, vimentin localization was diffuse [1]. Vimentin networks have been implicated in cholesterol transport to the ER [128-130]. Consistent with this, cells overexpressing ORP4S had reduced cholesterol esterification, possibly because of a reduction in cholesterol trafficking to the ER due to disruption of the vimentin network [1]. Overexpression of OSBP also reduced cholesterol esterification [21], indicating that ORP4S, ORP4L and OSBP participate in a similar pathway to affect ACAT activity [1].

Since ORP4L did not co-localize with vimentin, a domain in ORP4L, but not ORP4S, may sequester ORP4L by inhibiting vimentin binding or by promoting stronger interaction with another compartment [1]. The PH domain is the most likely candidate for this role, either by interacting inter- or intramolecularly to block the vimentin-binding

domain or by enhancing localization of ORP4L to a specific compartment through its presumed interaction with phosphorylated PIs.

1.6 ORP5-11 (Subfamilies III, IV, V, VI)

While ORPs 5-11 have been identified and complete cDNA and genomic sequences are available in humans and mouse, the functions of these proteins have not been characterized. These ORPs are predicted to contain PH domains, although splice variants that lack the PH domain have been reported for ORP6, ORP7 and ORP9 [2,4]. ORP5 and ORP8 also have putative transmembrane domains (Fig. 1). mRNAs for ORPs 5-11 are expressed in a number of tissues but most highly in brain, kidney and liver [6]. Loading cells with acetylated-LDL increased mRNA expression of ORP6 by 2-fold, but did not affect expression of other ORPs [6]. However a detailed analysis of the role of ORP6 in lipid regulation has not been undertaken.

1.7 OSBP-related proteins in *Saccharomyces cerevisiae*

Seven OSBP homologues (designated OSBP homology (*OSH*) *1-7)* have been identified in *S. cerevisiae* [8]. Like mammalian ORPs, the sequence similarity in the yeast *OSH* genes is confined to the OSBP homology and PH domains. *OSH1*, *OSH2* and *OSH3* encode PH domain containing proteins with the greatest similarity in the OHD to the human ORPs of Subfamilies I, II and III (Table 1). The other four *OSH* genes encode truncated proteins lacking PH domains that have the best similarity to subfamilies V and VI, which are themselves closely related. The *OSH* genes have the least similarity to ORP5 or ORP8 (subfamily IV). Similar to human ORP1L, Osh1p and Osh2p also have

Table 1. Protein sequence similarity and identity between yeast and human OSBP homology domains (OHDs). Human ORP OHDs were defined according to Jawaorski *et al* and Moreira *et al* [4,15]. OHDs of Osh proteins were defined by alignment with the OSBP OHD. Sequences were aligned using MacVector (version 6.5.3) and a Blosum 30 algorithm with an open gap penalty of 10 and an extend gap penalty of 0.1. The upper number in each box represents the total percent similarity (identical plus similar), while the two bracketed numbers represent the percentage of identical and similar residues, respectively. The best identities for each Osh protein are shown in bold and are used to assign the Osh proteins to the ORP subfamilies (Fig. 1).

	OSH1	OSH2	OSH3	OSH4	OSH5	OSH6	OSH7
OSBP (I)	**51% (37/14)**	**51% (36/15)**	41% (26/15)	21% (13/8)	22% (12/10)	28% (15/13)	30% (16/14)
ORP1 (II)	43% (29/14)	42% (28/14)	40% (28/12)	28% (17/11)	31% (18/13)	32% (18/14)	34% (20/14)
ORP2 (II)	42% (28/14)	42% (29/13)	41% (28/13)	28% (18/10)	30% (17/13)	32% (18/14)	33% (18/15)
ORP3 (III)	45% (29/16)	49% (33/16)	**45% (30/15)**	25% (16/9)	25% (14/11)	36% (20/16)	35% (20/15)
ORP4 (I)	**48% (33/15)**	**50% (33/17)**	42% (26/16)	22% (12/10)	24% (12/12)	30% (16/14)	32% (17/15)
ORP5 (IV)	22% (12/10)	23% (13/10)	24% (14/10)	27% (16/11)	26% (15/11)	29% (19/10)	30% (20/10)
ORP6 (III)	47% (29/18)	48% (32/16)	43% (29/14)	25% (15/10)	27% (14/13)	34% (18/16)	35% (18/17)
ORP7 (III)	45% (29/16)	47% (30/17)	**44% (29/15)**	23% (13/10)	24% (13/11)	34% (18/16)	35% (17/18)
ORP8 (IV)	19% (13/6)	20% (14/6)	23% (14/9)	24% (15/9)	23% (13/10)	28% (17/11)	28% (17/11)
ORP9 (V)	31% (19/12)	30% (18/12)	31% (16/15)	**36% (22/14)**	**36% (20/16)**	**45% (30/15)**	**45% (32/13)**
ORP10 (VI)	30% (17/13)	31% (19/12)	30% (16/14)	**33% (19/14)**	**34% (19/15)**	**42% (28/14)**	**43% (29/14)**
ORP11 (VI)	31% (18/13)	31% (18/13)	29% (15/14)	31% (18/13)	33% (18/15)	40% (26/14)	42% (29/13)
Sub-family	I	I	III	V/VI	V/VI	V/VI	V/VI

Table 1

ankyrin repeats [8].

An extensive study in *S. cerevisiae* examined the effects of deleting each of the *OSH* genes independently and in combination with each other [8]. While none of the genes were found to have an essential role, and any one of them could compensate for the loss of the other six, deletion of all seven was lethal, indicating that they constitute an essential gene family [8]. Using an *OSH*-null yeast strain that expressed Osh2p under the control of a methionine-regulated promoter, Beh and co-workers showed that the complete absence of *OSH* expression resulted in a 3- to 13-fold increase in the level of ergosterol and other yeast sterols [8]. Gene expression profiles of strains with individual deletions in each *OSH* gene showed distinct changes in the expression levels of 96 genes, indicating that even though Osh proteins may share a common overall function, they are not involved in common pathways. The majority of the genes whose expression was altered by deletion of the *OSH* genes were involved in membrane permeability and lipid homeostasis.

Both Osh1p and Osh2p showed the highest similarity to OSBP and ORP4, although they were also quite similar to ORPs 1, 2, 3, 6 and 7 (Table 1). This suggests a similar role to OSBP, ORP1L and ORP4L in cholesterol/ergosterol and lipid homeostasis (Sections 1.1.3, 1.2 and 1.5). An Osh1p-GFP fusion protein was localized to two distinct structures in the cell; the Golgi apparatus [25] and a sub-compartment of the ER termed the nucleus-vacuole (NV) junction [24,26]. The NV junction is a yeast-specific structure that is implicated in regulation of lipid metabolism [24,131], although its precise function is poorly defined. The ankyrin repeats regulated localization to the NV junction, while Golgi apparatus localization was regulated by the PH domain. Although Osh1p and

Osh2p contain N-terminal PH domains and ankyrin repeats, they have different localization patterns, supporting the concept that family members have similar roles in separate compartments of the cell. An Osh2p-GFP fusion protein was localized mainly to the PM and the site of yeast bud formation [24], indicating that it could be involved in ergosterol trafficking to the PM. In support of this concept, *OSH1* and *OSH2* deletion strains had normal ergosterol levels but the *osh1Δ* strain was sensitive to lovastatin, an inhibitor of HMG-CoA reductase, while the *osh2Δ* strain was sensitive to nystatin, which binds cholesterol in the PM [8]. Finally, both Osh1p and Osh2p were identified as part of a yeast protein complex that contained Fks1p, Opi1p, Stt4p and Scs2p, all of which are implicated in lipid or cell wall synthesis [132]. Scs2p is the yeast homologue of VAP-A, identified in this study as a protein partner for OSBP by yeast two-hybrid analysis. The yeast complex also contained Num1p, a protein involved in cytoskeletal interaction with the nucleus during nuclear migration into the bud, and Rpn10p, a component of the 26S proteasome. While all of these proteins may not directly interact, these data further implicate Osh1p and Osh2p in lipid homeostasis and cell cycle control [132].

Although Osh3p also has a PH domain, a GFP-fusion of Osh3p was found primarily in the cytosol [24]. Osh3p also has a Golgi dynamics (GOLD) domain, which is thought to mediate protein-protein interactions in the Golgi apparatus [2]. It is not known whether Osh3p PH and GOLD domains are required for the interaction of Osh3p with its protein partners. Osh3p was shown to interact with Rok1p (by yeast two-hybrid analysis), a DEAD-box RNA helicase that suppressed a nuclear fusion defect caused by the loss of *KEM1*, a cytoplasmic exoribonuclease [133-135]. Purified Kem1p promoted the polymerization of microtubules and is implicated in nuclear fusion during mating,

chromosome transmission and nuclear migration [133,136]. High-level expression of Osh3p enhanced the *kem1* defect, thus implicating Osh3p as a negative regulator of these processes [133]. Expression of Osh3p was also induced by the α-mating factor in a mitogen activated protein (MAP) kinase/*STE12*-dependent manner [133]. However, Osh3p was not essential for yeast mating, implying that other members of the *OSH* family may compensate for its loss [133]. Interestingly, an *OSH6* like gene was found in the mating-type (MAT) locus of *Candida albicans* and could represent another Osh protein involved in this process [12]. Yeast mating requires polarized membrane growth, redirection of vesicle transport and remodeling of the cell wall [137]. Osh3p could play a role in these processes by regulating membrane content or lipid trafficking.

The filamentous growth pathway and the α-factor-induced mating process are regulated by a number of the same signalling molecules, including the transcription factor Ste12p. High-level expression of Osh3p induced filamentous growth, suggesting it could function parallel to or downstream of *STE12* [133]. Finally, Osh3p is upregulated by induction of the unfolded protein response (UPR) and could be involved in controlling the membrane growth required to accommodate excess proteins in the ER during stress [2]. Collectively, these data show that Osh3p is involved in diverse cellular functions but mechanisms are still unclear.

Osh4/Kes1p was originally identified as an OSBP homologue implicated in ergosterol synthesis [9]. This was supported by data from the *OSH* gene deletion study [8], which showed that yeast lacking *OSH4/KES1* were less sensitive to nystatin, even though ergosterol content was normal. Although Osh4/Kes1p consists almost entirely of the OHD and displays limited sequence identity to OSBP (Table 1), its localization to the

Golgi apparatus was dependent on PI-4-P generation by Pik1p, but not by Stt1p activity and PI-4-P production at the PM [138]. However, unlike OSBP, regions within the OHD, including the consensus sequence HHPP and a putative PH domain found in the C-terminal portion of the OHD were involved in localization to the Golgi apparatus. The putative Osh4/Kes1p PH domain bound several phosphorylated PI species *in vitro* and showed the greatest affinity for PI-4,5-P_2 [138]. This is similar to the study by Xu *et al*, which demonstrated that ORP1S and ORP2, both truncated members of the ORP family that lack PH domains, bound phosphatidic acid and PI-3-P [118].

Osh4/Kes1p was characterized as a *sec14*^{ts} bypass mutant and a negative regulator of vesicle biogenesis from the Golgi apparatus (Sections 1.2 and 1.3) [120]. It is the only member of the *OSH* family member that supports *sec14*^{ts} bypass [8]. Other genes able to bypass the *sec14*^{ts} mutation when deleted included *SAC1*, which resulted in increased conversion of PI to phosphoinositol containing sphingolipids and increased DAG content [139], and the enzymes of the CDP-choline biosynthetic pathway, which resulted in decreased PC synthesis and increased DAG levels [140]. These data support a model wherein Sec14p functions to maintain a pool of DAG in the Golgi apparatus that is required to maintain vesicle biogenesis. Presumably, loss of Sec14p results in depletion of this pool, thereby altering the lipid composition of the Golgi apparatus and preventing vesicle biogenesis. Compensatory changes to increase DAG levels in bypass mutants such as *osh4/kes1Δ*, would allow vesicle biogenesis to proceed. Thus vesicle formation from the Golgi apparatus requires a balance between the inhibitory effects of Osh4/Kes1p and stimulatory effects of Sec14p [120].

OSH5/HES1 and *OSH6* were the only genes that when individually deleted caused increased ergosterol levels. In addition, deletion of either gene resulted in similar gene expression profiles [8]. As well, *OSH5/HES1* was shown to be involved in exogenous cholesterol accumulation in a *upc-2* yeast strain under aerobic conditions [141]. How Osh5p and Osh6P are in involved in ergosterol regulation in not known.

1.8 ORP expression in other species

The ORP family is structurally conserved across a variety of species. As with the human and mouse [11] ORPs, the main similarity is in the OHD, but the absolutely conserved mammalian sequence of EQVSHHPP (Fig. 1) is shortened to HHPP in non-mammalian species.

D. melanogaster has four ORP genes. One of them, designated OSBP-Dm, was originally identified in a screen for *D. melanogaster* cDNAs that could overcome cell cycle arrest induced by overexpression of Wee1p in *S. pombe* [14]. Wee1p inhibits the cell cycle control protein $p34^{cdc2}$, implicating OSBP-Dm in regulation of cell cycle progression [14]. OSBP-Dm is ~50% identical to both OSBP and ORP4 and there are several regions that are absolutely conserved between all three proteins, including the conserved OHD sequence EQVSHHPP and the region of OSBP required for dimerization. Insects cannot synthesize sterols, but acquire them from their diet. Thus OSBP-Dm is unlikely to regulate sterol synthesis, but could be involved in sterol transport. The three other ORP genes in *D. melanogaster* have PH domains [4,6].

Five ORPs have been identified in *C. elegans* [4,6,10,142], one of which was shown to interact with bone morphogenetic protein (BMP) receptor-associated molecule

(BRAM) as part of the transforming growth factor (TGF)-β signalling pathway regulating body length [10]. As well, twelve OSBP homologues have been identified in *A. thaliana*, a widely used model for plant genetics and development [4,18]. The genes from these two organisms are predicted to encode proteins both with and without PH domains. Finally, five ORP genes, all of which encode shorter non-PH domain containing proteins, have been identified in *D. discoidium* [13]. One of these genes, OSBPa, was implicated in the progression from a migrating body to culmination.

2 Project Aim

As discussed, the members of the ORP family are involved in diverse cellular functions, the best characterized of which is the regulation of cholesterol and lipid metabolism and transport. Although a role for OSBP in the regulation of cholesterol and SM synthesis had been determined, it was unclear whether these effects were direct or indirect. The aim of this project was to investigate the function of OSBP and the ORP family by identifying its protein partner(s) by yeast two-hybrid analysis, glutathione-*S*-transferase pull-down assays and co-immunoprecipitation. Functional analysis of relevant interactions was then undertaken in inducibly overexpressing CHO cell lines.

The results of this study support past work demonstrating a role for OSBP and oxysterols in the regulation of ceramide trafficking. The work presented here is the first to define OSBP and VAP-A as regulators of protein and ceramide export from the ER. Moreover, we have defined an interaction network of proteins centered around VAP-A that includes several members of the ORP family, suggesting that VAP-A is a central regulator of OSBP and ORP function. Investigation of the roles of these proteins and the significance of their interactions with VAP-A is the first step in determining the precise mechanism of action of this protein family.

3 Materials and Methods

3.1 Materials

Tissue culture media, G418, hygromycin B, sodium dodecyl sulphate (SDS), deoxynucleotide triphosphate (dNTP)s, V5 monoclonal antibody, and Vent, Platinum Taq and Taq polymerases were obtained from Invitrogen Life Sciences. Tet-on system plasmids, CHO-Tet-on cells and TALON resin were obtained from Clontech. Reagents for yeast and bacteria media, polyethylene glycol (PEG) 3400 and ethylene-diaminetetra-acetic acid (EDTA) were from EM Science. Tris-HCl and protease inhibitor cocktail tablets were from Roche Diagnostics. Protein A-Sepharose, glutathione-Sepharose and enhanced chemiluminescence kits were from Amersham Pharmacia Biosciences. Gene Editor site-directed mutagenesis kits and herring sperm DNA were purchased from Promega. Morph site-directed mutagenesis kits were from 5'-3' Inc. All restriction enzymes were from New England Biolabs or Invitrogen. Gene Clean II kits used to purify DNA for ligations were from QBio Gene. T7 sequencing kits were from USB Corp. Sequencing, PCR and mutagenic primers were purchased from Cortec DNA Service Laboratories Inc. Potassium acetate was from Fisher Scientific. Ethylene-glycol-(*bis*)(β-aminoethyl ether)-N,N,N',N'-tetra-acetic acid (EGTA) was from BDH. Reagents and equipment for SDS-PAGE and secondary goat anti-mouse (GAM) and anti-rabbit antibodies (GAR) coupled to horseradish peroxidase were from Bio-Rad. Triton X-100 (TX-100) was from Pierce. *N*-(4,4-difluoro-5-(2-thienyl)-4-boro-3α,4α-diaza-*s*-indacene-3-pentanoyl)sphingosine (C_5-DMB-ceramide) and Alexa-fluor conjugated secondary antibodies were from Molecular Probes. Monoclonal antibodies to protein disulphide isomerase (PDI) and the KDEL motif (recognizes glucose-regulated protein (78

kDa)/immunoglobulin binding protein (GRP74/BiP) and GRP94) and a polyclonal calnexin antibody were from Stressgen. A caveolin polyclonal antibody was from Transduction Laboratories. Bovine serum albumin (BSA), fatty acid-free BSA, nutrient supplements, amino acids, fluorescein isothiocyanate (FITC)-lentil lectin, propidium iodide and a monoclonal tubulin antibody were from Sigma Aldrich. A p58 polyclonal antibody was provided by Dr. Jaakko Saraste (University of Bergen, Norway). Giantin polyclonal antibody was provided by Dr. Douglas Hogue (Dalhousie University). A Sec31 polyclonal antibody was supplied by Dr. Fred Gorlick (Yale University, USA). An ARF GTPase activating protein (ARF-GAP) antibody was supplied by Dr. Rick Singer (Dalhousie University). Polyclonal antibodies against lamin A/C and poly(ADP ribose) polymerase (PARP) were purchased from Santa Cruz Biotechnology Inc. Monoclonal antibody 414 directed against a common epitope found in Nup62 and related components of the nuclear pore complex was from Berkeley Antibody Co. A human B-cell library in pACT was supplied by Dr. Chris Barnes (Dalhousie University). pVSVG-GFP was supplied by Dr. Jennifer Lippincott-Schwartz (NIH, MA, USA). A plasmid encoding ORP1L was supplied by Dr. Vessa Olkkonen (National Public Health Institute, Helsinki, Finland). A plasmid encoding ORP3(1d) was supplied by Dr. Mark Kirkland (Geelong Hospital, Geelong, Australia). All other chemicals were of reagent grade.

3.2 Methods

3.2.1 Polymerase chain reaction (PCR)

PCR was performed using a Perkin Elmer 2400 GeneAmp PCR system. Reactions contained Vent polymerase (1 U), 1 μM of each primer, 0.4 mM dNTPs and 2

mM Mg^{2+} in a total volume of 50 µl. Individual primers used in PCR reactions are listed in Appendix 1. Samples were denatured at 98°C for 5 minutes (min) before performing 30 amplification cycles consisting of denaturation at 98°C for 30 seconds (s), annealing at a temperature determined by the T_ms of the primers for 45 s and extension at 76°C for 2 min. A final incubation at 76°C for 5 min was done to achieve full extension of PCR products. In order to add 3' adenosine nucleotides to Vent PCR products, allowing them to be cloned into pCR2.1-TOPO, 0.4 mM dNTPs and Taq buffer were added to 25 µl of PCR reaction (final volume of 50 µl) and incubated for 15 min at 72°C with Taq polymerase (1 U).

PCR amplification with Platinum Taq polymerase (1 U) used a similar protocol except that primers were used at 2 µM each and extensions were performed at 68°C. Since 3' adenosines are added by Platinum Taq polymerase, the additional incubation with Taq polymerase was not necessary.

3.2.2 Plasmid preparation

3.2.2.1 Construction of OSBP plasmids

Yeast two-hybrid vectors containing full-length rabbit OSBP cDNAs were prepared as follows. pAS1-CYH2-OSBP (pAS1-OSBP) was prepared by PCR amplification of the rabbit OSBP cDNA from pCMV2-OSBP using Vent polymerase and primers ON1 and ON3 to create 5' and 3' *Nde1* and *BamH1* sites, respectively. pACT2-OSBP was prepared in the same manner, except that primers ON2 and ON3 were used to create *Nco1* and *BamH1* sites. PCR products were subcloned into pCR2.1-TOPO (Invitrogen Life Sciences) before cloning into *Nde1*/*BamH1*-digested pAS1 or

NcoI/BamH1-digested pACT2. A *NotI/BstEII* fragment from pCMV2-OSBP was later subcloned into pAS1-OSBP to reduce the chance of PCR error.

pCMV2-OSBP S381A was made by Dr. A. Mohammadi (Ridgway lab) using the Morph site-directed mutagenesis kit and pCMV2-OSBP Δ432-435 was made using primer ON29 and the Gene Editor site-directed mutagenesis kit. pAS1-OSBP S381A and pAS1-OSBP Δ432-435 were made by subcloning the *NotI/BstEII* fragments from pCMV2-OSBP S381A or pCMV2-OSBP Δ432-435 into pAS1-OSBP digested with the same enzymes. Other mutations in pAS1-OSBP were made using primers ON20-28 and the Morph site-directed mutagenesis kit or the Gene Editor site-directed mutagenesis kit and confirmed by sequencing. A pAS1 construct containing only the ligand binding domain of OSBP (pAS1-OSBP 351-809) was prepared by PCR amplification of this region of the cDNA from pCMV2-OSBP using Vent polymerase and primers ON4 and ON3 to create 5' and 3' *NdeI* and *BamH1* sites, respectively. The PCR product was subcloned into pCR2.1-TOPO, digested with *NdeI/BamH1* and ligated into pAS1 digested with the same enzymes.

The construction of pTRE-OSBP, pTRE-OSBP W174A, pTRE-OSBP Δ132-182, pCMV2-OSBP ΔPH and pCMV2-OSBP Δ92-125 has been described previously [21,143]. pCMV2-OSBP Δ132-182 and pCMV2-OSBP W174A were made in the same fashion. pCMV2-OSBP truncation mutants were prepared by Dr. A Mohammadi using site directed mutagenesis to insert stop codons at amino acid residues 218, 268 and 443.

pGEX3X-OSBP 80-187 was prepared by Dr. A. Mohammadi by PCR amplification of this region of the cDNA from pCMV2-OSBP using primers to create 5' and 3' *EcoR1* and *BamH1* sites, respectively. The PCR product was subcloned first into

pCR2.1-TOPO and then into pGEX3X digested with *EcoR1* and *BamH1*. The W174A mutation was introduced into pGEX3X-OSBP 80-187 using ON29 and the Gene Editor site-directed mutagenesis kit.

3.2.2.2 Construction of VAP-A plasmids

pACT2-VAP-A was prepared by subcloning the *Nco1* fragment containing the entire open reading frame of VAP-A from pACT-VAP-A (cDNA obtained from the yeast two-hybrid library screen) into *Nco1*-digested pACT2 and sequencing to confirm the orientation. pAS1-VAP-A was prepared by subcloning the *Nde1/BamH1* fragment from pACT2-VAP-A into pAS1 digested with the same enzymes. pACT2-VAP-A Δ43-49, pACT2-VAP-A 1-160 and pACT2-VAP-A ΔTM (introduces a stop codon at residue 221 to delete the transmembrane domain) were prepared by site directed mutagenesis using the Morph kit and primers ON30, ON31 and ON32. Mutations were confirmed by sequencing.

pGEX3X-VAP-A was prepared by PCR amplification of the cDNA from pACT-VAP-A using Vent polymerase and primers ON5 and ON6 to create 5' and 3' *EcoR1* and *BamH1* sites, respectively. pTRE-VAP-A and pTRE-VAP-A ΔTM were prepared in a similar manner as follows. Primer ON7 was used to create 5' *EcoR1* sites in conjunction with primer ON8 to create a 3' *BamH1* site at residue 220 (removes the transmembrane domain) or primer ON9 to create a 3' *BamH1* site at the end of the cDNA. All PCR products were first subcloned into pCR2.1-TOPO before cloning into the appropriate vectors digested with *EcoR1* and *BamH1* and verified by sequencing.

3.2.2.3 Construction of ORP4 plasmids

pAS1-ORP4S and pACT2-ORP4S were prepared by ligating the *Nco1-Xho1* fragment from pcDNA3-ORP4S [1] into pAS1 digested with *Nco1* and *Sal1* or pACT2 digested with *Nco1* and *Xho1*. pAS1-ORP4L was created by a two step ligation process. First, the cDNA was PCR amplified from pcDNA3-ORP4L [1] using Vent polymerase and primers ON11 and ON12 to create 5' and 3' *Nde1* and *Sal1* sites, respectively, and subcloned into pCR2.1-TOPO. An ORP4L fragment from the 5' *Nde1* site to a unique internal *Nde1* site was subcloned into *Nde1*-digested pAS1 and the orientation confirmed by restriction mapping. This vector was then digested with *Nco1* and *Sal1* and a second ORP4L fragment produced by digesting pcDNA3-ORP4L with *Nco1* and *Xho1* was ligated. pACT2-ORP4L was constructed using a similar protocol, except that an *Nco1* site was created at the 5' end of the cDNA by PCR using ON13 in conjunction with primer ON12. The PCR product was subcloned into pCR2.1-TOPO and the *Nco1* fragment from the 5' end to a unique internal *Nco1* site was cloned into pACT2-ORP4S digested with *Nco1*. Orientation was determined by restriction mapping and the cDNA insert was sequenced.

3.2.2.4 Construction of ORP9 plasmids

The ORP9S cDNA was amplified from pME18S-FL-ORP9S (Helix Research Institute, Chiba Japan) by Cheng Wang (Ridgway lab) using Vent polymerase and primers to create 5' and 3' *HindIII* and *Xho1* sites, respectively. The PCR product was cloned into *HindIII/Xho1*-digested pcDNA3.1V5/His, generating pcDNA3-ORP9S with in-frame epitope tags at the C-terminus.

The 5' end of ORP9L was amplified from a liver cDNA library using nested PCR and a reverse primer downstream of an internal *HindIII* site in conjunction with a forward primer containing a *HindIII* site. PCR products were subcloned into pCR2.1-TOPO, the inserts sequenced and a cDNA containing the entire 5' end was identified by comparison to the genomic sequence and cDNA databases. This cDNA was ligated into *HindIII*-digested pcDNA3-ORP9S. Orientation was determined by restriction mapping and the cDNA insert was sequenced.

pTRE2-ORP9S and pTRE2-ORP9L constructs were also prepared by Cheng Wang. Briefly, pTRE2-ORP9S was prepared by ligating the *HindIII/Pme1* fragment of pcDNA3-ORP9S into pTRE2 digested with *HindIII* and *EcoRV*. pTRE-ORP9L was prepared by simultaneously ligating the *HindIII/HindIII* and *HindIII/Pme1* fragments from pcDNA3-ORP9L into pTRE2 digested with *HindIII* and *EcoRV*.

pAS1-ORP9S was prepared by PCR amplification of the cDNA from pcDNA3-ORP9S using Platinum Taq polymerase and primers ON14 and ON15 to create 5' and 3' *Nco1* and *Xma1* sites, respectively. The PCR product was subcloned into pCR2.1-TOPO and the *Nco1/BamH1* fragment (the *BamH1* site in the pCR2.1-TOPO multi-cloning site was used) was ligated into *Nco1/BamH1*-digested pAS1. pACT2-ORP9S was constructed by subcloning the *Nco1-Sal1* fragment of pAS1-ORP9S into pACT2 digested with *Nco1* and *Xho1*. pAS1-ORP9L and pACT2-ORP9L were constructed using site directed mutagenesis (primer ON33) to introduce an *Nco1* site at the 5' end of pCDNA3-ORP9L. The resulting vector was then digested with *Nco1* and *Xho1* and ligated into *Nco1/Sal1*-digested pAS1 or *Nco1/Xho1*-digested pACT2.

3.2.2.5 Construction of Int6/eIF3e plasmids

pAS1-Int6/eIF3e was prepared by PCR amplification of the cDNA from pcDNA3.1/GS-Int6/eIF3e (Invitrogen) using Vent polymerase and primers ON16 and ON17 to create 5' *NcoI* and *NdeI* sites for insertion into pACT2 and pAS1, respectively, in conjunction with ON18 to create 3' *BamHI* sites. PCR products were subcloned into pCR2.1-TOPO and the *NdeI/BamHI* or *NcoI/BamHI* fragments were ligated into *NdeI/BamHI*-digested pAS1 or *NcoI/BamHI*-digested pACT2, respectively. Due to an internal *NcoI* site in Int6/eIF3e, the ligation into pACT2 was a two-step process: the *NcoI/BamHI* fragment was ligated in first, followed by the *NcoI/NcoI* fragment. The orientation of the second fragment was confirmed by restriction analysis. The PCI domain of Int6/eIF3e (nucleotides 915-1338, amino acids 305-446) was amplified from this region of the cDNA from pcDNA3-GS-Int6/eIF3e by PCR using Vent polymerase and primers ON19 and ON18 to create 5' and 3' *NcoI* and *BamHI* sites, respectively. The PCR product was first subcloned into pCR2.1-TOPO and then into pACT2 digested with *NcoI* and *BamHI*.

3.2.3 Yeast two-hybrid analysis

3.2.3.1 Routine yeast transformation

Overnight cultures of yeast strain PJ69 (ATCC #201450) were grown in YPD media. The culture was back-inoculated to an optical density $(OD)_{600}$ of 0.25 in YPD and allowed to grow for 4 hours (h) with shaking at 30°C. The yeast were harvested by centrifugation at 1,000*g*, washed once with sterile distilled water and resuspended in 50 µl TE/LiAc (10 mM Tris-HCl (pH 7.5), 1 mM EDTA, 100 mM lithium acetate). The

yeast was then mixed with 50 μg denatured herring sperm DNA (carrier), 1 μg each of the plasmids of interest and 300 μl of 40% polyethylene glycol (PEG) 3500 in TE/LiAc. The samples were incubated at 30°C for 30 min, heat shocked at 42°C for 15 min, plated on appropriate media and incubated at 30°C for three to five days.

Plates that supported growth only if the yeast expressed two interacting proteins (interaction-selective plates) contained yeast nitrogen base (Difco) without amino acids (13.4 g/l), glucose (20 g/l), methionine, lysine and uracil. Plates that selected for the transformed plasmids (transformation-control plates), but not for interaction, also contained adenine and histidine. The pAS1 plasmid conferred growth in the absence of tryptophan and the pACT or pACT2 plasmids conferred growth in the absence of leucine. All supplements were used at 0.002% (w/v) except lysine and methionine, which were used at 0.003% (w/v).

3.2.3.2 High efficiency transformation for yeast two-hybrid library screens

Prior to initiating the yeast two-hybrid screens, yeast strain PJ69 was transformed with pAS1 containing the cDNA of interest and expression was confirmed by Western blotting using monoclonal antibody 11H9 to detect OSBP, pan ORP antibody 170 to detect OSBP 351-809 and the VAP polyclonal antibody to detect VAP-A. Non-specific interactions or promoter activation by the pAS1 constructs were determined by co-transforming with pSE1111, while non-specific interactions or promoter activation in the presence of the pACT2 constructs were determined by co-transforming with pSE1112. pSE1111 and pSE1112 encode pACT-Sucrose Non Fermenting (SNF)4 and

pAS1-SNF1, respectively and are commonly used in conjunction as positive controls or as negative controls with other cDNAs of interest.

A human B-cell yeast two-hybrid library in pACT was screened in the following manner. Yeast harbouring pAS1-OSBP, pAS1-OSBP 351-809, pAS1-VAP-A, pAS1-ORP9S or pAS1-ORP9L were grown at 30°C to an OD_{600} of less than 0.8 in synthetic media lacking tryptophan. The yeast culture was then back-inoculated to an OD_{600} of 0.25 in YPD and allowed to grow until the OD_{600} was 0.6 (~4 h). The yeast were collected by centrifugation at 20°C for 10 min at 1,000*g*, washed once with sterile water, resuspended in 8 ml TE/LiAc and mixed with 20 mg denatured herring sperm DNA and 200 μg of the human B-cell library. PEG 3500 (60 ml of 40% (w/v) in TE/LiAc) was added and the yeast were incubated at 30°C for 30 min. Dimethyl sulfoxide (DMSO) (7 ml of 10% (v/v) solution) was added dropwise with constant swirling, yeast were incubated at 42°C for 15 min and then on ice for 5 min. The transformation mixture was mixed by swirling the flask every 5 min during incubations. The yeast were then sedimented by centrifugation at 1,000*g* for 5 min at 20°C, washed once with sterile water, resuspended in 5 ml TE and aliquots of 200 μl were spread on interaction-selective plates. Diluted aliquots were also grown on transformation-control plates to determine transformation efficiency. The interaction-selective plates were incubated at 30°C for up to one week.

3.2.3.3 Identification and characterization of yeast two-hybrid positive clones

Overnight cultures of the colonies from interaction-selective plates were grown in synthetic media lacking leucine as described in Section 3.2.3.1. Plasmids were isolated

from the overnight cultures using a yeast plasmid isolation protocol (Section 3.2.3.4) or the Y-DER Yeast DNA Extraction kit (Pierce), transformed into JF1754 by electroporation (a DH5α strain deficient in leucine biosynthesis) and grown on M9 leucine-deficient agar plates with 100 μg/ml ampicillin (plates contained 4 g/l glucose, 0.0033% (w/v) histidine, 0.0033% (w/v) methionine, 0.0025% (w/v) thiamine and M9 salts (55 mM NaH_2PO_4, 22 mM KH_2PO_4, 8.5 mM NaCl and 23 mM NH_4Cl)). Colonies from these plates were grown in Luria Bertani (LB) media containing ampicillin (100 μg/ml) and plasmids were isolated using alkaline lysis and ethanol precipitation [144]. Plasmids isolated from JF1754 colonies were co-transformed into PJ69 with pAS1-OSBP, pAS1-OSBP 351-809, pAS1-VAP-A, pAS1-ORP9S or pAS1-ORP9L to confirm interactions, or with pSE1112 to eliminate false positives. The identity of cDNA clones was determined by sequencing and basic local alignment search tool (BLAST) searches against EST and genomic databases.

3.2.3.4 Plasmid isolation from yeast

Yeast cultures (5 ml) were grown overnight at 30°C in synthetic media lacking leucine. The cultures were harvested by centrifugation (1,000*g* for 5 min at 20°C) and resuspended in 500 μl of 1 M sorbitol, 0.1 M EDTA (pH 7.5). Zymolyase 100,000 (50 μg) was added and the sample incubated at 37°C for 1 h to dissolve the cell wall. Yeast were collected by centrifugation, resuspended in 500 μl of 50 mM Tris-HCl (pH 7.4), 20 mM EDTA and mixed with 50 μl of 10% SDS. The samples were incubated at 65°C for 30 min to lyse the cells and 200 μl of 5 M potassium acetate was added to precipitate proteins and SDS. Samples were incubated on ice for 1 h, cellular debris was removed by

centrifugation at 20°C for 5 min and the plasmids and DNA were precipitated from the supernatant with an equal volume of isopropanol. DNA was isolated by brief (10 second) centrifugation and washed once with 70% ethanol. The resulting DNA was resuspended in 10 µl sterile water.

3.2.4 Mammalian cell culture

3.2.4.1 Routine maintenance of mammalian cells

Untransfected CHO-Tet-on cells were maintained in Dulbecco's modified Eagle's medium (DMEM) containing 5% antibiotic-free Tet-system fetal calf serum (FCS) and 33 µg/ml proline (medium A) plus 300 µg/ml G418. CHO-K1 cells were maintained in DMEM containing 33 µg/ml proline and 5% FCS (medium C). COS cells and human embryonic kidney (HEK) cells were maintained in DMEM containing 10% FCS (medium E).

3.2.4.2 Transient transfection of mammalian cells

CHO-K1 cells were subcultured in medium C for 24 h prior to transient transfection of plasmids with Lipofectamine 2000. DMEM containing 33 µg/ml proline and Lipofectamine 2000 were combined in a 25:1 ratio and then mixed with an equal volume of DMEM (33 µg/ml proline) and 0.5 µg of plasmid DNA for every 1 µl of Lipofectamine 2000. This mixture was incubated at 20°C for 5 minutes, diluted 5-fold with DMEM (33 µg/ml proline). Cells were washed once with DMEM and the Lipofectamine 2000/DNA mixture was added to the cells and allowed to incubate for 5 h before adding an equal volume of medium C containing an additional 5% FCS. A

complete media change was done 24 h later and the cells were harvested 48 h after transfection.

Transient expression of ORP9S in CHO cells required a 10:1 ratio of DMEM (33 μg/ml proline) to Lipofectamine 2000 and 0.3 μg of plasmid DNA for every 1 μl of Lipofectamine 2000. As this concentration of Lipofectamine 2000 and DNA was very toxic to the cells, it was important that the cells be nearly confluent at the time of transfection.

COS cells were subcultured in medium E for 24 h prior to transient transfection with 2.2 μg plasmid DNA per 60 mm dish using the DEAE/dextran method [145] and harvested after 48 h. Cells were transfected in medium E.

3.2.4.3 Generation and maintenance of inducibly and stably expressing cell lines

CHO-Tet-on cells were subcultured in medium A for transfections. pTRE-VAP-A, pTRE-VAP-A ΔTM, pTRE-ORP9S or pTRE-ORP9L (10 μg plasmid per 100 mm dish, plus 1 μg/ml pTK-hyg vector to confer hygromycin B resistance) were transfected into CHO-tet-on using the calcium phosphate transfection method [33]. Cells were selected in medium A containing 600 μg/ml G418 and 200 μg/ml hygromycin B (medium B) for approximately two weeks to allow colonies to form. The colonies were isolated (see Section 3.2.4.4), cultured in medium B and screened by Western blotting after 48 h induction with 2 μg/ml doxycycline. V5 monoclonal antibody was used to detect ORP9S and ORP9L and a VAP polyclonal antibody was used to detect VAP-A and VAP-A ΔTM. Highly expressing clones were further purified by limiting dilution subcloning in medium B for 10-20 days. Overexpression levels in clonal lines were

characterized both by Western blotting and immunofluorescence. Cell lines were maintained in medium B, but for experiments were subcultured in medium A for 24 h before inducing with doxycycline.

CHO-K1-Tet-off cell lines expressing OSBP, OSBP ΔC-PH and OSBP W174A were maintained in medium B containing 1 μg/ml doxycycline [143]. Cells were washed twice with sterile phosphate-buffered saline (PBS) prior to subculturing in medium A (± doxycycline) for experiments. A second medium change (fresh medium A ± doxycycline) was done the following day in order to remove residual doxycycline and induce expression of OSBP and OSBP W174A. Unless otherwise stated, cells were induced for 72 h.

The CHO-OSBP cell line has been described elsewhere [21]. CHO-OSBP cells were maintained in medium C containing 300 μg/ml G418 (medium D) and subcultured in medium C for experiments.

3.2.4.4 Colony isolation for inducible cell lines

Once CHO-tet-on colonies were clearly visible after selection in G418 and hygromycin B, their locations were marked on the underside of the culture dish. The dish was then washed once with DMEM and 1 ml of 0.25% (w/v) trypsin was added. Approximately 20 μl of DMEM was then added to the dish directly on top of the cell colony. The colony was immediately removed by aspiration into a pipette tip and placed in 2 ml of medium B in a 35 mm dish. The plate was not moved during colony selection to prevent colony dispersion and the introduction of cells that were not part of the colony. Once cells had grown sufficiently (~75% confluent), they were split into three 60 mm

dishes; one for a stock culture and two for determination of relative overexpression by Western blotting following induction for 48 h with 2 μg/ml doxycycline.

3.2.5 Antibodies and immunoblotting

A VAP polyclonal antibody was generated in rabbits against a GST-VAP-A fusion protein. GST-VAP-A was prepared in the following manner. An overnight culture of DH5α harboring pGEX3X-VAP-A was grown to an OD_{600} of less than 0.8 and 5 ml was added to 1 litre of LB broth containing ampicillin (100 μg/ml). The culture was grown at 37°C with constant shaking to an OD_{600} of 0.4-0.5, at which time the culture was moved to 25°C and induced with isopropyl-1-thio-β-D-galactopyranoside (IPTG) for 3 h. GST-VAP-A was extracted by lysozyme and TX-100 treatment and purified by affinity chromatography on glutathione-Sepharose 4B [146]. Rabbits were immunized with 150 μg GST-VAP-A in 1 ml 50% Freunds complete adjuvant and were boosted after 4 and 7 weeks with 75 μg GST-VAP-A in 1 ml 50% Freunds incomplete adjuvant. The VAP polyclonal antibody detects both endogenous and overexpressed VAP-A as well as endogenous VAP-B.

An ORP9-specific polyclonal antibody was raised in rabbits against amino acids 90 to 288 of ORP9 fused to GST. GST-ORP9 was purified by Cheng Wang in the same manner as GST-VAP-A except that induction with IPTG was done at 37°C. Rabbits were immunized with 150 μg of GST-ORP9 and boosted after 4, 7 and 10 weeks with 75 μg GST-ORP9. The ORP9 polyclonal recognizes both transfected and endogenous ORP9 and does not cross-react with OSBP, ORP1, ORP2 or ORP4.

The ORP4 polyclonal antibody was raised in rabbits as described previously [1]. It recognizes both endogenous and overexpressed ORP4S and ORP4L, and does not cross react with OSBP, ORP1, ORP2, ORP3 or ORP9.

OSBP monoclonal antibody 11H9 (kindly supplied by Dr. J. Goldstein, University of Texas, Southwestern Medical Centre, Dallas, TX) detects only overexpressed OSBP (rabbit). Antibody 170 was raised in rabbits against the C-terminal 100 residues of ORP1 fused to GST. This antibody recognizes ORP1, ORP2, ORP4 and OSBP, but not ORP3 or ORP9. All other antibodies were purchased from suppliers or were gifts from other researchers (Section 3.1).

SDS-PAGE and immunoblotting was carried out using standard techniques. Briefly, protein samples were heated to 90°C for 3 min in reducing buffer (62.5 mM Tris-HCl, pH 6.8, 10% glycerol, 2% SDS, 5% β-mercaptoethanol) and separated by SDS-PAGE. Proteins were transferred to nitrocellulose membranes at 100V in Tris-buffered glycine containing 20% (v/v) methanol for 1 h at 4°C. Nitrocellulose filters were incubated with primary antibodies for 1 h at room temperature in Tris-HCl (pH 7.4), 150 mM NaCl, (Tris-buffered saline (TBS)), 0.1% Tween-20 and 5% (w/v) skim milk powder (Blotto), washed three times for 10 min each in Blotto and incubated for 1 h with a secondary antibody coupled to horseradish peroxidase (HRP). Filters were then washed three times for 10 min each in Blotto, followed by a 2 min wash in TBS prior to development by the enhanced chemiluminescence method.

3.2.6 Indirect immunofluorescence

Cells cultured on glass coverslips were fixed in 3% (v/v) formaldehyde for 15 min at 20°C, permeabilized with 0.05% (v/v) TX-100 for 10 min at –20°C and blocked with 1% (w/v) BSA in PBS immunofluorescence buffer (PBS-IF, 10 mM Na_2HPO_4 (pH 7.4), 225 mM NaCl, 2 mM $MgCl_2$) for 15 min at 20°C [33]. Alternatively, cells were permeabilized with 0.05% (w/v) saponin for 1 min on ice to remove cytosolic proteins prior to formaldehyde fixation and TX-100 permeabilization. In experiments investigating localization of lamin A/C or giantin, cells were fixed and permeabilized with methanol/acetone (1:1, v/v) for 15 min at -20°C. Coverslips that were to be immunostained for giantin were air dried and blocked with 1% (w/v) BSA in PBS-IF. Coverslips that were to be immunostained for lamin A/C were placed in 1% BSA (w/v) in PBS-IF immediately following methanol/acetone fixation. Primary antibodies were used in conjunction with cross-adsorbed secondary GAR or GAM antibodies conjugated to Alexa Fluor-488, -555, or –647, FITC or Texas red (TXR). Incubations with polyclonal antibodies were done first, followed by incubation with GAR secondary antibodies, monoclonal antibodies and GAM secondary antibodies. Primary and secondary antibody incubations were in 1% BSA (w/v) in PBS-IF (1 ml) for 1 h and coverslips were washed three times between antibody incubations with 1% (w/v) BSA in PBS-IF (2 ml) for 15 min. Lentil lectin was incubated with coverslips for 2 h in 1% (w/v) BSA in PBS-IF (1 ml) and washed as described above. Coverslips were mounted on glass slides using 2.5% (w/v) 1,4-diazadicyclo[2.2.2]octane in 50 mM Tris-HCl and 90% (v/v) glycerol (DABCO) and sealed with clear nail polish. Fluorescence images were obtained

using a Zeiss Axiovert 100M Laser Scanning Confocal Microscope 510 and imported into Adobe Photoshop for analysis.

3.2.7 Protein quantification

Protein concentration was determined by a μLowry assay [147]. Proteins from samples that contained TX-100, which interferes with the μLowry assay, were precipitated prior to assay. Briefly, samples were diluted to 1 ml in dH_2O, mixed with 100 μl of 0.15% sodium deoxycholate for 10 min at 20°C, 100 μl 72% trichloroacetic acid (TCA) was added and samples were subjected to centrifugation at 20°C for 15 min. The supernatant was removed and precipitated proteins or samples that did not contain TX-100 were diluted in 400 μl dH_2O, mixed with 400 μl Solution A (equal volumes of 10% SDS, 0.8 M sodium hydroxide, dH_2O and CTC (10% sodium carbonate, 0.1% copper sulfate, 0.2% potassium tartarate)) and incubated at 20°C for 10 min. Solution B (5X dilution of Folin-Ciocalteu reagent in dH_2O) (200 μl) was added and the samples were incubated at 20°C for a further 30 min. The absorbance at 660 nm was determined and used to calculate protein concentration by comparison to a BSA standard curve (2 to 20 μg).

3.2.8 GST-VAP-A pull-down assays

CHO-K1 or COS cells were transiently transfected as described in Section 3.2.4.2. Cells were rinsed once with 2 ml of cold PBS, scraped into 1 ml PBS and collected by centrifugation for 30 seconds at 10,000*g*. Cell pellets were solubilized on ice for 15 min in 100 μl/dish (60 mm) of lysis buffer (10 mM phosphate pH 7.4, 150 mM

NaCl, 5 mM KCl, 2 mM EDTA, 2 mM EGTA, 0.5% TX-100 and 1X protease inhibitor) and subjected to centrifugation at 16,000*g* for 15 min at 4°C. Aliquots of the supernatant (20 µl) were incubated with GST-VAP-A or GST for 45 min at 20°C with constant gentle shaking, and a 1:1 slurry of glutathione-Sepharose (30 µl) was added for an additional 30 min at 20°C. Sepharose beads were collected by centrifugation and washed three times with PBS containing 0.1% TX-100. Samples were resuspended in 10 µl 5X SDS sample buffer, heated to 90°C for 3 min, resolved on SDS-PAGE and analyzed by immunoblotting.

3.2.9 Co-immunoprecipitation

CHO cell lines constitutively overexpressing OSBP or inducibly overexpressing OSBP, OSBP W174A, ORP9S or ORP9L were used to confirm the interactions identified by yeast two-hybrid analysis *in vivo*. CHO-tet-ORP9S and CHO-tet-ORP9L cells were cultured in medium A ± 2 µg/ml doxycycline for 48 h and CHO-tet-OSBP and CHO-tet-OSBP W174A cells were cultured in medium A ± 1 µg/ml doxycycline for 72 h. CHO-OSBP cells were cultured in medium C for 48 h. Cells were rinsed once with 2 ml of cold PBS, scraped into 1 ml PBS and collected by centrifugation for 30 seconds at 10,000*g*. Cell pellets were solubilized on ice for 15 min in 20 µl/dish (60 mm) of lysis buffer (described in Section 3.2.8) and subjected to centrifugation at 16,000*g* for 15 min at 4°C. Supernatants (20 µl) were incubated with antibodies for 4 h at 4°C with constant gentle shaking. Protein A-Sepharose (30 µl of a 1:1 slurry in PBS with 0.1% TX-100) was added and the samples were mixed by constant gentle shaking for 30 min at 20°C. Sepharose beads were collected by centrifugation and washed three times with 1 ml PBS

containing 0.1% TX-100. The samples were heated to 90°C in SDS sample buffer under reducing conditions, separated by SDS-PAGE and analyzed by immunoblotting.

3.2.10 Ceramide trafficking

Trafficking of ceramide from the ER to the Golgi apparatus was examined using a fluorescent ceramide analogue that mimics trafficking of endogenous ceramide [148]. Cells were cultured on glass coverslips and protein expression in CHO-tet-VAP-A or VAP-A ΔTM cells was induced for 48 h with the addition of 2 μg/ml doxycycline, or in CHO-tet-OSBP-WT or CHO-tet-OSBP-W174A cells, by the removal of doxycycline for 72 h. C_5-DMB-ceramide/BSA (fatty acid-free) (1:1 mol) complex was prepared by dissolving 50 nmol of C_5-DMB-ceramide in ethanol and adding it dropwise to 10 ml DMEM containing 3.4 mg fatty acid-free BSA while vortexing. This solution was diluted with DMEM to a working solution of 1.25 μM C_5-DMB-ceramide/BSA for experiments. Cells were washed three times with DMEM at 4°C and loaded with the C_5-DMB-ceramide/BSA complex for 30 min at 4°C, after which cells were washed three times with DMEM containing 0.34 mg/ml fatty acid-free BSA and either fixed or transferred to 37°C. After incubation for various time periods at 37°C, cells were washed again with DMEM containing 0.34 mg/ml fatty acid-free BSA and fixed with 3% formaldehyde in PBS-IF. Coverslips were washed with PBS-IF and mounted on glass slides with DABCO. Since C_5-DMB-ceramide cannot be permanently fixed, images were taken immediately to ensure that it did not diffuse. Images were obtained using an Axiovert 200M fluorescence microscope equipped with a 100X objective and an Axiocam HRC image capture system and imported into Adobe Photoshop for analysis.

3.2.11 VSVG-GFP transport

The role of VAP-A and OSBP in protein trafficking from the ER to the Golgi apparatus was examined using tso45-VSVG-GFP (VSVG-GFP), a temperature sensitive mutant of VSVG that is maintained in the ER at 40°C, but is exported to the Golgi apparatus and PM at 32°C. This construct was tagged with GFP on the cytoplasmic tail [149]. CHO-tet-VAP-A or CHO-tet-VAP-A ΔTM cells were induced for 36 h with 2 μg/ml doxycycline or, in CHO-tet-OSBP-WT or OSBP-W174A cells, by the removal of doxycycline for 60 h. Cells were transiently transfected with a plasmid encoding VSVG-GFP (pVSVG-GFP) using Lipofectamine 2000 as described in Section 3.2.4.2 and incubated at 40°C for 5 h, after which a complete media change was performed (medium A containing 10 mM Hepes pH 7.4 ±doxycycline). After 7 h, cells were either fixed immediately or transferred to a water bath at 32°C for 5 to 60 min before fixation. Cells were fixed and permeabilized using formaldehyde and TX-100 as described in Section 3.2.6 and immunostained for VAP or OSBP to confirm overexpression. Fixation of cells for the zero time point was done at 40°C in prewarmed PBS-IF/3% formaldehyde to prevent transport of VSVG-GFP during fixation.

3.2.12 Analysis of membrane association of VAP-A

The detergent solubility and membrane association of VAP-A was investigated by separating light and heavy membranes into TX-100-soluble and -insoluble fractions by centrifugation. Expression of VAP-A or VAP-A ΔTM was induced by the addition of 2 μg/ml doxycycline for 0, 12, 24 or 48 h. Cells were harvested in PBS, collected by centrifugation and lysed in PBS containing 2 mM EDTA, 2 mM EGTA and 1X protease

inhibitor cocktail by 20 passages through a 23-gauge needle. A heavy membrane fraction was isolated by centrifugation at 10,000*g* for 15 min. The supernatant (light membrane and cytosol) was then subjected to centrifugation at 400,000*g* for 15 min to separate the cytosol and light membrane fractions. The heavy and light membrane pellets were resuspended in the lysis buffer (described above) plus 1% TX-100 and subjected to centrifugation at 400,000*g* for 15 min at 4°C to isolate TX-100-soluble and -insoluble fractions. The presence of VAP-A and OSBP in the samples was determined by immunoblotting.

3.2.13 Isolation of lipid rafts on sucrose density gradients

Lipid rafts were resolved by discontinuous sucrose density gradient centrifugation of TX-100 cell extracts. CHO-K1 cells were first labeled to equilibrium with 5 μCi [^{3}H]cholesterol for 24 h. Cells were grown in 100 mm dishes, harvested in PBS and lysed on ice for 15 min in 400 μl/dish MBS buffer (25 mM Na-MES, (pH 6.5), 150 mM NaCl, 2 mM EDTA, 1X protease inhibitors) containing 1% (v/v) TX-100. Samples were then mixed with an equal volume of MBS buffer containing 80% (w/v) sucrose, placed in a centrifuge tube and layered with 2.5 ml of 35% (w/v) sucrose in MBS and 2 ml of 5% (w/v) sucrose in MBS. Samples were subjected to centrifugation in a Beckman L8 55 ultracentrifuge using an SW55 swinging bucket rotor for 16 h at 200,000*g* and allowed to stop without braking. Fractions (0.5 ml) were collected by needle puncture of the centrifuge tube just above the 40%/35% sucrose interface. All manipulations prior to fraction collection were performed on ice. Fractions were assayed

by Western blotting for VAP, OSBP and caveolin 1, and the amount of [^{3}H]cholesterol in each fraction was quantified on a Beckman LS 6500 scintillation counter.

3.2.14 VAP-A/tubulin binding assay

The association of VAP-A with tubulin was investigated using the microtubule-associated protein (MAP) spin-down assay kit (Cytoskeleton Inc.) according to manufacturer's protocols. CHO-K1 cells were harvested in PBS, collected by centrifugation and lysed on ice for 15 min in 200 µl/100 mm dish of Hepes buffered-saline ((HBS) 25 mM Hepes, pH 7.4, 100 mM NaCl) containing 1% TX-100 (v/v) and 1X protease inhibitor cocktail. A soluble fraction was isolated by centrifugation at 50,000*g* for 80 min at 4°C in a Beckman L8 55 ultracentrifuge using an SW55 swinging bucket rotor fitted with adaptors and the protein concentration determined by the µLowry assay (Section 3.2.7). Tubulin was prepared by resuspending lyophilized protein in G-PEM (80 mM PIPES pH 6.9, 1 mM $MgCl_2$, 1 mM EGTA (PEM), 1 mM GTP) at 5 mg/ml, adding additional GTP (1 mM) and snap-freezing 20 µl aliquots immediately in liquid nitrogen. For experiments, tubulin was thawed in a 20°C water bath, immediately transferred to ice, mixed with 2.5 µl of cushion buffer (50% glycerol in PEM) and incubated at 35°C for 20 min. After the incubation, tubulin was diluted 10-fold with G-PEM (35°C) containing 20 µM taxol to generate 5 – 10 µm long stabilized microtubules (10 nM). Microtubules were then mixed with cell extracts (10-50 µg), incubated at 20°C for 30 min, layered on top of 100 µl of cushion buffer containing 20 µM Taxol in 500 µl centrifuge tubes and subjected to centrifugation at 50,000*g* for 80 min in an SW55 swinging bucket rotor. Volumes equivalent to the original supernatant (50 µl) (unbound

proteins) and the cushion buffer (100 µl) were removed, the pellets (tubulin and bound proteins) were resuspended in SDS sample buffer (1X) and the samples analyzed by SDS-PAGE and Coomassie staining or Western blotting.

3.2.15 PH domain binding to phospholipid vesicles

A sedimentation assay was used to measure the binding of a GST-OSBP-PH fusion protein to phosphatidylcholine (PC) vesicles containing 5 mol% of various other phospholipids. GST-OSBP fusion proteins (residues 80-187) encompassed the entire PH domain and were either wildtype or had a tryptophan to alanine mutation at residue 174 (W174A). Fusion proteins were prepared as described in Section 3.2.5, except that the induction with IPTG was done at 37°C. PC (95 mol%) was mixed with other phospholipids (5 mol%) in $CHCl_3$:methanol (1:1, v/v) (phosphatidylserine (PS) and PI) or $CHCl_3$:methanol:HCl (1:1:0.1, v/v) (PI-4,5-P_2, PI-4-P). The lipids were dried under nitrogen and resuspended in HBS at a final concentration of 25 mM phospholipid. Vesicles were prepared by sonication for 5 min in a bath sonicator, followed by 10 freeze-thaw cycles in liquid nitrogen and room temperature water. For experiments, vesicles were diluted with HBS to a range of concentrations from 50 µM to 5 mM phospholipid. Vesicles (100 µl) were incubated with fusion protein for 5 min at 20°C before being subjected to centrifugation at 400,000*g* for 15 min. The supernatant was removed and the pellet washed once with HBS before being resuspended by sonication in 100 µl of the same buffer. Equal volumes of the supernatant (unbound) and pellet (bound) were resolved by SDS-12% PAGE and proteins were detected by staining with Coomassie Blue.

4 Results

4.1 Identification of protein-protein interactions by yeast two-hybrid analysis

4.1.1 VAP-A interacts with OSBP

In order to identify OSBP interacting proteins, yeast two-hybrid analysis was performed using full-length OSBP as bait to screen a human B-cell library. A vector encoding OSBP expressed as an N-terminal fusion protein with the DNA binding domain of the GAL4 transcription factor (pAS1-OSBP) was constructed and expression in *S. cerevisiae* yeast strain PJ69 was confirmed by immunoblotting (Fig. 4A). As in mammalian cells, OSBP was expressed in yeast as a doublet on SDS-PAGE. No growth on interaction-selective plates was detected when pAS1-OSBP was co-transformed with pSE1111, suggesting it was a suitable candidate for yeast two-hybrid analysis. Screening of a human B-cell library using OSBP as bait resulted in the cloning of 18 VAP-A cDNAs, all which encoded full-length proteins. VAP-A and OSBP interacted in yeast regardless of which was expressed as a fusion protein with the DNA binding domain or transcriptional activation domain, indicating that this was not a false positive interaction. The B-cell library was also screened using N-terminally truncated OSBP (pAS1-OSBP 351-809) as bait but again only VAP-A cDNAs were cloned.

Given that VAP-A is an integral membrane protein, it is unusual that it was cloned by yeast two-hybrid analysis, which is biased towards soluble proteins that can be targeted to the nucleus. It may be that the transmembrane domain is removed in yeast, allowing the soluble portion of the protein to enter the nucleus. In support of this, when VAP-A is overexpressed in CHO-tet-on cells, a cleavage product very similar in size to that of VAP-A ΔTM is observed (Fig. 15). However, this is unlikely, since removal of the

Figure 4. Expression of wildtype and mutant forms of OSBP and VAP-A in *S. cerevisiae* yeast strain PJ69. Yeast (PJ69) transformed with pAS1, pAS1-OSBP, pAS1-OSBP mutants, pAS1-VAP, pACT2-VAP-A or pACT2-VAP-A mutants were grown overnight in selective media to mid-log phase, collected by centrifugation for 5 min at 1000*g* at 20°C, washed with 5 ml sterile distilled water and resuspended in 250 µl sterile water. 5X SDS buffer was added (100 µl), the tubes were filled to the meniscus with glass beads and the samples were shaken on the Bead Beater for 1 min. Equal volumes of sample (20 µl) were separated by SDS-PAGE and immunoblotted with monoclonal OSBP antibody 11H9 or VAP polyclonal antibody.

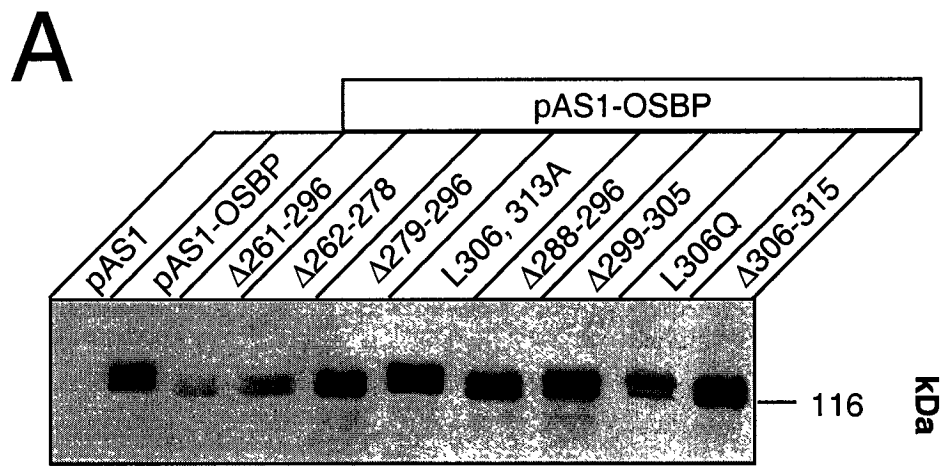
A
pAS1-OSBP
pAS1
pAS1-OSBP
Δ261-296
Δ262-278
Δ279-296
L306, 313A
Δ288-296
Δ299-305
L306Q
Δ306-315
116
kDa

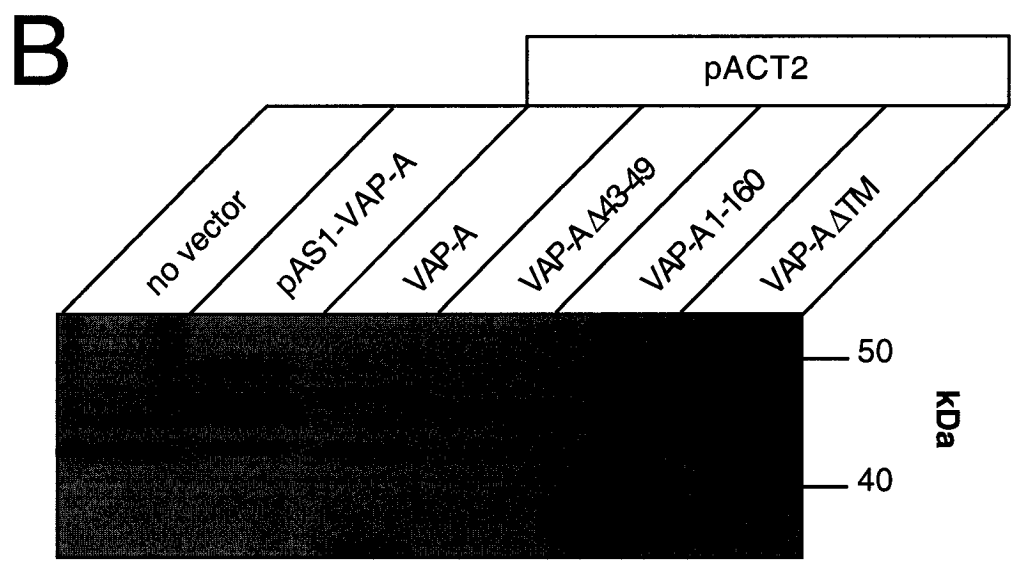
B
pACT2
no vector
pAS1-VAP-A
VAP-A
VAP-AΔ43-49
VAP-A1-160
VAP-AΔTM
50
40
kDa

Figure 4

transmembrane domain prevents interaction with OSBP (Table 3). It is also possible that the transmembrane domain aggregates such that exposure of hydrophobic residues is minimized, rendering VAP-A soluble and allowing it to enter the nucleus.

Like the ORP family, orthologues of VAP-A have been identified in a wide range of species from yeast to man [16,143,150-158]. VAP-A is a type II transmembrane protein that localizes to the ER, Golgi apparatus and ERGIC (ER/Golgi apparatus intermediate compartment) [159-161]. The overall structure, which is representative of all VAP orthologues, consists of a conserved 19 amino acid cytoplasmic N-terminal region (the VAP consensus domain), a coiled-coil region thought to be involved in protein:protein interactions and a C-terminal transmembrane domain (Fig. 5). VAP-A is also referred to as VAP-33 [155,162] and shares 60% amino acid sequence identity with VAP-B or ER/Golgi apparatus 30 kDA protein (ERG30) [161].

Both VAP-A and VAP-B are ubiquitously expressed in mammalian cells and have been implicated in vesicle trafficking and fusion in an ER/Golgi pathway [151,153,156,159-161,163]. VAP-A interacts with a number of proteins involved in these processes such as VAP-B, VAMP1 and VAMP2, as well as several SNAREs (soluble N-ethylmaleimide-sensitive factor (NSF) attachment protein (SNAP) receptor) and SNARE adaptors including αSNAP, NSF, syntaxin 1A, rbet1 and rsec22 [156,159,160]. This group of interactions suggests that VAP-A is a component of the fusion machinery or is a protein chaperone that blocks inappropriate interactions and increases the specificity of vesicle targeting within the secretory pathway [160].

Figure 5. Structural features of VAP-A. Schematic representation of VAP-A showing conserved domains and topology in ER membrane. Numbers indicate amino acid residues.

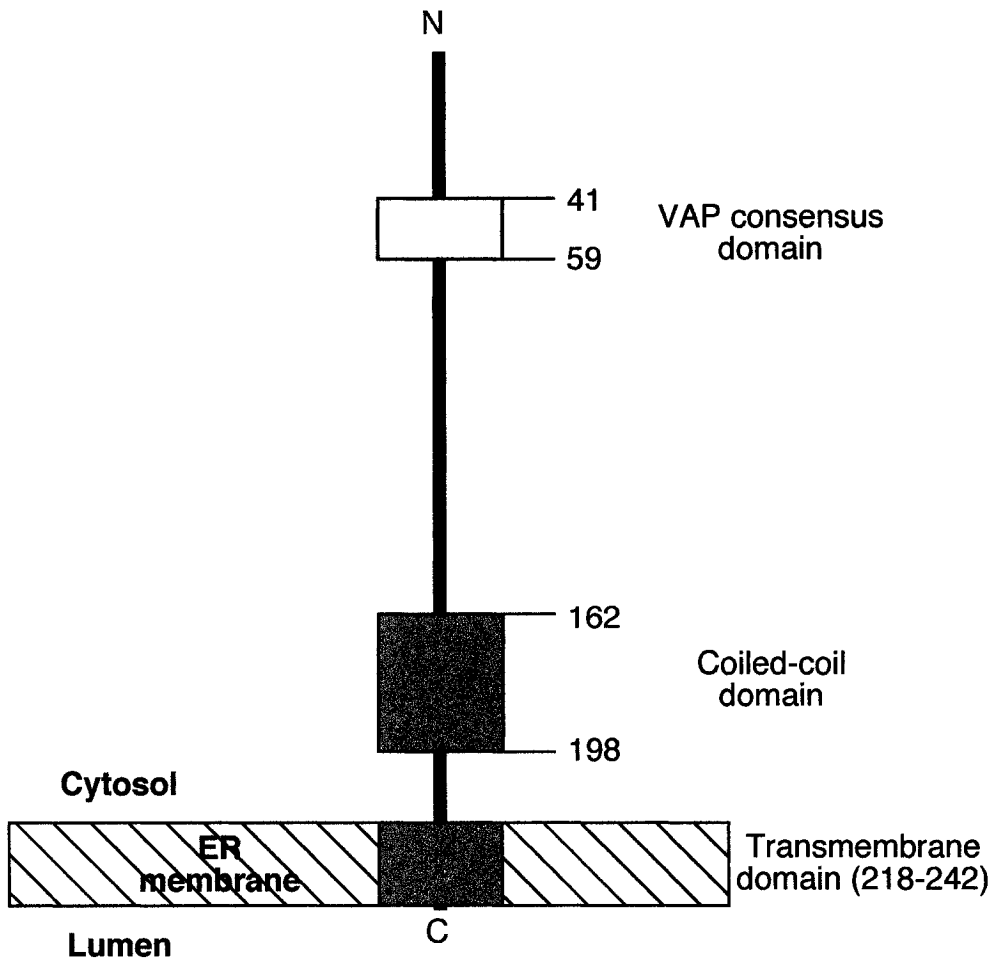
N
41
59
VAP consensus domain
162
198
Coiled-coil domain
Cytosol
ER membrane
Transmembrane domain (218-242)
Lumen
C

Figure 5

4.1.2 ORP9 is a VAP-A interacting protein

In an effort to further elaborate the VAP-A/OSBP interaction network, a second yeast two-hybrid screen was performed using full-length VAP-A as bait. The expression of pAS1-VAP-A was confirmed in yeast strain PJ69 (Fig. 4B) and growth on interaction-selective plates was not supported when pAS1-VAP-A was co-expressed with pSE1111, making it a suitable candidate for yeast two-hybrid analysis. Screening a human B-cell library using VAP-A as bait resulted in the cloning of an uncharacterized member of the ORP family, ORP9, as well as 13 full-length VAP-A cDNAs, thus confirming VAP-A multimerization [159]. As the ORP9 cDNA isolated from the library was truncated and rearranged (Fig. 6), complete cDNAs for full-length ORP9L and its truncated splice variant ORP9S were obtained and cloned into pAS1 and pACT2 in order to confirm their interaction with VAP-A. Both ORP9S and ORP9L interacted with VAP-A regardless of whether they were expressed as fusion proteins with the GAL4 DNA binding domain or activation domain.

The partial ORP9 cDNA isolated from the screen was analyzed in an attempt to identify the VAP-A interacting domain. The partial cDNA contained an inversion of ~250 basepairs (bp) at the 3' end, but because of suspected secondary structure formed by complementary sequences, we were unable to obtain complete sequence data. However, we were able to use unique internal *BamH1* and *BglII* sites in conjunction with *BglII* sites at the 5' and 3' ends of the cDNA to map the site of the inversion. In order to determine the nature of the ORP9 library clone, it was digested with *Xho1* to release the entire ORP9 insert (Fig. 6A), *BamH1* or *BglII* (Fig. 6B). When the partial cDNA was digested with *BglII*, three bands were visible, at ~900, 600 and 200 bp. The ~900 bp band

Figure 6. Structure of the partial ORP9 cDNA cloned from a human B-cell yeast two-hybrid library. *(A) Xho1* digests of the partial ORP9 cDNA separated on a 1% agarose gel. *(B) BglII* and *BamH1* digests of the partial ORP9 cDNA separated on a 2% agarose gel. *(C)* Schematic representation of full-length ORP9S cDNA in pACT showing *Xho1*, *BamH1* and *BglII* sites. *(D)* Schematic representation of the partial ORP9 cDNA in pACT showing *Xho1*, *BamH1* and *BglII* sites, restriction fragments, and sequence orientation with respect to wildtype cDNA. The partial ORP9 cDNA does not contain the initiator AUG codon and the *XhoI* and *BglII* sites at the 3' end are derived from the pACT vector. Abbreviations: *DL*, DNA ladder; *bp,* base pair.

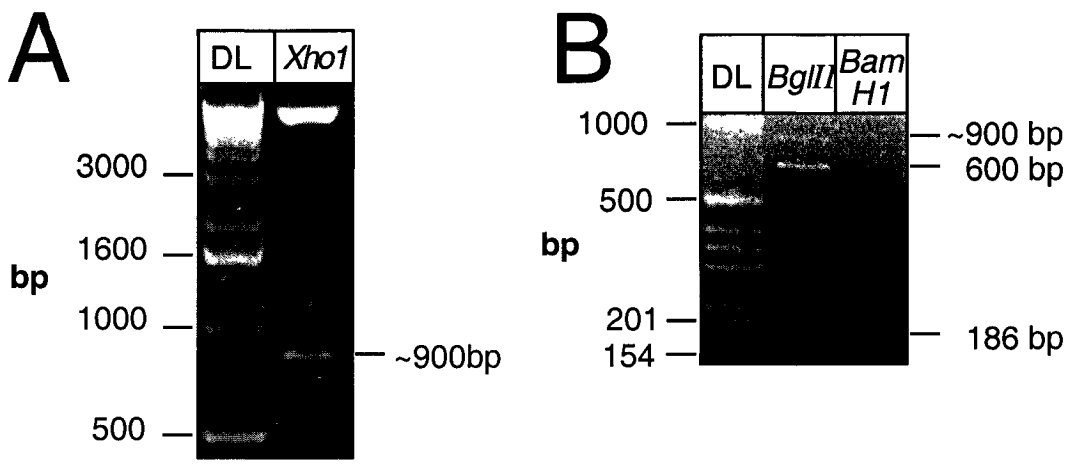

C

ORP9S (wild-type)

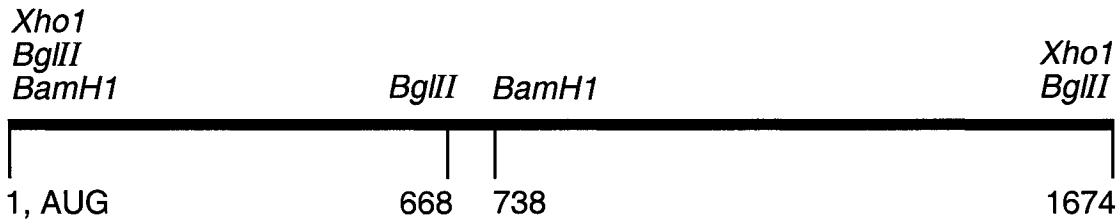

D

ORP9 partial cDNA

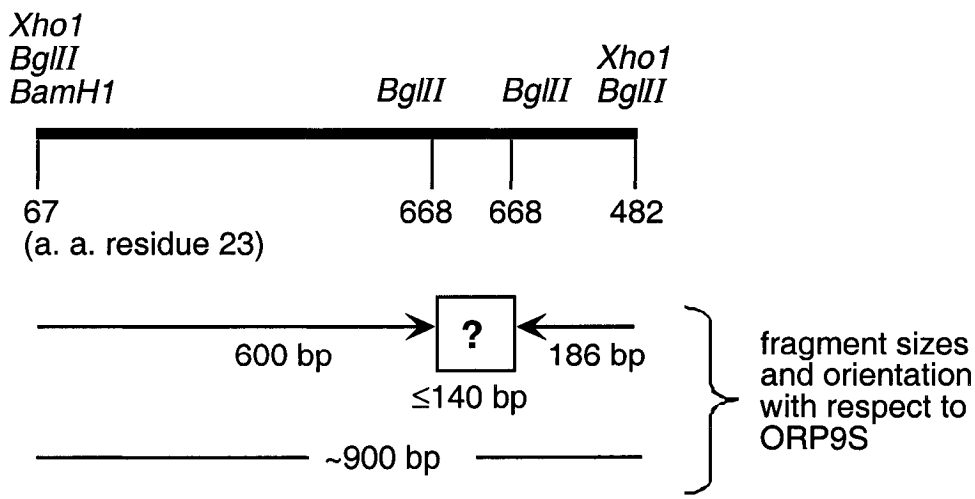

Figure 6

100bp

likely represents partially digested DNA (digestion could have been incomplete due to the formation of secondary structure), while the 600 bp band represents the fragment from the 5' end of the clone to the first *BglII* site, which corresponds to the unique *BglII* site in the wildtype ORP9S cDNA. The existence of the smaller band indicates that a *BglII* site was also included in the inverted sequence (Fig. 6D). Since sequencing of the 3' end of the cDNA showed that it started at nucleotide 482 of ORP9S the size of this band was determined to be 186 bp. This leaves only the region between the two *BglII* sites, which could not be identified. Digestion with *BamH1* did not produce any fragments (Fig. 6B), indicating that this site was not present in the partial cDNA. Since the *BamH1* site is 70 bp 3' to the *BglII* site, the maximum size of the fragment is 140 bp. Although we were unable to determine the site of the inversion, restriction analysis and sequencing of the partial cDNA allowed us to localize the binding region of VAP-A to amino acids 23-246 of ORP9S (residues 188 and 411 of ORP9L).

4.1.3 Identification of ORP9 interacting proteins

In an effort to gain insight into the function(s) of ORP9S and ORP9L, yeast two-hybrid screens were performed using ORP9S and ORP9L as bait to identify protein partners. While expression of ORP9S or ORP9L from the pAS1 vectors could not be confirmed in yeast by Western blotting due to the high background with the ORP9 polyclonal antibody, both were able to confer growth on interaction-selective plates when co-expressed with pACT2-VAP-A, functionally confirming their expression. As well, neither ORP9S nor ORP9L supported growth on interaction-selective plates when co-expressed with pSE1111, making ORP9S and ORP9L suitable candidates for yeast two-

hybrid analysis. Screening of the human B-cell library with pAS1-ORP9S resulted in the cloning of importin-α and RED/IK cytokine (Table 2). Screening with pAS1-ORP9L identified Int6/eIF3e, zinc finger protein 207 and the β subunit of proteasome activator 28 (PA28). As well, more than 30 VAP-A cDNAs were isolated.

The interaction of ORP9S and ORP9L with Int6/eIF3e was further investigated. Like ORP9, the Int6/eIF3e cDNA isolated from the B-cell library was rearranged, in this case with an inversion of 66 bp at the 5' end of the clone (Fig. 7). As a result there are 22 nonsense amino acids between the GAL4 transcription activation domain and the start of the Int6/eIF3e coding sequence. Since no stop codons were found in this sequence, the Int6/eIF3e sequence after the inversion was expressed in frame. The Int6/eIF3e cDNA isolated from the B-cell library encoded the C-terminal quarter of the protein (amino acids 339 to 445), which contains the proteasome/COP9 signalosome/translation initiation factor 3 (PCI) domain (amino acids 304-445). PCI domains are found in several components of the proteasome, COP9 signalosome (CSN) and protein translation complex (Int6/eIF3e). In *S. pombe*, the orthologue of Int6/eIF3e, Yin6p, has been shown to interact with and regulate the assembly of the proteasome [171]. The CSN has also been implicated in the regulation of some proteasome-mediated degradation events [172].

Since the Int6/eIF3e cDNA we cloned was incomplete, a full-length cDNA was obtained from Invitrogen and cloned into pAS1 (pAS1-Int6/eIF3e) and pACT2 (pACT2-Int6/eIF3e) both to confirm its interaction with OPR9L and to investigate its interaction with VAP-A, OSBP, ORP4S, ORP4L and ORP9S. A second construct expressing only the PCI domain was also generated and cloned into pACT2 (pACT2-Int6/eIF3e-PCI). Full-length Int6/eIF3e did not interact with any of the proteins tested by yeast two-hybrid

Table 2. Identity of cDNAs isolated in yeast two-hybrid screens with pAS1-ORP9S and pAS1-ORP9L. Plasmids were isolated from yeast growing on interaction-selective plates, transformed into DH5α strain JF1754 and plated on M9 plates lacking leucine and containing ampicillin (100 μg/ml) (Section 3.2.3.3). Plasmids were isolated from bacteria, sequenced and identified using BLAST software (NCBI). Interactions were reconfirmed with ORP9S and ORP9L and checked against irrelevant proteins to identify false positives. ✓ interaction; X, no interaction.

Clone	ORP9S	ORP9L	Proposed Role	Reference
Importin-α	✓	X	Nuclear import	Gorlich *et al* (1996) *Cell* **87**, 21-32 [164]
RED/IK cytokine	✓	X	Down regulation of HLA II (antigen presentation)	Krief *et al* (1994) *Oncogene* **9** 3449-56 [165] Assier et al (1999) Gene 230, 145-54 [166]
Int6/eIF3e	✓	✓	Protein degradation and translation initiation	Asano *et al* (1997) *JBC* 272, 23477-80 [167] Diella *et al* (1997) *DNA Cell Biol* 16, 839-47 [168]
Zinc finger protein 207	X	✓	DNA binding protein, transcription factor (?)	Pahl *et al* (1998) *Genomics* 33, 410-12 [169]
β subunit of PA28 (proteasome activator)	X	✓	Regulates affinity of PA28 for proteasome, involved in antigen generation and presentation on MHC I	Song *et al* (1997) *JBC* 272, 27994-00 [170]

Table 2

Figure 7. Structure of partial pACT-Int6/eIF3e cDNA cloned from a human B-cell yeast two-hybrid library. *(A)* Schematic view of the structure of the full-length Int6/eIF3e cDNA showing region coding for the PCI domain. *(B)* Schematic view of the structure of the partial Int6/eIF3e cDNA showing site of inversion, sequence direction with respect to wildtype Int6/eIF3e and truncated PCI domain encoding region.

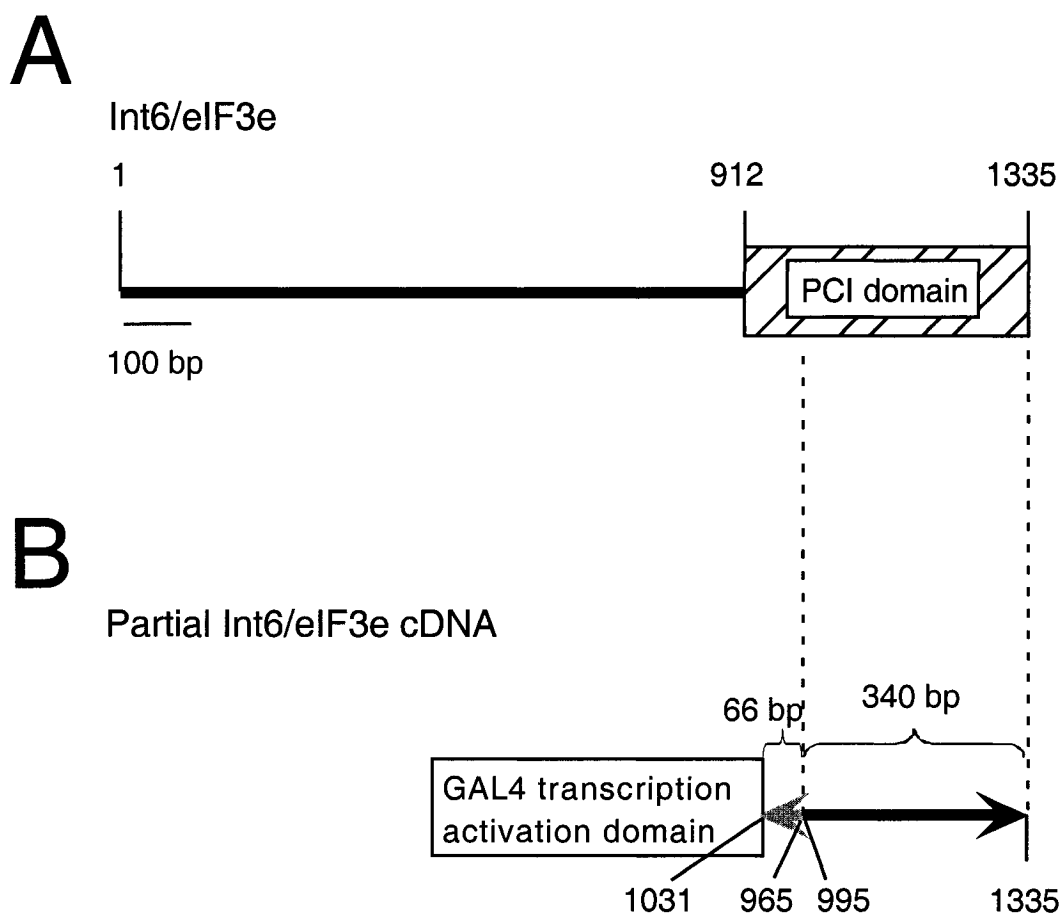
A
Int6/eIF3e
1
912
1335
PCI domain
100 bp
B
Partial Int6/eIF3e cDNA
66 bp
340 bp
GAL4 transcription
activation domain
1031
965
995
1335

Figure 7

analysis. However, the PCI domain construct interacted with both ORP9 variants, but not with VAP-A, OSBP, ORP4S or ORP4L.

4.1.4 Characterization of interactions between ORP family members and VAP-A by yeast two-hybrid analysis

The regions of OSBP and VAP-A involved in homodimerization, as well as the VAP-A domain(s) responsible for binding OSBP, ORP9S and ORP9L were further investigated using the yeast two-hybrid system. Mutations were made in pAS1-OSBP or pACT-VAP-A and their expression in *S. cerevisiae* yeast strain PJ69 was confirmed by Western blotting (Fig. 4A and 4B). Mutants were co-transformed into yeast strain PJ69 in conjunction with wildtype OSBP or VAP-A, and growth on interaction-selective plates was determined (Table 3). The mutations made in pAS1-OSBP were designed to investigate the role of several different domains and sequence motifs in homodimerization and VAP-A binding: OSBP Δ261-296, OSBP Δ262-278, OSBP Δ279-296 and OSBP Δ288-296 were made in order to confirm and further define the dimerization region [33]; OSBP L306, 313A, OSBP Δ299-305 and OSBP L306Q disrupted a potential leucine zipper; OSBP Δ306-315 deleted a potential SNARE V2 homology region; OSBP Δ432-435 deleted a conserved sequence in the OHD; and OSBP 351-809 expressed only the C-terminal half of the protein (location of mutations is shown in Fig. 9). Only OSBP 351-809, OSBP Δ261-296, OSBP Δ262-278 and OSBP Δ279-296 failed to homodimerize with full-length OSBP, confirming and further defining the dimerization region to residues 261-288 (Table 3). All of the OSBP mutants interacted with VAP-A, indicating that none of the deleted regions were essential for binding.

Both VAP-A and VAP-B have been shown to homodimerize by non-reducing SDS-PAGE, yeast two-hybrid analysis and GST pull-down assays [153,159,161]. In order to further investigate the homodimerization of VAP-A and its interaction with OSBP, three regions of VAP-A were mutated in pACT2-VAP-A; part of the VAP consensus domain in the amino terminus was deleted (VAP-A Δ43-49), VAP-A was truncated prior to the coiled-coil domain (VAP-A 1-160) and the transmembrane domain was deleted (VAP-A ΔTM) (location of mutations is shown in Fig. 9). All of the mutants interacted with wildtype VAP-A, showing that none of the deleted regions were necessary for homodimerization (Table 3). Since previous work showed that a VAP-B truncation mutant expressing residues 1-140 did not homodimerize [161], residues 140-160 of VAP-A may be involved in dimerization. However, this region has very little sequence similarity between VAP-A and VAP-B and may be involved in isoform-specific functions rather than dimerization.

The interaction of VAP-A and the VAP-A mutants with OSBP, ORP4S, ORP4L, ORP9S and ORP9L was also investigated by yeast two-hybrid analysis (Table 3). All of the VAP-A mutations prevented interaction with OSBP. As the interaction of each VAP-A mutant with itself was not tested, it is possible that the individual mutants failed to form homodimers and that this lack of dimerization prevented interaction with OSBP. This is unlikely, as all three mutants dimerized with wild type VAP-A (Table 3). Only VAP-A Δ43-49 failed to interact with ORP9S and ORP9L, evidence that the VAP consensus sequence may be involved in the interaction of VAP-A with the ORP family (Table 3). Wild-type VAP-A did not interact with ORP4S or ORP4L by yeast two-hybrid analysis. However, ORP4L and VAP-A were shown to interact via GST pull-down

assays (Section 4.2.2) thus the yeast two-hybrid data may not fully reflect the situation in mammalian cells.

Finally, the yeast two-hybrid system was used to further define interactions among OSBP and ORP family members (Table 3). The ORP4 polyclonal antibody could not be used to confirm expression of pAS1-ORP4S or pAS1-ORP4L in yeast due to a high background on immunoblots. However, ORP4L interacted with OSBP and thus can be assumed to be expressed. On the other hand, ORP4S did not interact with any of the proteins tested and there is no direct evidence of its expression in yeast. ORP4L had the same OSBP mutant binding profile as OSBP, showing that OSBP dimerizes or interacts with ORP4 via the conserved dimerization domain. Interestingly, ORP4L did not homodimerize, indicating that it may not be folded correctly in yeast, an explanation supported by its lack of interaction with VAP-A in this system (ORP4L and VAP-A interact by GST pull-down analysis). OSBP did not interact with ORP4S or either form of ORP9, and ORP4S and the ORP9 variants did not homodimerize or interact with each other.

4.2 *In vitro* interaction of GST-VAP-A with members of the ORP family.

The VAP-A/OSBP and VAP-A/ORP9 interactions seen by yeast two-hybrid analysis were confirmed *in vitro* by GST pull-down analysis. As well, GST pull-down assays were used to further characterize the region of OSBP involved in VAP-A binding and to investigate the interaction of several other ORP family members with VAP-A.

In order to confirm and characterize the interaction of OSBP with VAP-A, TX-100 extracts of COS cells that had been transiently transfected with wildtype or mutant

Table 3. Interactions of ORP family members and VAP-A detected by yeast two-hybrid analysis. The interaction of ORP4S, ORP4L, ORP9S, ORP9L, OSBP and VAP-A with themselves and each other, as well as with mutants of VAP-A and OSBP was investigated using the yeast two-hybrid system. All plasmids were co-transfected into yeast strain PJ69 and yeast were grown at 30°C (Section 3.2.3.1). VAP-A mutations were made in pACT2-VAP-A and OSBP mutations were made in pAS1-OSBP. All other interactions were confirmed by expressing the cDNAs as fusion proteins with both the GAL4 DNA-binding domain (pAS1) and activation domain (pACT2), except Int6/eIF3e-PCI, which was investigated only as a fusion with the transcription activation domain in pACT2. Multiple transformants that grew on transformation-control plates were restreaked on interaction-selective plates to confirm or disprove the interactions. ✓ interaction, X no interaction, - no data.

	VAP-A	OSBP	ORP4S	ORP4L	ORP9S	ORP9L
VAP-A	✓	✓	X	X	✓	✓
VAP-A Δ43-49	✓	X	-	-	X	X
VAP-A Δ 161	✓	X	-	-	✓	✓
VAP-A Δ TM	✓	X	-	-	✓	✓
OSBP WT	✓	✓	X	✓	X	X
OSBP Δ 261-296	✓	X	-	X	-	-
OSBP Δ 262–278	✓	X	-	X	-	-
OSBP Δ 279–296	✓	X	-	X	-	-
OSBP Δ 288–296	✓	✓	-	✓	-	-
OSBP Δ 306–315	✓	✓	-	✓	-	-
OSBP L306A,L313A	✓	✓	-	✓	-	-
OSBP Δ 299–305	✓	✓	-	✓	-	-
OSBP L306Q	✓	✓	-	✓	-	-
OSBP S371A	✓	✓	-	✓	-	-
OSBP – LBD (360-809)	✓	X	-	X	-	-
ORP 4 Short	X	X	X	X	X	X
ORP 4 Long	X	✓	X	X	X	X
ORP 9 Short	✓	X	X	X	X	X
ORP 9 Long	✓	X	X	X	X	X
Int6/eIF3e	X	X	X	X	X	X
Int6/eIF3e - PCI domain	X	X	X	X	✓	✓

Table 3

OSBP cDNAs were prepared and incubated with GST or GST-VAP-A. Wild-type OSBP was recovered from TX-100 extracts by binding to increasing amounts of GST-VAP-A (0 - 10 μM) but not to GST (1 μM) or glutathione beads alone (Fig. 8A). Since binding of OSBP was optimal at 1 μM GST-VAP-A, this concentration was used in all subsequent experiments. OSBP with partial or complete deletions of the PH domain, or mutation of the conserved tryptophan 174 to alanine, also bound quantitatively, demonstrating that the PH domain was not required for binding to VAP-A (Fig. 8B). The phosphorylation state of OSBP was also not involved in VAP-A interaction since pretreatment of cells with okadaic acid or staurosporin to hyperphosphorylate or dephosphorylate OSBP, respectively, did not affect binding (Fig. 8B). Several deletion and truncation mutants of OSBP were also investigated. OSBP truncated at amino acid 443 bound GST-VAP-A but truncations closer to the N-terminus (OSBP 1-217 and OSBP 1-267) did not (Fig. 8C). As well, partial deletion of a conserved sequence at the N-terminus of the OHD (Δ432-435) did not affect binding of OSBP to GST-VAP-A (Fig. 8D). This, combined with the yeast two-hybrid data showing that VAP-A interacted with OSBP 351-809, allowed us to narrow the VAP-A binding domain of OSBP to residues 351 to 431 (Fig. 9). This region overlaps with the ligand-binding region of OSBP and the OHD [2,4,6,7].

GST pull-down assays were also used to confirm the interaction of VAP-A with ORP9S and ORP9L. CHO-K1 cells were transiently transfected with pcDNA3-ORP9S and pcDNA3-ORP9L, as well as empty vector and pCMV2-OSBP. TX-100 extracts of cells were prepared and incubated with GST or GST-VAP-A (Fig. 10). OSBP, ORP9S and ORP9L bound GST-VAP-A but not GST. Based on the assay input, the binding efficiency was approximately 25%. These and subsequent experiments used a GST-VAP-

Figure 8. Identification of the VAP-A-binding domain in OSBP by GST pull-down assays. Samples in all panels were treated in the following manner. OSBP cDNAs were transiently overexpressed in COS cells for 48 h and TX-100 cell lysates were prepared (Section 3.2.8). Lysates (20 μl) were incubated with 1 μM GST-VAP-A (+) or GST (-) in PBS (pH 7.4) for 45 min at 20°C, glutathione-Sepharose (30 μl of a 1:1 slurry) was added for 30 min, beads were collected by brief centrifugation and washed 3 times with 0.5 ml PBS and 0.1% TX-100. Samples were separated by SDS 8%-PAGE (panels A, B and D) or SDS 10%-PAGE (panel C and E) and immunoblotted with monoclonal OSBP antibody 11H9. *(A)* TX-100 extract of cells expressing wildtype OSBP was incubated with GST-VAP-A (0, 0.5, 1, 2.5, 5 or 10 μM), 1 μM GST or glutathione beads. *(B)* TX-100 extracts of cells expressing OSBP, OSBP PH domain mutants or OSBP-transfected cells pretreated with 1 μM okadaic acid (increase phosphorylation) or 1 μM staurosporin (decrease phosphorylation) for 60 min. *(C)* TX-100 extracts of cells expressing C-terminally truncated forms of OSBP. *(D)* TX-100 extracts of cells expressing OSBP or OSBP Δ 432-435. *(E)* Input for panels A, B and D, representing 25% of extract in the binding assay. Abbreviations: +, GST-VAP-A; -, GST; *OKA,* okadaic acid; *STS,* staurosporin.

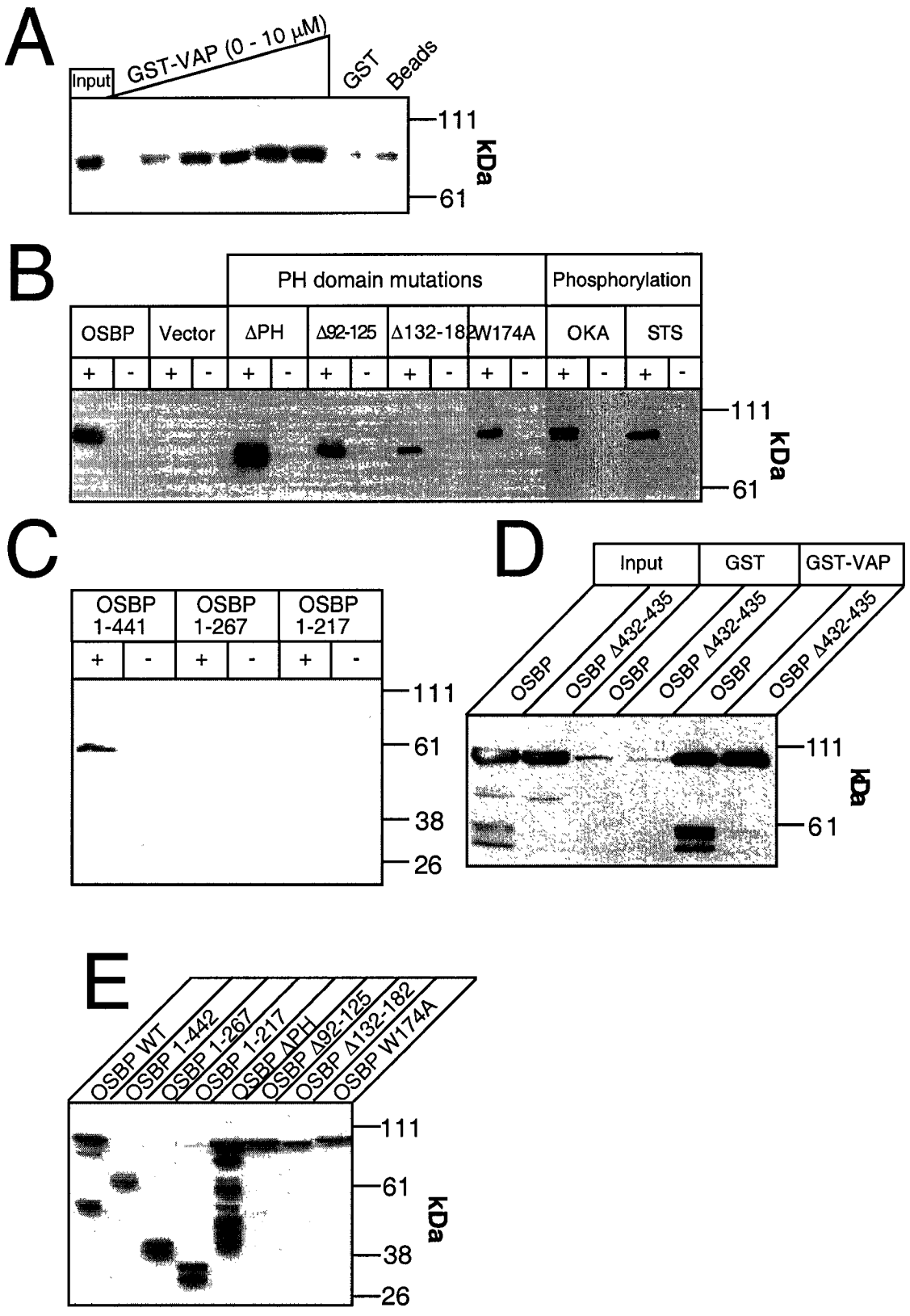
A
Input
GST-VAP (0 - 10 μM)
GST
Beads
111
61
kDa
B
PH domain mutations
Phosphorylation
OSBP
Vector
ΔPH
Δ92-125
Δ132-182
W174A
OKA
STS
111
61
kDa
C
OSBP 1-441
OSBP 1-267
OSBP 1-217
111
61
38
26
D
Input
GST
GST-VAP
OSBP
OSBP Δ432-435
111
61
kDa
E
OSBP WT
OSBP 1-442
OSBP 1-267
OSBP 1-217
OSBP ΔPH
OSBP Δ92-125
OSBP Δ132-182
OSBP W174A
111
61
38
26
kDa

Figure 8

Figure 9. Summary of interactions between OSBP and VAP-A by yeast two-hybrid and GST pull-down analysis. For yeast two-hybrid analysis, wildtype and mutant forms of OSBP and VAP-A were co-transformed into *S. cerevisiae* yeast strain PJ69 and grown on synthetic media as described for Table 3. Results of the GST binding assays are described in Figure 8. Abbreviations: *G/A*, glycine/alanine rich region; *Dim*, dimerization domain; *VCD*, VAP consensus domain; *CCD*, coiled coil domain.

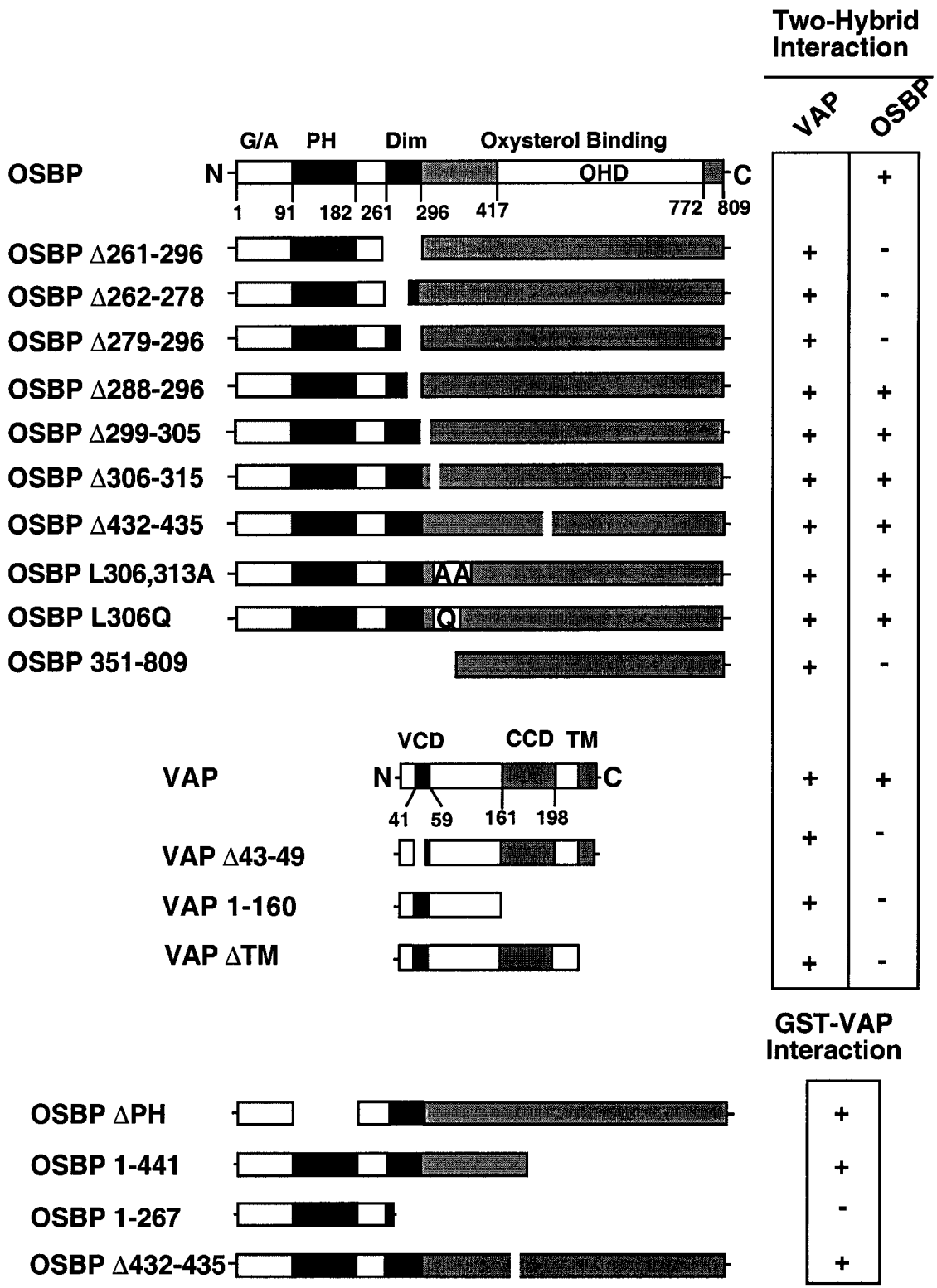
Two-Hybrid Interaction
VAP
OSBP
G/A
PH
Dim
Oxysterol Binding
OSBP
N
OHD
C
1
91
182
261
296
417
772
809
OSBP Δ261-296
OSBP Δ262-278
OSBP Δ279-296
OSBP Δ288-296
OSBP Δ299-305
OSBP Δ306-315
OSBP Δ432-435
OSBP L306,313A
AA
OSBP L306Q
Q
OSBP 351-809
VCD
CCD
TM
VAP
N
C
41
59
161
198
VAP Δ43-49
VAP 1-160
VAP ΔTM
GST-VAP Interaction
OSBP ΔPH
OSBP 1-441
OSBP 1-267
OSBP Δ432-435

Figure 9

Figure 10. Interaction of ORP9S and ORP9L with GST-VAP-A. TX-100 cell extracts were prepared from transiently transfected CHO-K1 cells expressing ORP9S, ORP9L, OSBP or a vector control (Section 3.2.8). Lysates were incubated with 1 μM GST or GST-VAP-A as described in the legend to Figure 8, separated by SDS 8%-PAGE and immunoblotted for ORP9S and ORP9L with V5 monoclonal antibody or OSBP with monoclonal antibody 11H9. The samples from cells transfected with empty vector were probed with the V5 monoclonal antibody. Input represents 25% of the extract used in the binding assay. Abbreviations: +, GST-VAP-A; -, GST.

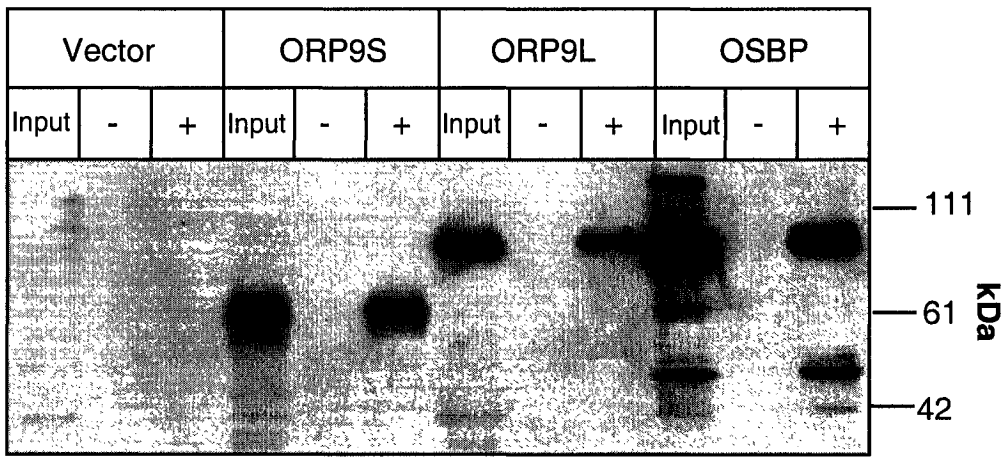
Vector
ORP9S
ORP9L
OSBP
Input
-
+
Input
-
+
Input
-
+
Input
-
+
111
61
42
kDa

Figure 10

A preparation that did not bind OSBP as efficiently as the original preparation used in the experiments described in Figure 8.

Finally, binding of ORP1L, ORP3(1d) and ORP4L to GST-VAP-A was investigated. TX-100 extracts of CHO-K1 or COS cells transiently transfected with appropriate cDNAs were prepared, incubated with GST or GST-VAP-A and binding was analyzed by Western blotting (Fig. 11). ORP1L, along with endogenous OSBP was pulled down with VAP-A (Fig. 11A). If ORP1L bound GST-VAP-A as part of an OSBP-containing complex, the amount of ORP1L in the bound fraction would probably be reduced relative to OSBP. Since their ratio in the bound sample was the same as the input, ORP1L probably bound GST-VAP-A independently of OSBP. Approximately 10% of ORP1L bound GST-VAP-A, indicating a weak or transient interaction. The interaction of GST-VAP-A and ORP3(1d), a splice variant in which exons 9 and 12 are absent [5] (Section 1.4), was also very weak (Fig. 11B). Although ORP4L and VAP-A did not interact directly by yeast two-hybrid assay, they interact weakly via a GST pull-down assay (Fig 11C). The presence of endogenous OSBP in the ORP3(1d) and ORP4L samples was not determined because of antibody specificities, but is assumed to be present (ORP3(1d) was detected with a V5 monoclonal tag antibody and ORP4L was detected with an ORP4-specific polyclonal antibody, while pan ORP polyclonal antibody 170 was used to detect ORP1L). Although these interactions all appeared weak, no interactions were detected in the GST controls, showing that the interactions were specific. It is possible that the endogenous ligand of some of the ORPs is VAP-B rather than VAP-A, and that the interaction detected in GST pull-down assays is indirect and due to the interaction of the ORP with endogenous VAP-B, which is able to

Figure 11. Interaction of ORP1L, ORP3(1d) and ORP4L with GST-VAP-A. CHO-K1 and COS cells were transiently transfected and TX-100 extracts were prepared (Section 3.2.8). Lysates were incubated with 1 μM GST or GST-VAP-A as described in the legend to Figure 8, separated by SDS 8%-PAGE and immunoblotted for ORP1L (ORP antibody 170), ORP3(1d) (V5 monoclonal antibody) or ORP4L (ORP4 polyclonal antibody). Input represents 25% of extract used in the binding assay except for ORP4L, which represents 100%. *(A)* TX-100 extract of CHO K1 cells transiently expressing ORP1L. *(B)* TX-100 extract of COS cells transiently expressing ORP3(1d). *(C)* TX-100 extract of CHO-K1 cells transiently expressing ORP4L.

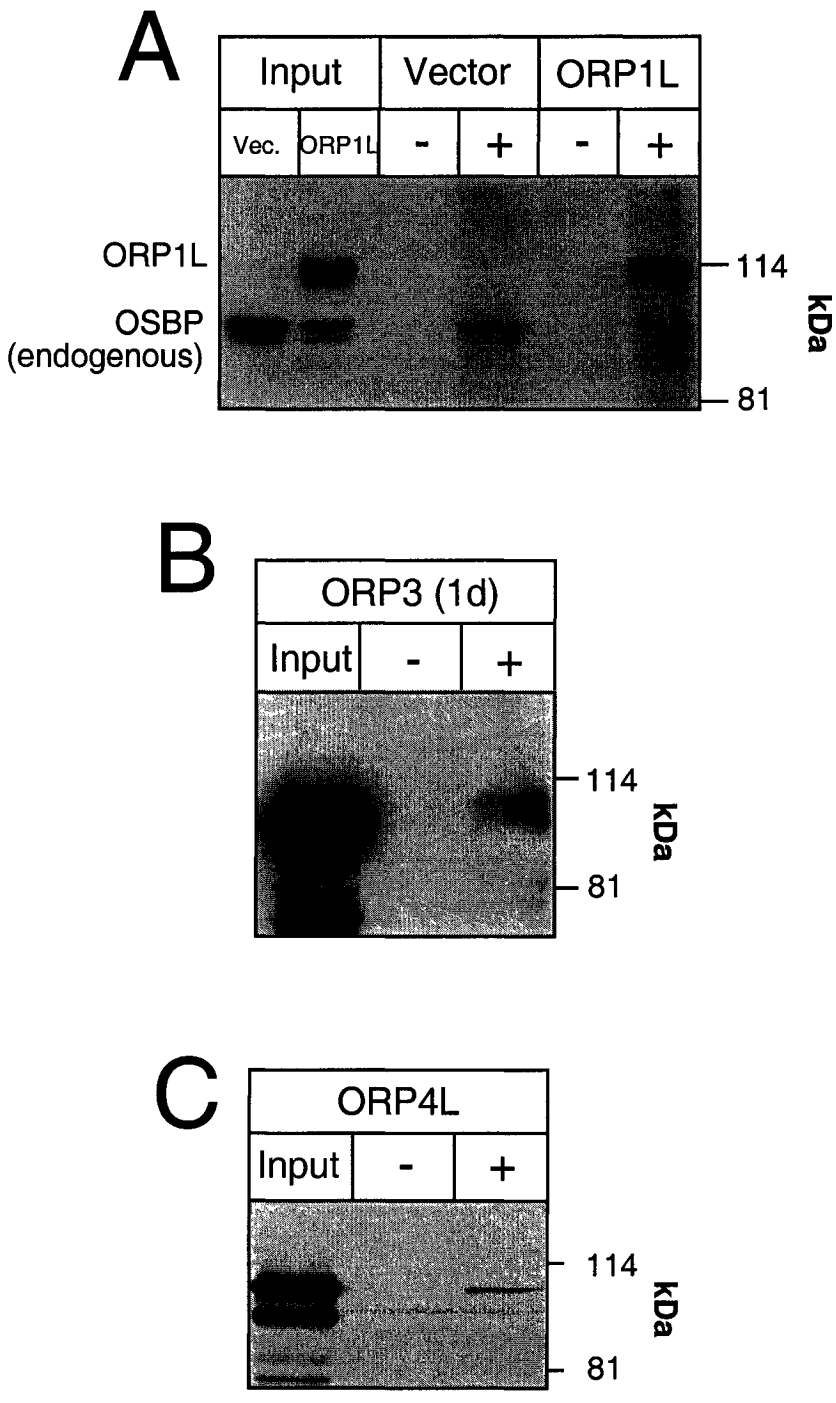
A
Input
Vector
ORP1L
Vec.
ORP1L
-
+
-
+
ORP1L
OSBP
(endogenous)
114
81
kDa
B
ORP3 (1d)
Input
-
+
114
81
kDa
C
ORP4L
Input
-
+
114
81
kDa

Figure 11

heterodimerize with GST-VAP-A. It is also possible that the interaction of the overexpressed ORP with GST-VAP-A is through an endogenous VAP-A-interacting ORP found in the cell extract.

4.3 Co-immunoprecipitation of VAP-A with OSBP and ORP9

4.3.1 Co-immunoprecipitation of VAP-A and OSBP

To confirm the interaction of VAP-A and OSBP seen by yeast two-hybrid and GST pull-down analysis, co-immunoprecipitation studies were carried out. To facilitate this, a polyclonal antibody against full-length VAP-A was prepared. By immunoblotting the VAP polyclonal antibody recognized proteins at 30, 33 and 65 kDa in CHO-K1 cell TX-100 soluble cell extracts (Fig. 12A). Overexpressed VAP-A in CHO-K1 cells co-migrated with the 30 kDa protein, confirming its identity as VAP-A (see Fig. 15). Pre-incubation of the antibody with GST-VAP-A blocked detection of both the 30 and the 33 kDa proteins, but not the 65 kDa protein (Fig. 12A), confirming that the 30 kDa protein was VAP-A and indicating that the 33 kDa protein could be either a modified form of VAP-A or VAP-B [161]. Since overexpressed VAP-A was not observed to undergo a size shift due to phosphorylation or palmitoylation (data not shown), it is assumed that the 33 kDa protein is VAP-B. The 65 kDa protein could be an incompletely dissociated VAP dimer [159], but this is unlikely as it was present under reducing and denaturing conditions and was still detected in the presence of GST-VAP-A.

The VAP-A/OSBP complex was immunoprecipitated from CHO-OSBP cells using the VAP polyclonal antibody and OSBP monoclonal antibody 11H9 (Fig. 12B). The VAP polyclonal antibody precipitated OSBP very weakly compared with direct

Figure 12. Co-immunoprecipitation of VAP and OSBP. *(A)* CHO-K1 cells were subcultured in medium C for 48 h and TX-100 lysates were prepared (Section 3.2.8). Lysates were heated for 5 min in the presence or absence of β-mercaptoethanol, separated by SDS-PAGE and immunoblotted with the VAP polyclonal antibody in the presence or absence of GST-VAP-A (5 μg/ml). *(B)* CHO-OSBP cells were subcultured in medium C for 2 days before harvesting and preparing TX-100 extracts. Lysates (25 μl) were immunoprecipitated with 2 μl of VAP polyclonal or VAP pre-immune serum, or 3 μl of OSBP monoclonal antibody 11H9 or SREBP monoclonal antibody 7B4 (irrelevant monoclonal antibody, negative control) (Section 3.2.9). Samples were separated by SDS 10%-PAGE and immunoblotted with OSBP monoclonal antibody 11H9 or VAP polyclonal antibody. *(C)* CHO-tet-OSBP and CHO-tet-OSBP W174A cells were induced for 72 h in medium A by the removal of doxycycline. Cells cultured in medium A containing 1 μg/ml doxycycline served as negative controls. Co-immunoprecipitation was performed as described in Panel B. Abbreviations: *BME*, β-mercaptoethanol, *PI*, pre-immune serum; *IA*, irrelevant antibody; *IP*, antibody used for immunoprecipitation; *IB*, antibody used for immunoblotting; *NA*; no addition; *DOX*, doxycycline.

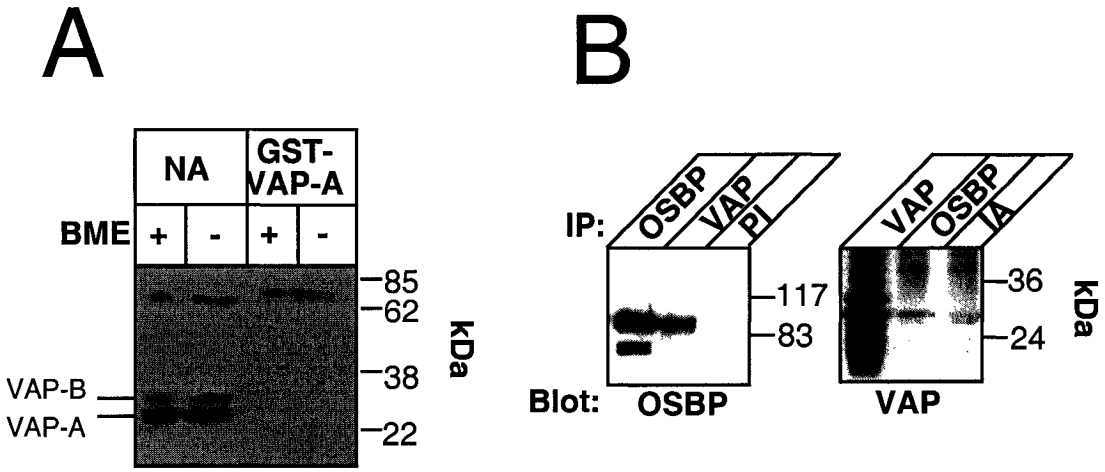
A
NA
GST-VAP-A
BME
+
-
+
-
85
62
38
22
kDa
VAP-B
VAP-A
B
IP:
OSBP
VAP
PI
VAP
OSBP
IA
117
83
36
24
kDa
Blot:
OSBP
VAP

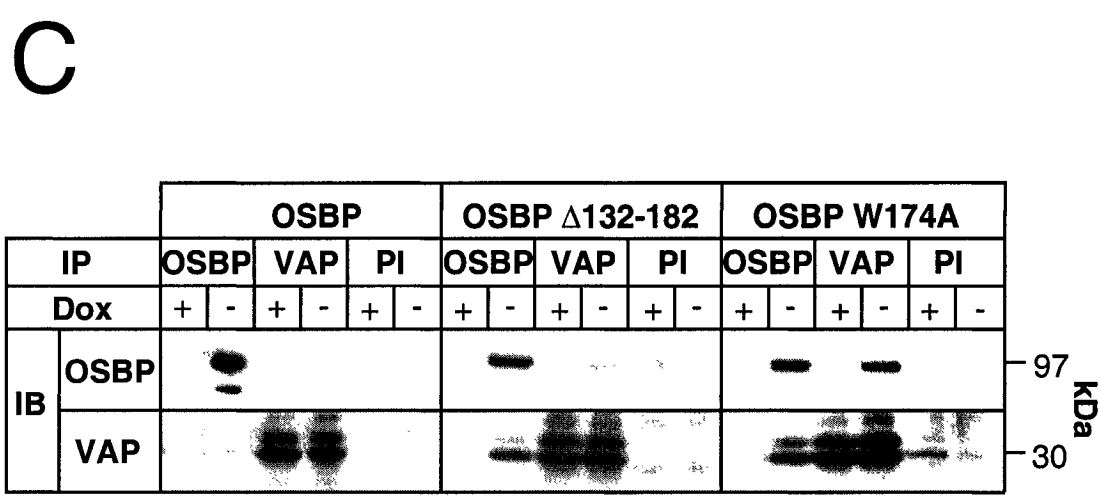
C
OSBP
OSBP Δ132-182
OSBP W174A
IP
OSBP
VAP
PI
OSBP
VAP
PI
OSBP
VAP
PI
Dox
+
-
+
-
+
-
+
-
+
-
+
-
+
-
+
-
+
-
IB
OSBP
VAP
97
30
kDa

Figure 12

immunoprecipitation by 11H9, but as the pre-immune serum did not precipitate OSBP, the interaction was specific. Repeated attempts to co-immunoprecipitate endogenous or overexpressed VAP using monoclonal and polyclonal OSBP antibodies were unsuccessful.

Mutation of the conserved PH domain tryptophan to alanine (W174A) or the deletion of the C-terminal 50 residues of the PH domain (OSBP Δ132-182) resulted in constitutive membrane association of OSBP [143]. Since VAP-A is also membrane localized, its interaction with these mutants was investigated to determine if there was enhanced interaction with VAP-A (Fig. 12C). CHO-tet-off cell lines that express OSBP, OSBP W174A or OSBP Δ132-182 by removal of doxycycline for 3 days were induced approximately 6- to 8-fold in comparison to endogenous OSBP 3 days after removal of doxycycline [143]. No interactions were detected in uninduced cells when immunoprecipitated with the VAP polyclonal or the OSBP monoclonal antibody 11H9. In induced CHO-tet-OSBP cells, co-immunoprecipitation of OSBP by the VAP polyclonal antibody or co-immunoprecipitation of VAP-A by the OSBP monoclonal antibody was very weak and could only be detected with long exposure times (data not shown). In contrast, the VAP polyclonal antibody co-immunoprecipitated OSBP from induced CHO-tet OSBP W174A cells almost as efficiently as the OSBP monoclonal antibody, and the OSBP monoclonal antibody co-immunoprecipitated VAP-A almost as efficiently as the VAP polyclonal antibody. Thus the W174A mutation appears to significantly stabilize the interaction of OSBP and VAP-A. The co-immunoprecipitation of VAP-A and OSBP Δ132-182 from induced CHO-tet OSBP Δ132-182 was intermediate between OSBP W174A and wildtype OSBP. These co-

immunoprecipitations were specific, since no OSBP or VAP-A was detected in samples immunoprecipitated with the VAP pre-immune serum. While the interaction of OSBP with VAP-B has not been characterized, a significant amount of VAP-B was co-immunoprecipitated by the OSBP antibody. The relative level of VAP-A and VAP-B in samples immunoprecipitated with the VAP polyclonal antibody is approximately equal while an enrichment of VAP-A can be see in samples co-immunoprecipitated with the OSBP antibody, suggesting that the interaction may be indirect. Due to difficulties in maintaining expression of OSBP Δ132-182, we focused on the CHO-tet-OSBP and CHO-tet-OSBP W174A cell lines in subsequent experiments (Section 4.5).

4.3.2 Co-immunoprecipitation of VAP-A and ORP9 from CHO-tet-on cell lines

In order to confirm the interaction of VAP-A with ORP9S and ORP9L observed by yeast two-hybrid and GST pull-down analysis, we developed CHO-K1-tet-on cell lines that expressed ORP9S or ORP9L (CHO-tet-ORP9S and CHO-tet-ORP9L) in the presence of doxycycline, and carried out co-immunoprecipitation experiments.

To enable detection of the proteins, C-terminal-V5 epitopes were included and a polyclonal antibody that detects both ORP9 variants was developed. ORP9L, but not ORP9S, was detected in uninduced CHO-tet-on cells (Fig. 13A). Although some or all of this could be due to expression from the tet-regulated promoter, this is not likely, as ORP9 was not detected by Western blotting or immunofluorescence with the V5 antibody, indicating that transfected ORP9L is not expressed. As well, endogenous ORP9L was detected by immunoblotting in CHO-K1 and HEK cells (see Fig. 29). By Western blotting analysis, addition of 2 μg/ml doxycycline to CHO-tet-ORP9L cells for

Figure 13. Inducible expression of ORP9 in CHO-tet-on cells. CHO-tet-ORP9S and CHO-tet-ORP9L cells were subcultured in medium A for 24 h, induced with doxycycline and TX-100 cell lysates were prepared (Section 3.2.8). Samples were resolved by SDS 8%-PAGE (Panel A and immunoblots probed with ORP9 polyclonal antibody in Panels C and D), SDS 7%-PAGE (Panel B) or SDS 10%-PAGE (immunoblots probed with V5 monoclonal antibody in Panels C and D), transferred to nitrocellulose and immunoblotted for ORP9S and ORP9L with the ORP9 polyclonal antibody or V5 monoclonal antibody. *(A)* Comparison of endogenous ORP9 to induced ORP9S and ORP9L after 48 h induction with 2 μg/ml doxycycline. Samples contained 2 μg of protein (except for NA10X which contained 20 μg). *(B)* Comparison of bands detected by ORP9 polyclonal antibody and V5 monoclonal antibody. Samples probed with ORP9 polyclonal antibody contained 2.5 μg protein and samples probed with monoclonal antibody V5 contained 7.5 μg protein. *(C)* CHO-tet-ORP9S and ORP9L cells were induced with 2 μg/ml doxycycline for varying amounts of time. *(D)* CHO-tet-ORP9S and ORP9L cells were induced for 48 h with varying amounts of doxycycline. Abbreviations: *NA*, no addition; *DOX*, doxycycline; *S*, ORP9S; *L*, ORP9L.

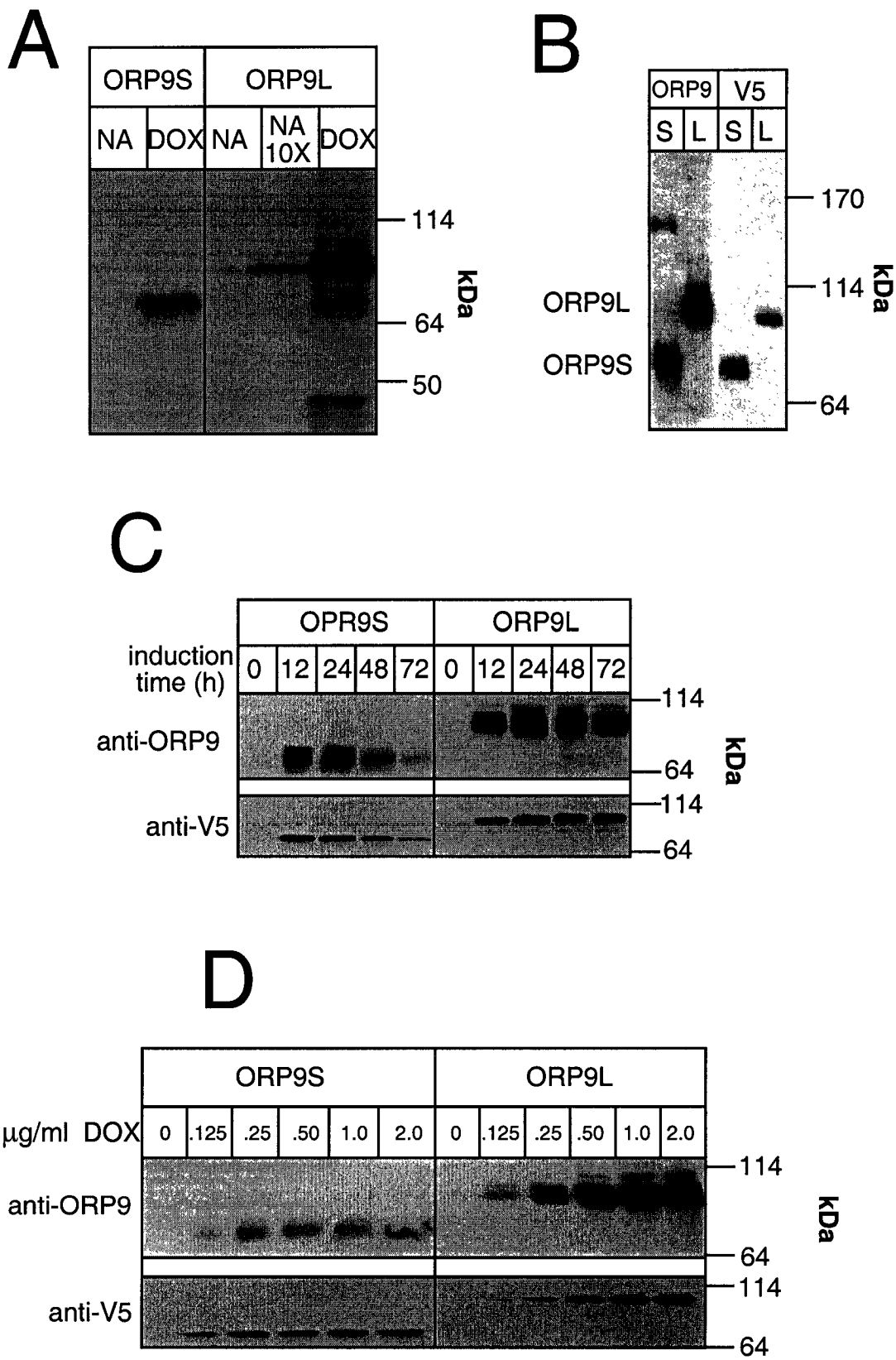
A
ORP9S
ORP9L
NA
DOX
NA
NA 10X
DOX
114
64
50
kDa
B
ORP9
V5
S
L
S
L
170
114
64
kDa
ORP9L
ORP9S
C
induction time (h)
OPR9S
ORP9L
0
12
24
48
72
0
12
24
48
72
anti-ORP9
anti-V5
114
64
114
64
kDa
D
µg/ml DOX
ORP9S
ORP9L
0
.125
.25
.50
1.0
2.0
0
.125
.25
.50
1.0
2.0
anti-ORP9
anti-V5
114
64
114
64
kDa

Figure 13

24 h resulted in a very high induction of ORP9L compared to the uninduced controls (Fig. 13A), while the expression of ORP9S appeared to be slightly lower than that of ORP9L. Both the ORP9-specific polyclonal antibody and the V5 monoclonal antibody were used to detect the ORP9 variants. However, the pattern of proteins detected by these two antibodies was quite different (Fig. 13B). The doublet seen when samples were probed with the V5 monoclonal antibody was also visible when samples were immunoblotted with the ORP9 polyclonal antibody, but the bands were much more diffuse and several slightly higher molecular weight forms were detected by the ORP9 polyclonal antibody. The multiple bands seen in both ORP9S and ORP9L samples immunoblotted with the ORP9 polyclonal antibody, but undetectable by the V5 monoclonal antibody, suggest that ORP9S and ORP9L could be post-translationally modified and the V5 epitope was blocked as a result.

The time course and dose response for ORP9S and ORP9L induction were determined (Fig. 13C and 13D). Maximal induction was seen after 24 h with 2 μg/ml doxycycline in both CHO-tet-ORP9S and ORP9L cell lines, after which time ORP9S expression decreased, while ORP9L expression remained relatively constant (Fig. 13C). Decreased expression of ORP9S was due to extensive cell detachment and death after 24 h. When the dose response of ORP9S and ORP9L induction was determined at 48 h, maximal induction of ORP9S was seen with 0.25 μg/ml doxycycline, while maximal induction of ORP9L was observed with 2 μg/ml doxycycline (Fig. 13D). However, a greater number of CHO-tet ORP9S cells remained alive at 48 h post-induction when induced with lower concentrations of doxycycline, compared to extensive cell death at 48 h post-induction with higher concentrations of doxycycline (see Fig. 29).

ORP9L appeared to be expressed at slightly higher levels than ORP9S, presumably due to the toxicity of ORP9S expression (Fig. 13). The weaker ORP9S signal detected by the ORP9 polyclonal antibody could also be due to fewer epitopes, as the induction level appeared more similar when the proteins were detected with the V5 monoclonal antibody. Only one band was seen in V5-immunoblotted samples in Figures 13C and 13D because 10%-PAGE gels were used, resulting in compression of the bands, while 8%-PAGE gels were used for separation of samples immunoblotted with the ORP9 polyclonal antibody.

In order to confirm the interaction of VAP-A with ORP9S and ORP9L seen by yeast two-hybrid and GST pull-down analysis, co-immunoprecipitation of VAP-A/ORP9 complexes from CHO-tet-ORP9S and ORP9L cell lines was performed (Fig. 14). No interactions were detected in the uninduced control cells when immunoprecipitated with VAP or ORP9 polyclonals or V5 monoclonal antibodies. In induced cells, the VAP antibody was able to co-immunoprecipitate both ORP9S and ORP9L, while the ORP9 antibody co-immunoprecipitated VAP-A. The co-immunoprecipitations were specific, since no ORP9S, ORP9L or VAP-A was detected in samples immunoprecipitated with the ORP9 pre-immune serum. Less VAP-A was co-immunoprecipitated by the V5 antibody (bands become visible after longer exposures) than by the ORP9 polyclonal antibody, even though the V5 monoclonal and ORP9 polyclonal antibodies immunoprecipitated similar amounts of ORP9. It is possible that steric effects associated with the interaction of the V5 monoclonal antibody with ORP9S or ORP9L prevent interaction with VAP-A. A number of ORP9 isoforms are detected by the ORP9 polyclonal antibody that are not detected by the V5 monoclonal antibody (see Fig. 13),

Figure 14. Co-immunoprecipitation of VAP and ORP9 from CHO-tet-on cell lines. CHO-tet-ORP9S (Panel A) and CHO-tet-ORP9L (Panel B) cells were subcultured in medium A for 24 h before inducing with 2 μg/ml doxycycline for 48 h. Uninduced cells served as negative controls. TX-100 cell lysates were prepared (Section 3.2.9) and samples were immunoprecipitated with 0.5 μl of V5 monoclonal antibody, 2 μl of ORP9 polyclonal antibody, 2 μl of VAP polyclonal antibody or 2 μl of ORP9 preimmune serum. Co-immunoprecipitations were performed as described in the legend to Figure 12. Samples were separated by SDS 10%-PAGE and immunoblotted with V5 monoclonal antibody or VAP polyclonal antibody. Abbreviations: *PI*, preimmune serum; *DOX*, doxycycline; *IP*, antibody used for immunoprecipitation; *IB*, antibody used for immunoblotting.

A

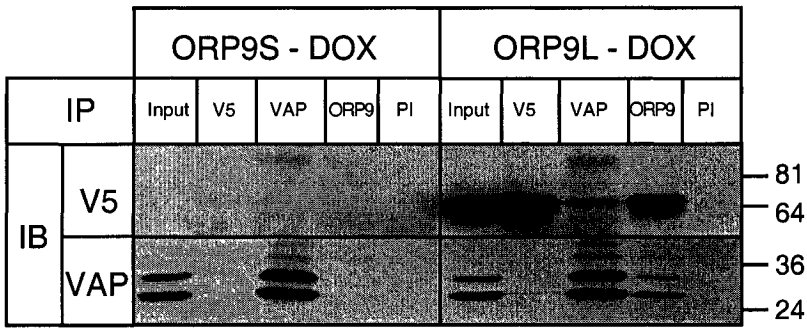
ORP9S - DOX
ORP9L - DOX
IP
Input
V5
VAP
ORP9
PI
Input
V5
VAP
ORP9
PI
IB
V5
VAP
81
64
36
24

B

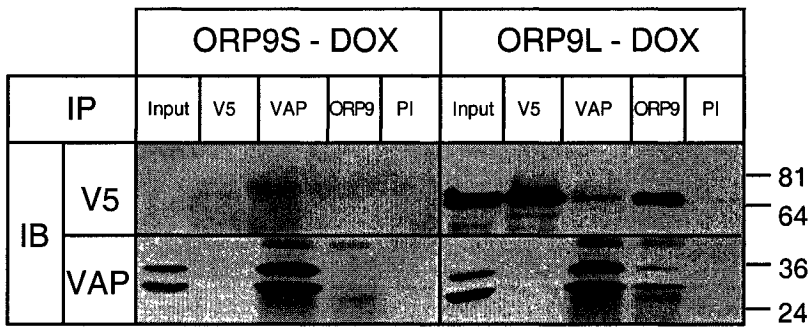
ORP9S - DOX
ORP9L - DOX
IP
Input
V5
VAP
ORP9
PI
Input
V5
VAP
ORP9
PI
IB
V5
VAP
81
64
36
24

Figure 14

thus potential post-translational modification of ORP9 could enhance interaction with VAP-A. VAP-B was also immunoprecipitated by the ORP9 polyclonal antibody.

4.4 Characterization of VAP-A and its role in protein and ceramide trafficking

4.4.1 Cellular localization of endogenous and overexpressed VAP-A

To investigate the localization and function of VAP-A, CHO-K1-tet-on cell lines were developed that inducibly overexpressed VAP-A (CHO-tet-VAP-A) or VAP-A with the transmembrane domain (TM) deleted (CHO-tet-VAP-A ΔTM) in the presence of doxycycline. Overexpression was seen in both cell lines 12 h post-induction with 2 μg/ml doxycycline and levels increased progressively up to 72 h (Fig. 15A). It is notable that overexpression of wildtype VAP-A resulted in a species that co-migrated with VAP-A ΔTM. Since OSBP and VAP-A interact, we investigated whether VAP-A overexpression affected OSBP expression and phosphorylation (Fig. 15B). Based on the relative increase in the upper band of the OSBP doublet, OSBP was hyperphosphorylated in response to the overexpression of VAP-A but not VAP-A ΔTM. This was confirmed by *in vivo* [^{32}P] labelling of cells overexpressing VAP-A and VAP-A ΔTM (data not shown). Expression of VAP-B was not altered by overexpression of VAP-A.

The subcellular localization of overexpressed VAP-A, VAP-A ΔTM and OSBP in CHO-tet-VAP-A and CHO-tet-VAP-A ΔTM cells was determined by fractionation into cytosolic and TX-100-soluble and -insoluble membrane fractions (Fig. 16). Endogenous VAP-A and VAP-B were found primarily in the heavy membrane fractions (0 h). Induction of VAP-A expression caused a progressive increase of VAP-A in all fractions except the cytosol (Fig. 16A). VAP-A ΔTM was found primarily in the cytosol,

Figure 15. Inducible overexpression of VAP-A and VAP-A ΔTM increases OSBP phosphorylation. CHO-tet-VAP-A and CHO-tet-VAP-A ΔTM cells were subcultured in medium A and staggered additions of 2 μg/ml doxycycline were made to induce cells for 12, 24, 48 or 72 h (Panel A) or 12, 24 or 48 h (Panel B). Cells subcultured in medium A for 72 or 96 h served as uninduced controls. TX-100 cell extracts were prepared (Section 3.2.8) and proteins (5 μg) were resolved by SDS 10%-PAGE and immunoblotted with the VAP polyclonal antibody (Panel A) or the pan-ORP polyclonal antibody 170 (Panel B). Abbreviation used: *P*, phosphorylated.

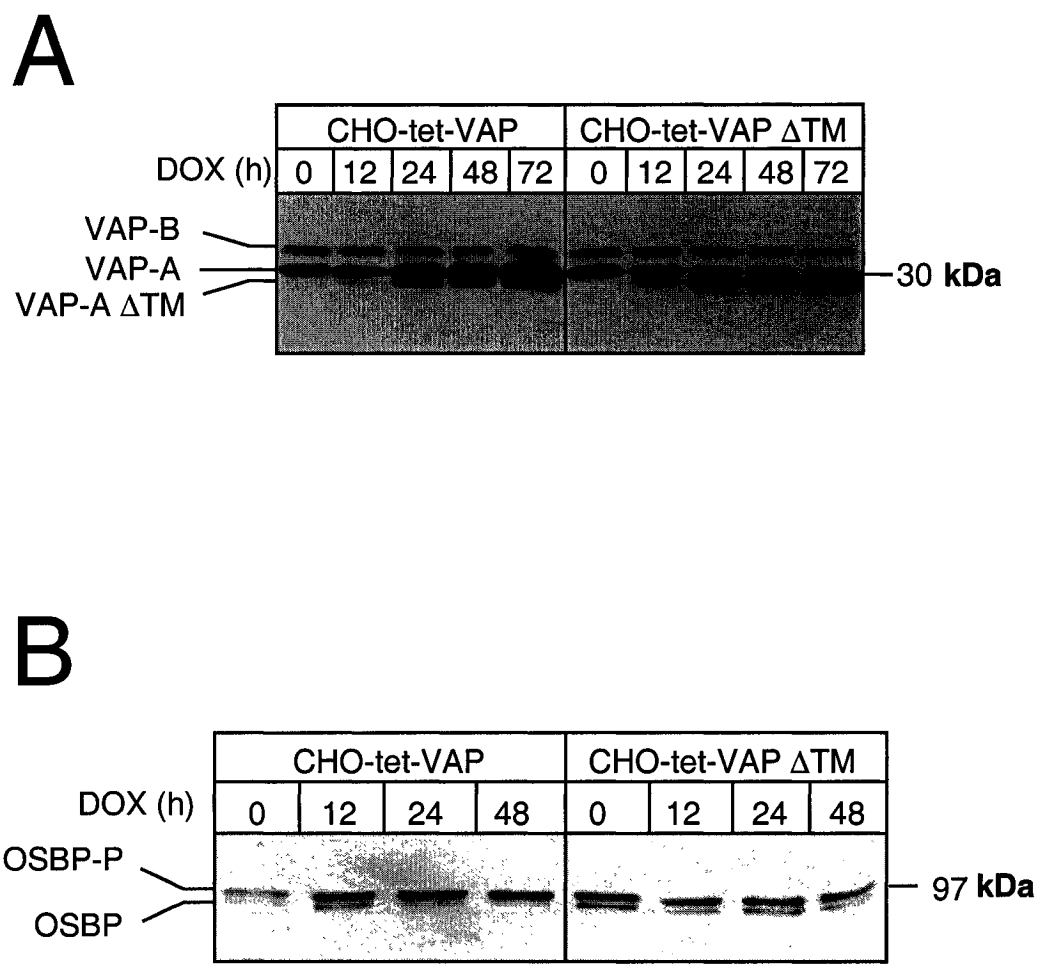
A
CHO-tet-VAP
CHO-tet-VAP ΔTM
DOX (h)
0
12
24
48
72
0
12
24
48
72
VAP-B
VAP-A
VAP-A ΔTM
30 kDa
B
CHO-tet-VAP
CHO-tet-VAP ΔTM
DOX (h)
0
12
24
48
0
12
24
48
OSBP-P
OSBP
97 kDa

Figure 15

Figure 16. Membrane association and TX-100-solubility of endogenous and overexpressed VAP-A. CHO-tet-VAP-A (Panel A) and CHO-tet-VAP-A ΔTM (Panel B) cells were subcultured in medium A and staggered additions of 2 μg/ml doxycycline were made to induce expression for 12, 24 or 48 h. Cells subcultured in medium A for 72 h served as uninduced controls. Cells were harvested, fractionated into light and heavy membrane fractions and further fractionated into TX-100-soluble and -insoluble fractions (Section 3.2.12). Proteins (20 μg) were resolved by SDS 10%-PAGE and immunoblotted with pan-ORP polyclonal antibody 170 or the VAP polyclonal antibody.

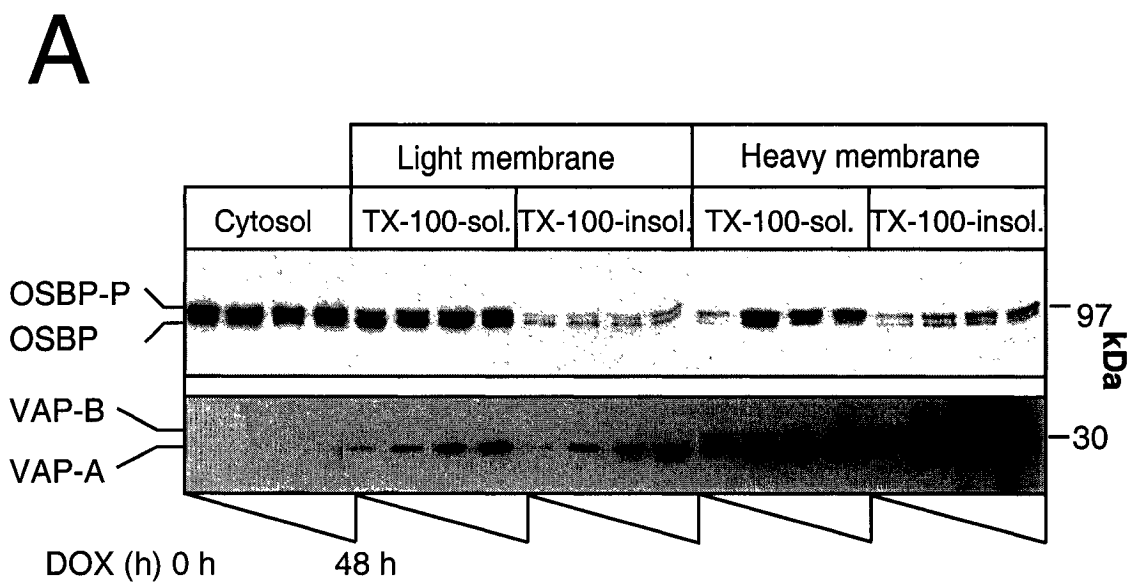
A
Light membrane
Heavy membrane
Cytosol
TX-100-sol.
TX-100-insol.
TX-100-sol.
TX-100-insol.
OSBP-P
OSBP
VAP-B
VAP-A
97
30
kDa
DOX (h) 0 h
48 h

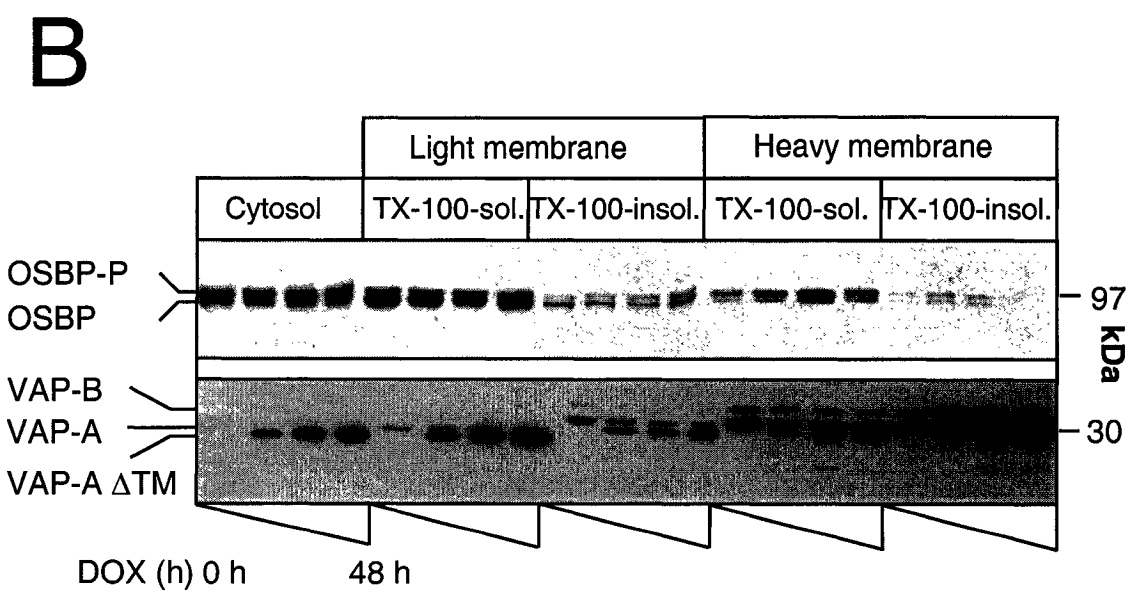
B
Light membrane
Heavy membrane
Cytosol
TX-100-sol.
TX-100-insol.
TX-100-sol.
TX-100-insol.
OSBP-P
OSBP
VAP-B
VAP-A
VAP-A ΔTM
97
30
kDa
DOX (h) 0 h
48 h

Figure 16

although a substantial amount was also found in the TX-100-soluble fraction of both heavy and light membranes (Fig. 16B). Although OSBP was primarily cytosolic in both induced and uninduced cells, induction of VAP-A or VAP-A ΔTM expression increased the proportion of OSBP in the TX-100 soluble fraction of heavy membranes. Induction of VAP-A or VAP-A ΔTM expression did not alter the expression or localization of endogenous VAP-B.

The localization of endogenous VAP in CHO-K1 cells, as well as overexpressed VAP-A and VAP-A ΔTM in CHO-tet-on cells, was monitored by indirect immunofluorescence (Fig. 17). Since the VAP polyclonal antibody recognizes both VAP-A and VAP-B, these two proteins cannot be distinguished from each other by immunofluorescence, hence the proteins detected by the VAP polyclonal antibody in immunofluorescence experiments will be referred to as VAP. In CHO-K1 and uninduced CHO-tet-on cells, endogenous VAP was localized to small vesicles in a diffuse ER-like network that was clustered around the Golgi apparatus and nucleus (Fig. 17A). This VAP-A expression by the addition of doxycycline to CHO-tet-VAP-A cells resulted in a pronounced increase in localization to the ER (Fig. 17B), as judged by co-localization with PDI (Fig. 18), a marker of the ER lumen. A significant portion of overexpressed VAP-A also co-localized with the Golgi apparatus marker FITC-lentil lectin. As expected, overexpressed VAP-A ΔTM was primarily cytosolic, although there was significant localization to the PM (Fig. 17B). Overexpression of VAP-A or VAP-A ΔTM did not alter the staining pattern of FITC-lentil lectin, indicating that the structure of the Golgi apparatus was not altered. Collectively these results show that in CHO-K1 cells,

Figure 17. Immunofluorescence localization of endogenous and overexpressed VAP-A and VAP-A ΔTM. *(A)* CHO-K1 cells were cultured on glass coverslips in medium C for 48 h before treating with 2.5 μg/ml 25OH for 1 h. Cells were fixed, permeabilized and processed for immunofluorescence (Section 3.2.6). Endogenous VAP was detected with VAP polyclonal antibody and GAR-FITC. *(B)* CHO-tet-VAP-A and CHO-tet-VAP-A ΔTM cells were cultured on glass coverslips in Medium A for 24 h before inducing expression with 2 μg/ml doxycycline for 24 h. Cells were fixed, permeabilized and processed for immunofluorescence (Section 3.2.6) using the VAP polyclonal antibody in conjunction with GAR-TXR (red). Lentil lectin-FITC (green) was used to identify the Golgi apparatus. Cells were photographed using a Zeiss Axiovert 100M Laser Scanning Confocal microscope 510 with a 100X objective. Images are single 0.2 μm slices. Abbreviations: *NA*, no addition; *DOX*, doxycycline.

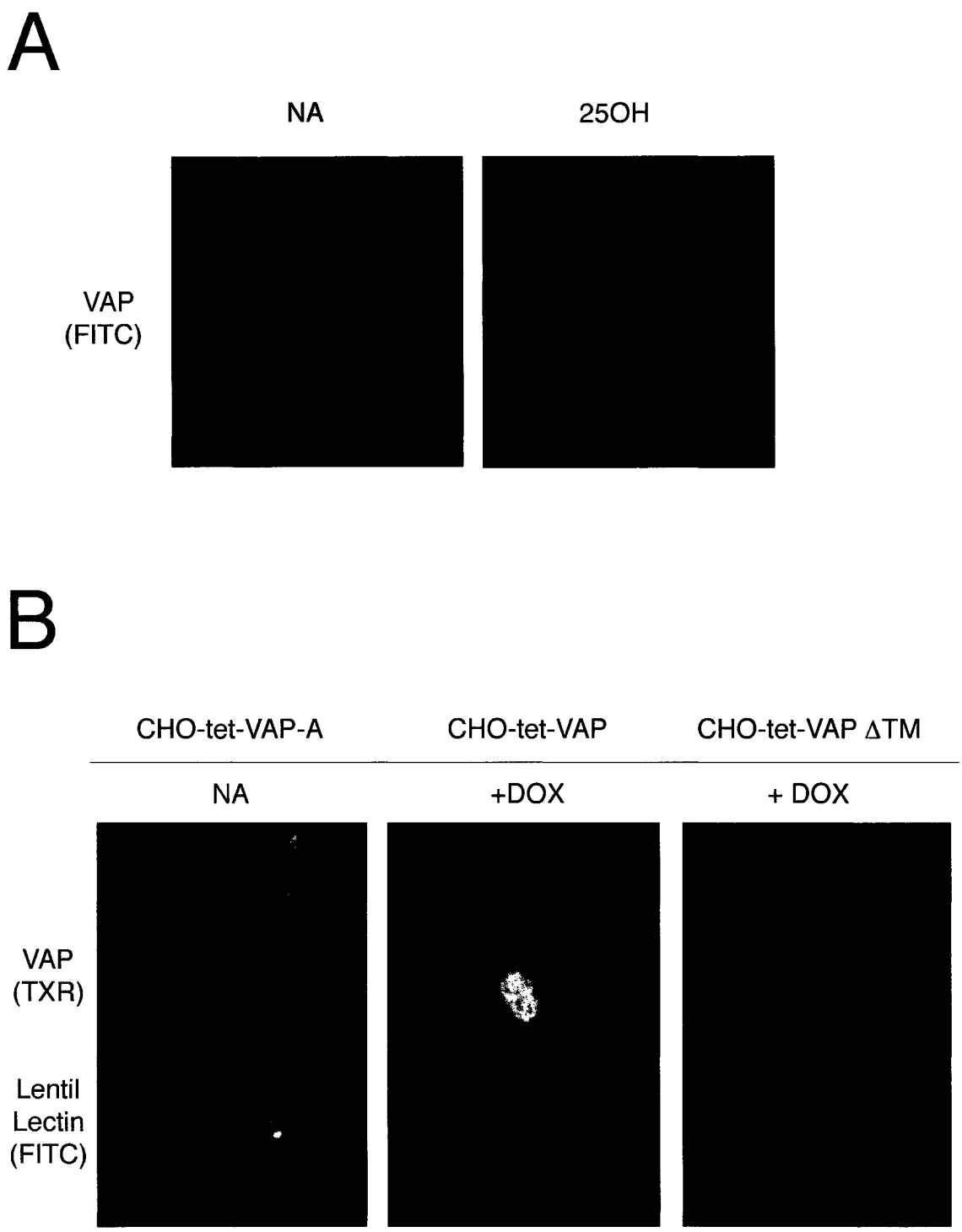
A
NA
25OH
VAP
(FITC)
B
CHO-tet-VAP-A
CHO-tet-VAP
CHO-tet-VAP ΔTM
NA
+DOX
+ DOX
VAP
(TXR)
Lentil
Lectin
(FITC)

Figure 17

Figure 18. Overexpressed VAP-A co-localizes with PDI in the ER. CHO-tet-VAP-A cells were cultured on glass coverslips in Medium A for 24 h before inducing with 2 μg/ml doxycycline for 48 h. Cells were fixed, permeabilized and processed for immunofluorescence using the VAP polyclonal antibody in conjunction with GAR-FITC and a PDI monoclonal antibody in conjunction with GAM-TXR (Section 3.2.6). Cells were photographed using a Zeiss Axiovert 100M Laser Scanning Confocal Microscope 510 with a 100X objective. Images are a projection of six 0.2 μm sections. Abbreviation used: *NA*, no addition.

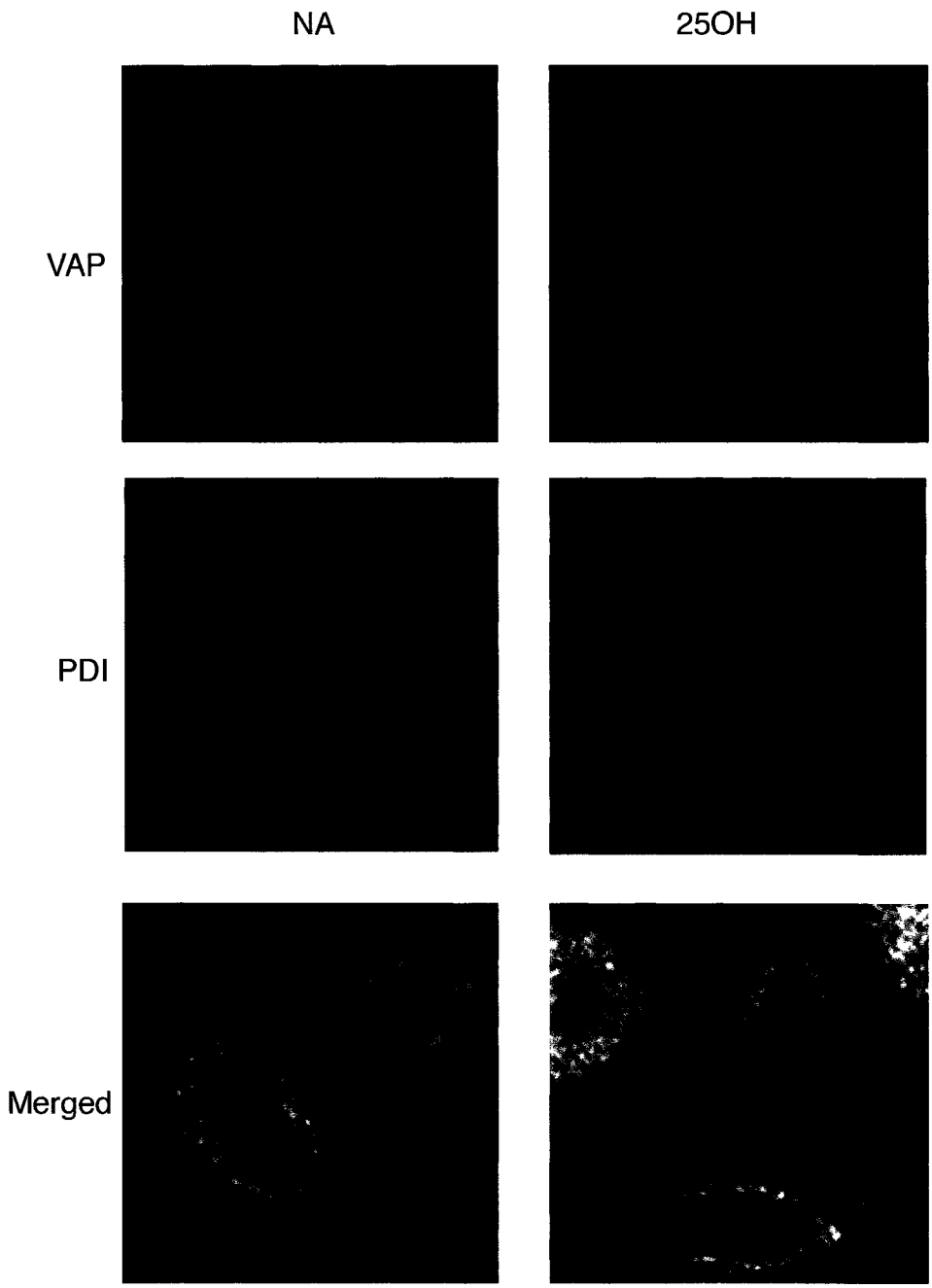

Figure 18

VAP-A is localized to TX-100 soluble and insoluble regions of the ER by the C-terminal TM domain.

4.4.2 Association of VAP-A with detergent-resistant membrane domains

Due to the localization of VAP-A in TX-100 resistant membrane fractions (Fig. 16), and its potential involvement in cholesterol and SM metabolism through its interaction with OSBP, the association of VAP-A with caveolae/DIGs in CHO-K1 cells was investigated (Fig. 19). CHO-K1 cells were treated with colchicine, taxol, nocodazole, lovastatin, cyclodextrin or bacterial SMase to alter intracellular cholesterol trafficking and synthesis, SM content and vesicle transport (Fig. 19A). Cells were harvested, lysed in Hepes buffer containing TX-100 at 4°C and subjected to centrifugation to separate detergent-insoluble membrane domains from soluble proteins. Distribution of VAP-A between the supernatant and pellet was unaltered in response to any of the treatments described above, indicating that VAP-A solubility was not affected by disrupting sterol or SM metabolism, or microtubule organization. While this demonstrated that the TX-100 solubility was not affected by sterol or SM composition, it did not address the involvement of VAP-A in the formation of DIGs or its presence in other types of detergent-resistant membranes. These domains are assembled in the Golgi apparatus prior to export to the PM, thus it is possible that VAP-A plays a role in their formation that could not be detected by the experiment described in Figure 19A. To address this issue, a light membrane fraction containing microsomes and nascent DIGs was prepared from CHO-K1 cells, solubilized with different detergents and separated into soluble and pellet fractions by centrifugation (Fig. 19B). Supernatant and pellet fractions were analyzed for

Figure 19. Endogenous VAP-A does not associate with caveolae. *(A)* CHO-K1 cells were subcultured in medium C for 48 h before treating with lovastatin (5 μM for 12 h), nocodazole (20 μg/ml for 1 h), taxol (20 μM for 1 h), colchicine (2 μM for 1 h), bacterial SMase (50 mU/ml for 1 h) or cyclodextran (5.0 mM for 45 min). Cells were harvested in PBS, collected by centrifugation, lysed (10 mM Hepes, 50 mM KCl, 1 mM dithiothreitol, 1 mM EDTA, 1% TX-100 and protease inhibitors) for 15 min on ice and subjected to centrifugation at 400,000*g* for 15 min. Proteins (5 μg) were separated by SDS 12%-PAGE and immunoblotted with the VAP polyclonal antibody. *(B)* CHO-K1 cells were subcultured in medium A for 48 h before preparing a light membrane fraction (Section 3.2.12). Membranes were solubilized in different detergents as indicated, and soluble and insoluble fractions were isolated by centrifugation at 400,000*g* for 15 min. Pellets were resuspended in a volume equal to the supernatant (50 μl) and samples (20 μl) were separated by SDS 12%-PAGE and immunoblotted with VAP and caveolin 1 polyclonal antibodies. *(C)* CHO-K1 cells were labeled with 5 μCi/dish [^{3}H]cholesterol for 24 h, harvested and separated on a discontinuous sucrose gradient (Section 3.2.13). Fractions from the gradient (20 μl) were separated by SDS 12%-PAGE and immunoblotted with VAP and caveolin 1 polyclonal antibodies, and for OSBP with pan-ORP polyclonal antibody 170. Fraction 1 contains the bottom fraction and as such contains all non-raft material. Abbreviations: *NA*, no addition; *col*, colchicine; *tax*, taxol; *noc*, nocodazole; *lov*, lovastatin; *CD*, cyclodextran; *Sm*, bacterial SMase.

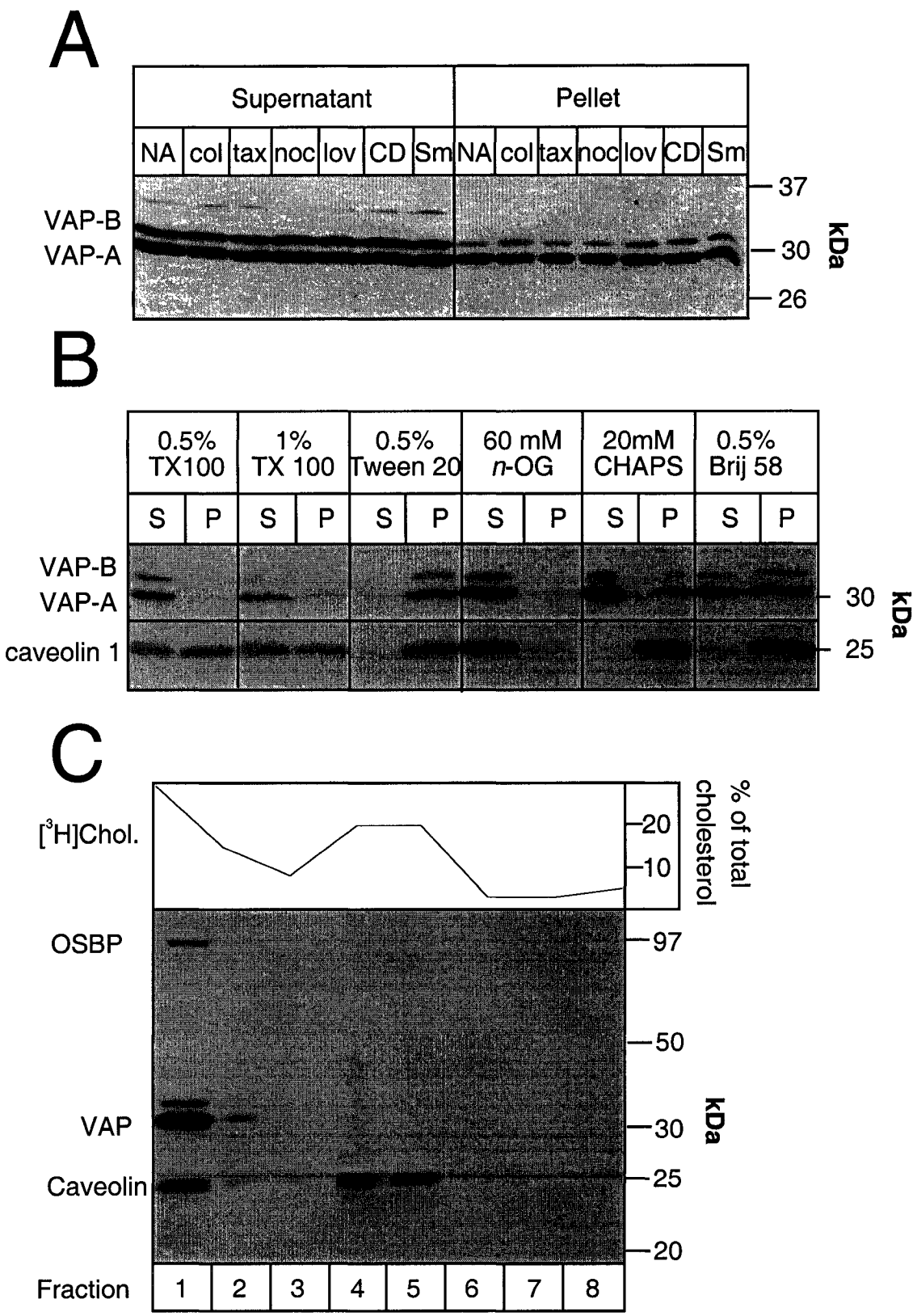
A
Supernatant
Pellet
NA col tax noc lov CD Sm NA col tax noc lov CD Sm
VAP-B
VAP-A
37
30
26
kDa
B
0.5% TX100
1% TX 100
0.5% Tween 20
60 mM n-OG
20mM CHAPS
0.5% Brij 58
S P S P S P S P S P S P
VAP-B
VAP-A
caveolin 1
30
25
kDa
C
[3H]Chol.
20
10
% of total cholesterol
OSBP
97
50
VAP
30
Caveolin
25
20
kDa
Fraction
1 2 3 4 5 6 7 8

Figure 19

VAP-A and caveolin by Western blotting. While VAP-A and caveolin co-fractionated to a limited extent in all detergents, the differences in fractionation in detergents such as TX-100 and CHAPS suggests that they do not extensively co-localize.

Finally, to determine if the limited amount of VAP-A that co-fractionated with caveolin 1 in Figure 19B was associated with caveolae/DIGs, CHO-K1 cell extracts were separated on discontinuous sucrose gradients (Fig. 19C). This fractionation technique allows for more precise co-localization of candidate proteins to DIGs/caveolae. CHO-K1 cells were pre-labeled for 24 h with [^{3}H]cholesterol in order to enable localization of caveolae on the sucrose gradients. TX-100 extracts of CHO-K1 cells were subjected to centrifugation and fractions were collected by needle puncture of the centrifuge tube. The fractions were then analyzed by Western blotting for the presence of OSBP, caveolin 1 and VAP-A and scintillation counting to detect [^{3}H]cholesterol. Although some VAP-A was in detergent resistant fractions (Fig. 19A and 19B), the absence of VAP-A in the caveolin 1/[^{3}H]cholesterol-enriched fractions of the sucrose gradient suggests that VAP-A does not localize to DIGs/caveolae. OSBP was also not detected in the caveolin 1/[^{3}H]cholesterol-enriched fractions.

4.4.3 Interaction of VAP-A with microtubules

Several lines of evidence indicate that VAP-A interacts with the microtubule network. A mouse orthologue of VAP-A co-localized with microtubules by electron microscopy [155], and a *D. melanogaster* orthologue has been shown to bind tubulin and regulate membrane contacts with the microtubule network [154]. In addition, the detergent insolubility of VAP-A (Fig. 19) indicated that it may be associated with

cytoskeletal elements. Therefore, the binding of VAP-A to microtubules was investigated (Fig. 20). A TX-100-soluble cell extract of CHO-K1 cells was incubated with tubulin. Samples were layered onto a cushion buffer, subjected to centrifugation and the supernatant (unbound proteins) and pellet (microtubule binding proteins) fractions analyzed by Western blotting for VAP-A (Fig. 20A). Although the amount of VAP-A in the pellet fraction in the presence of tubulin increased slightly compared to samples without tubulin (Fig. 20A), this appeared to be non-specific. Control experiments were performed (Fig. 20B) in which binding of a positive control (MAP, supplied with the kit) and negative control (BSA, supplied with the kit) to tubulin was investigated. A small amount of BSA was found in the pellet both in the presence and absence of tubulin indicating that some low-level non-specific binding is inherent to the assay. The localization of tubulin to the pellet fraction was confirmed, as was the appropriate localization of the positive control MAP.

4.4.4 Role of VAP-A in ceramide trafficking

Ceramide is synthesized in the ER and then exported to the Golgi apparatus where it is a precursor in the synthesis of SM and glycosphingolipid (reviewed in [173]). OSBP is implicated in this trafficking pathway (Section 1.1.3), as is its phosphorylation state (Section 1.1.4). Overexpression of VAP-A caused hyperphosphorylation of OSBP, potentially implicating VAP-A in the regulation of SM through its effects on OSBP (Section 4.4.1). Furthermore, VAP-A and VAP-B have been implicated in vesicle trafficking between the ER and Golgi apparatus [151,159-162]. These findings prompted us to investigate ceramide trafficking in the CHO-tet-VAP-A and VAP-A ΔTM cells

Figure 20. Lack of association of VAP-A with microtubules. Samples were incubated with (+ Tubulin) and without tubulin (NA), layered onto 100 µl of cushion buffer in a 500 µl centrifuge tube and subjected to centrifugation at 50,000*g* for 80 min. The supernatant (50 µl) and cushion buffer fractions were removed and the pellets resuspended in 50 µl G-PEM buffer (Section 3.2.14). Samples (30 µl) were separated by SDS 10%-PAGE. *(A)*. Binding of VAP-A in TX-100 extracts of CHO-K1 cells (10, 25 and 50 µg protein) to tubulin was assayed as described above. Proteins were transferred to nitrocellulose and analyzed by immunoblotting with the VAP polyclonal antibody. *(B)* Positive and negative control proteins supplied by the manufacturer were treated as described above and proteins detected by Coomassie Blue staining. Abbreviations: *S*, supernatant; *P*, pellet.

A

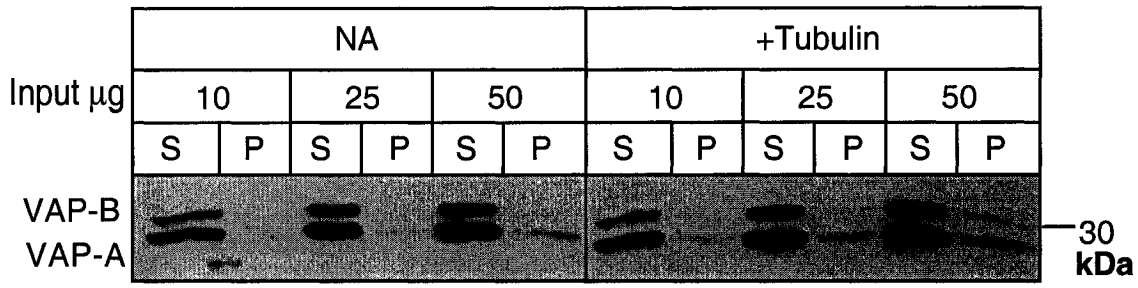
NA
+Tubulin
Input µg
10
25
50
10
25
50
S
P
S
P
S
P
S
P
S
P
S
P
VAP-B
VAP-A
30
kDa

B

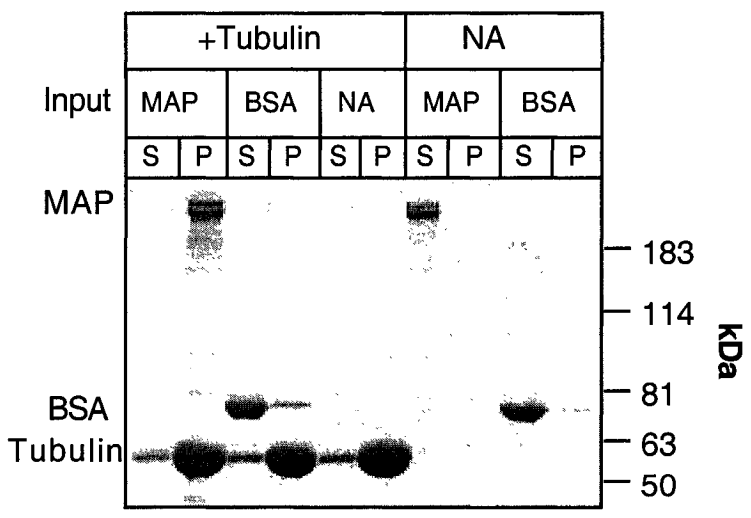
+Tubulin
NA
Input
MAP
BSA
NA
MAP
BSA
S
P
S
P
S
P
S
P
S
P
MAP
BSA
Tubulin
183
114
81
63
50
kDa

Figure 20

using C_5-DMB-ceramide, a fluorescent analogue that mimics transport of endogenous ceramide [148]. Cells were loaded with a C_5-DMB-ceramide/BSA complex at 4°C for 30 min and then shifted to 37°C for 5 or 45 min to allow transport (Fig. 21). Induction of VAP-A or VAP-A ΔTM did not cause any detectable differences in initial ceramide loading at 4°C (0 min) or trafficking to the Golgi apparatus after 5 or 45 min. As C_5-DMB-ceramide cannot be fixed sufficiently to withstand subsequent antibody incubations and washes to detect overexpressed VAP-A or VAP-A ΔTM, we were unable to visualize VAP and C_5-DMB-ceramide in the same cell. However, cells cultured in parallel and immunostained for overexpressed VAP-A or VAP-A ΔTM confirmed that more than 75% of cells were overexpressing.

4.4.5 Role of VAP-A in VSVG-GFP trafficking

The role of VAP-A and VAP-A ΔTM in protein trafficking was also investigated using VSVG-GFP. At 40°C, folding of VSVG-GFP is blocked at a late step and retained in the ER [174]. Correct folding of the protein, and subsequent transport to the Golgi apparatus and PM, occurs at 32°C and requires PDI, GRP78/BiP and calnexin [175]. CHO-tet-VAP-A and VAP-A ΔTM cells were transiently transfected with VSVG-GFP at 40°C for 12 h and then shifted to 32°C for varying amounts to time to allow transport from the ER (Fig. 22). At the non-permissive temperature of 40°C, VSVG-GFP was ER-localized in uninduced CHO-tet-VAP-A cells as well as in induced CHO-tet-VAP-A and VAP-A ΔTM cells. After 30 min at 32°C, VSVG-GFP had exited the ER and was strongly localized to the Golgi apparatus, but weakly localized to the PM in uninduced CHO-tet-VAP-A cells, and induced CHO-tet-VAP-A and VAP ΔTM cells.

Figure 21. Trafficking of C_5-DMB-ceramide was not altered by overexpression of VAP-A or VAP-A ΔTM. CHO-tet-VAP and CHO-tet-VAP ΔTM cells were cultured in Medium A for 24 h before inducing expression with 2 μg/ml doxycycline for 48 h. Cells were loaded with C_5-DMB-ceramide (Section 3.2.10) and either fixed immediately or shifted to 37°C for 5 or 45 min (Section 3.2.6). Photographs were taken immediately with an Axiovert 200M fluorescence microscope equipped with a 100X objective and an Axiocam HRC image capture system. Abbreviations: *NA*, no addition; *DOX*, doxycycline.

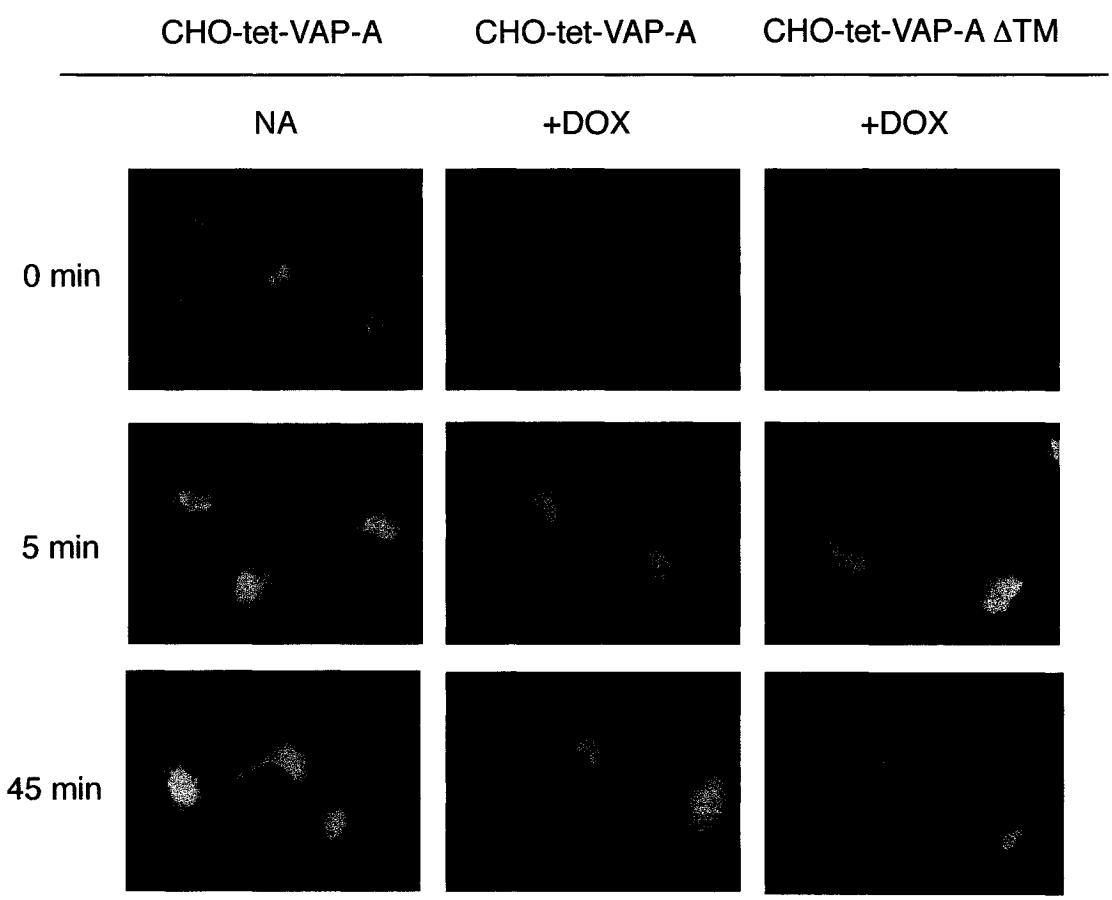
CHO-tet-VAP-A
CHO-tet-VAP-A
CHO-tet-VAP-A ΔTM
NA
+DOX
+DOX
0 min
5 min
45 min

Figure 21

Figure 22. Overexpression of VAP-A and VAP-A ΔTM did not affect transport of VSVG-GFP from the ER to the Golgi apparatus. CHO-tet-VAP and CHO-tet-VAP ΔTM cells were cultured on glass coverslips in Medium A for 24 h before inducing expression with 2 μg/ml doxycycline for 36 h and transiently transfecting with pVSVG-GFP for 12 h (Section 3.2.11). Cells were shifted to 32°C for 30 min, fixed, permeabilized and processed for immunofluorescence using the VAP polyclonal antibody in conjunction with Alex-fluor 555 (Section 3.2.6). Cells were photographed using a Zeiss Axiovert 100M Laser Scanning Confocal Microscope 510 with a 100X objective. Images are single 0.2 μm slices. Abbreviations: *NA*, no addition; *DOX*, doxycycline.

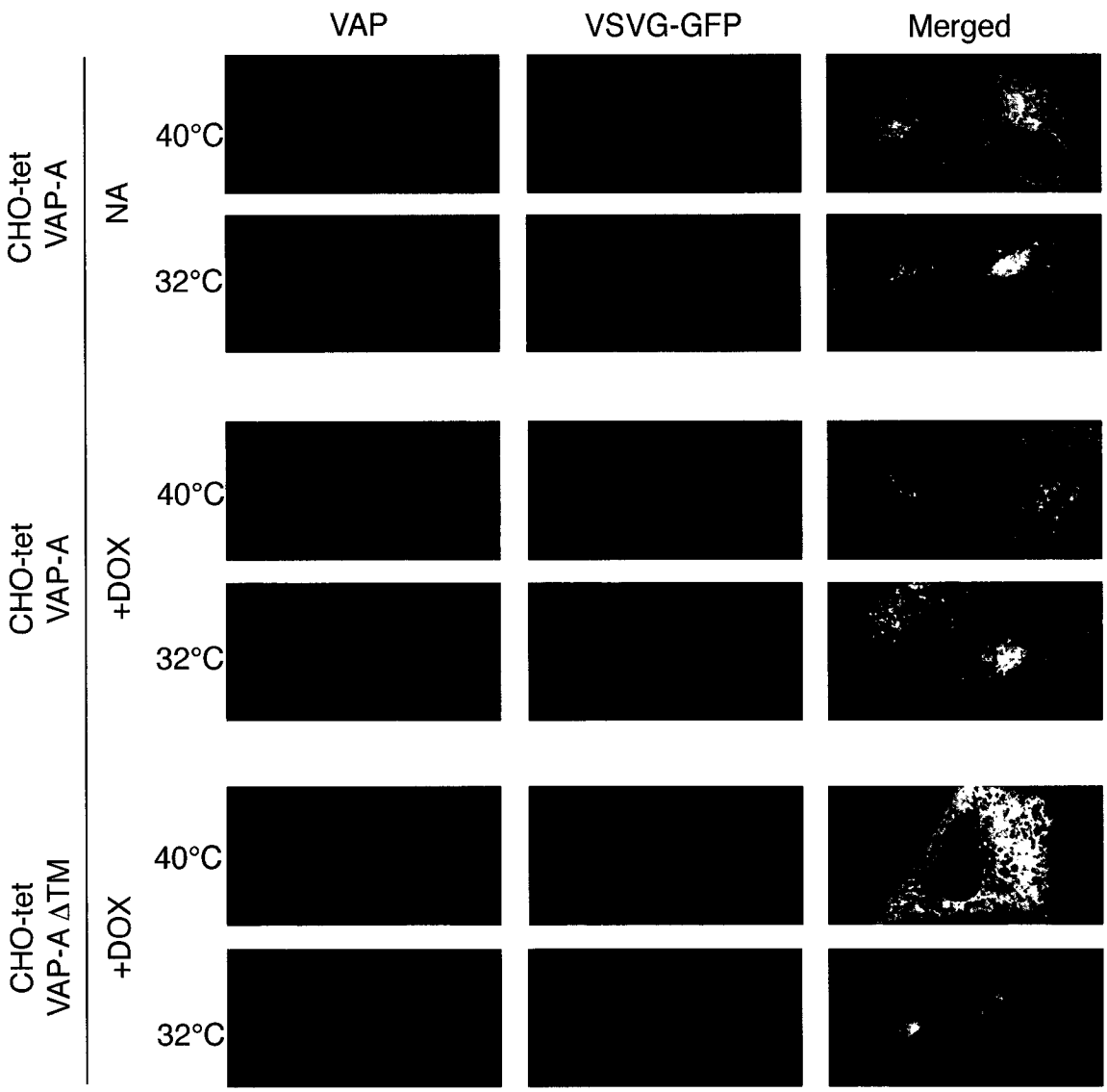
VAP
VSVG-GFP
Merged
CHO-tet VAP-A
NA
40°C
32°C
CHO-tet VAP-A
+DOX
40°C
32°C
CHO-tet VAP-A ΔTM
+DOX
40°C
32°C

Figure 22

Localization of VSVG-GFP in uninduced CHO-tet-VAP-A ΔTM cells was similar (data not shown). Thus, over-expression of VAP-A or VAP-A ΔTM did not affect export of VSVG-GFP from the ER to the Golgi apparatus and PM.

4.5 Role of VAP-A/OSBP interaction in ER export

4.5.1 Overexpression of OSBP W174A alters ER structure

Although the PH domain is not required for the interaction of OSBP with VAP-A (Fig. 8), this domain regulates OSBP localization to the Golgi apparatus and thus opposes ER localization of OSBP via its interaction with VAP-A. To investigate the role of the OSBP PH domain with respect to VAP-A interaction, CHO-tet-off cell lines that overexpressed wildtype or PH domain mutants of OSBP (CHO-tet-OSBP, CHO-tet-OSBP W174A and CHO-tet-OSBP Δ132-182) were developed and the site of interaction of VAP with OSBP and OSBP W174A was determined by indirect immunofluorescence (Fig. 23). In uninduced CHO-tet-OSBP cells, VAP was localized to an ER/vesicular compartment (Fig. 23 left panel), similar to the localization seen in CHO-K1 cells (Fig. 17). Localization of VAP in uninduced CHO-tet-OSBP W174A cells was similar (data not shown). Induction of OSBP expression by the removal of doxycycline did not alter VAP localization, and VAP and OSBP co-localized in the ER and Golgi apparatus (Fig. 23, middle panel). The partial localization of overexpressed OSBP to the ER indicates that some of the cytoplasmic/vesicular localization observed for endogenous OSBP may be weak ER localization. Induction of OSBP W174A resulted in dramatic re-localization of VAP to vesicle-like structures where it co-localized with OSBP W174A (Fig. 23, right

Figure 23. Co-localization of VAP with OSBP and OSBP W174A. CHO-tet-OSBP and CHO-tet-OSBP W174A cells were subcultured on glass coverslips in Medium A with or without doxycycline for 24 h before changing the media (medium A ± doxycycline) to remove residual doxycycline and induce expression of OSBP and OSBP W174A for 72 h. Cells were fixed, permeabilized and processed for immunofluorescence using the VAP polyclonal antibody in conjunction with GAR-FITC (green) and the OSBP monoclonal antibody 11H9 in conjunction with GAM-TXR (red) (Section 3.2.6). Cells were photographed using a Zeiss Axiovert 100M Laser Scanning Confocal Microscope 510 with a 100X objective. Images are single 0.2 μm slices. Abbreviations: *NA*, no addition; *DOX*, doxycycline.

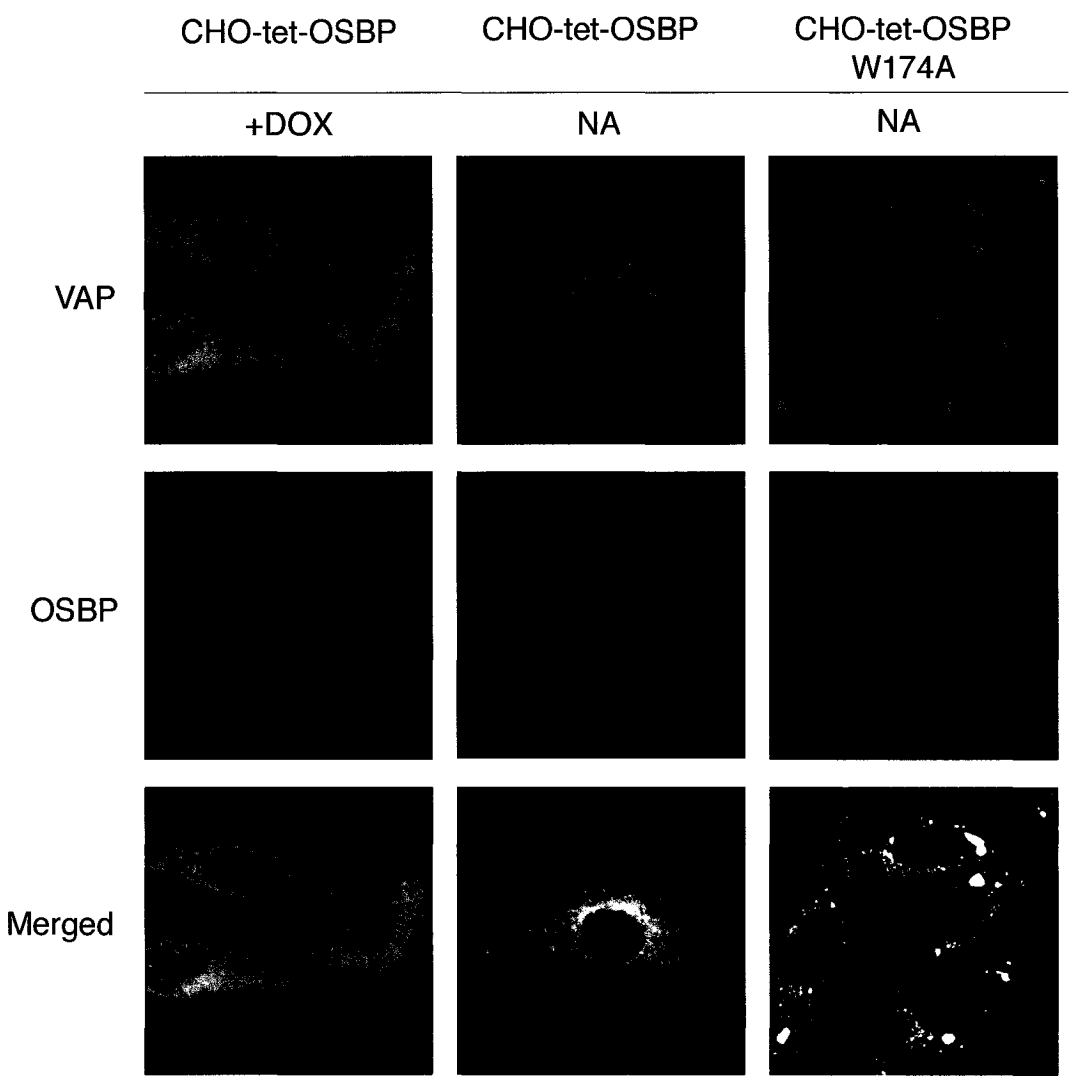
CHO-tet-OSBP
CHO-tet-OSBP
CHO-tet-OSBP W174A
+DOX
NA
NA
VAP
OSBP
Merged

Figure 23

panel). The co-localization of VAP and OSBP W174A in these structures confirms the enhanced interaction seen by co-immunoprecipitation (Fig. 12C).

The association of VAP and OSBP W174A with these unusual structures suggests they are modified organellar membranes, possibly ER-derived. In order to determine their origin, indirect co-immunofluorescence of VAP or OSBP in conjunction with a number of organellar markers was performed (Fig. 24). Localization of giantin, a marker of the Golgi apparatus [176], and β-COP, a coatomer protein found primarily in the Golgi apparatus [177], were unaltered in induced CHO-tet-OSBP W174A cells, indicating that the structures were not Golgi-derived and that induction of OSBP W174A did not alter the structure of the Golgi apparatus. However, ARF-GAP1, which is involved in COPI-mediated vesicle budding and cargo recruitment [178], co-localized with OSBP W174A in the membrane inclusions. p58, a marker of the ERGIC [179], and Sec31, a marker of the transitional ER and a component of the COPII coat machinery [180], were distributed throughout the cell in small punctate structures. Although some staining for each marker overlapped with the membrane inclusions, their localization was unaltered by induction of OSBP W174A. The lumenal ER protein PDI co-localized with VAP in the membrane inclusions, as did an antibody against the KDEL sequence that detects GRP94 and GRP78/BiP, lumenal ER-localized molecular chaperones required for protein folding [181]. As overall cellular morphology apart from the ER was unaltered in the OSBP-tet-W174A cells and ER resident proteins were localized to the structures induced by OSBP W174A expression, it is most likely that the membrane inclusions correspond to distorted regions of the ER membrane. It is noteworthy that these ER-

Figure 24. Expression of OSBP W174A induces irregular ER-derived membrane structures. CHO-tet-OSBP W174A cells were cultured on glass coverslips in medium A and induced by the removal of doxycycline for 72 h. Cells were immunostained with giantin, p58, Sec31 or ARF-GAP1 polyclonal antibodies in conjunction with Alexa–fluor GAR-488 (green) followed by monoclonal OSBP antibody 11H9 in conjunction with Alexa–fluor GAM-555 (red), or the VAP polyclonal antibody in conjunction with Alexa–fluor GAR-555 (red) followed by PDI or GRP94/BIP monoclonal antibodies in conjunction with Alexa–fluor GAM-488 (green) (Section 3.2.6). Cells were photographed using a Zeiss Axiovert 100M Laser Scanning Confocal Microscope 510 with a 100X objective. Images are single 0.2 μm slices.

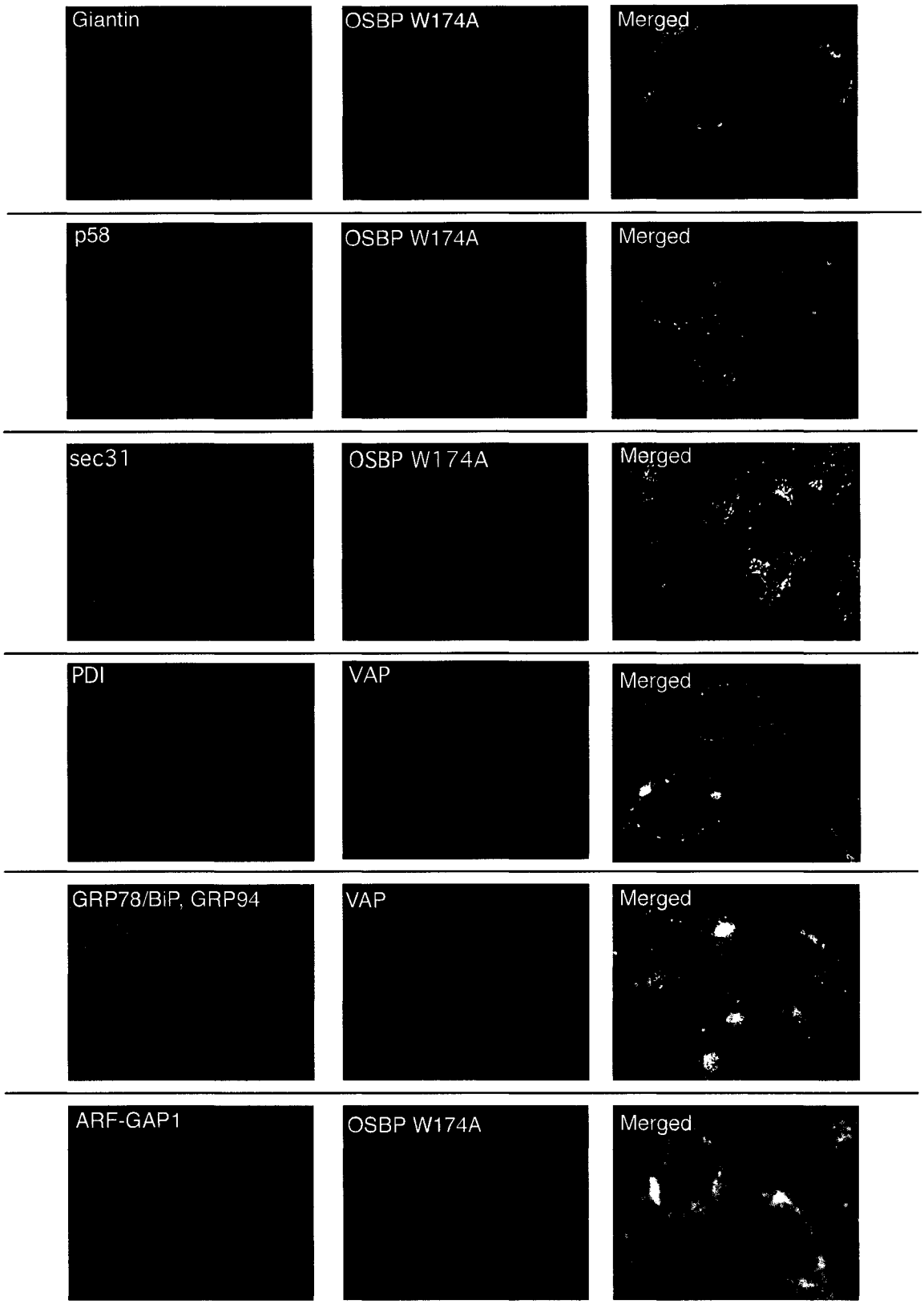
Giantin
OSBP W174A
Merged
p58
OSBP W174A
Merged
sec31
OSBP W174A
Merged
PDI
VAP
Merged
GRP78/BiP, GRP94
VAP
Merged
ARF-GAP1
OSBP W174A
Merged

Figure 24

derived structures seemed to concentrate lumenal proteins involved in protein folding and disulfide bond formation.

4.5.2 Involvement of VAP and OSBP in transport of VSVG-GFP

The indication that the OSBP W174A-induced ER structures were involved in protein folding and export pathways prompted us to investigate the effect of OSBP W174A on protein trafficking from the ER. For these experiments, CHO-tet-OSBP and CHO-tet-OSBP W174A cells were transiently transfected with pVSVG-GFP and transport from the ER was monitored by immunofluorescence (Fig. 25). In CHO-tet-OSBP cells expressing OSBP at 40°C, as well as in uninduced controls (data not shown), VSVG-GFP was ER-localized. Shifting the induced CHO-tet-OSBP cells to 32°C resulted in correct folding and export of VSVG-GFP to the Golgi apparatus. In induced CHO-tet-OSBP W174A cells at 40°C, VSVG-GFP accumulated in the ER-derived structures and co-localized with OSBP W174A. However, VSVG-GFP was folded and transported normally from the ER to the Golgi apparatus at 32°C. This suggests that the ER-derived structures are a site of accumulation of unfolded proteins and ER chaperones.

4.5.3 Ceramide transport in CHO-tet-OSBP and OSBP W174A cells

OSBP and oxysterols have been implicated in the regulation of ceramide transport to the Golgi apparatus [80,106]. Therefore, we investigated the effect of OSBP and OSBP W174A overexpression on trafficking of the fluorescent ceramide analogue, C_5-DMB-ceramide, from the ER to the Golgi apparatus (Fig. 26). In uninduced CHO-tet-OSBP and OSBP W174A cells and induced CHO-tet-OSBP cells, C_5-DMB-ceramide

Figure 25. VSVG-GFP transport in CHO-tet-OSBP and OSBP W174A cells. CHO-tet-OSBP or CHO-tet-OSBP W174A cells were cultured on glass coverslips as described in the legend to Figure 23, induced for 60 h and transfected with VSVG-GFP for 12 h at 40 °C (Section 3.2.11.) Cells were either fixed immediately (40°C) or switched to the transport-permissive temperature of 32°C for 1 h prior to processing for immunofluorescence using monoclonal OSBP antibody 11H9 in conjunction with GAM-555 (red) (Section 3.2.6). Cells were photographed using a Zeiss Axiovert 100M Laser Scanning Confocal Microscope 510 with a 100X objective. Images are single 0.2 μm slices.

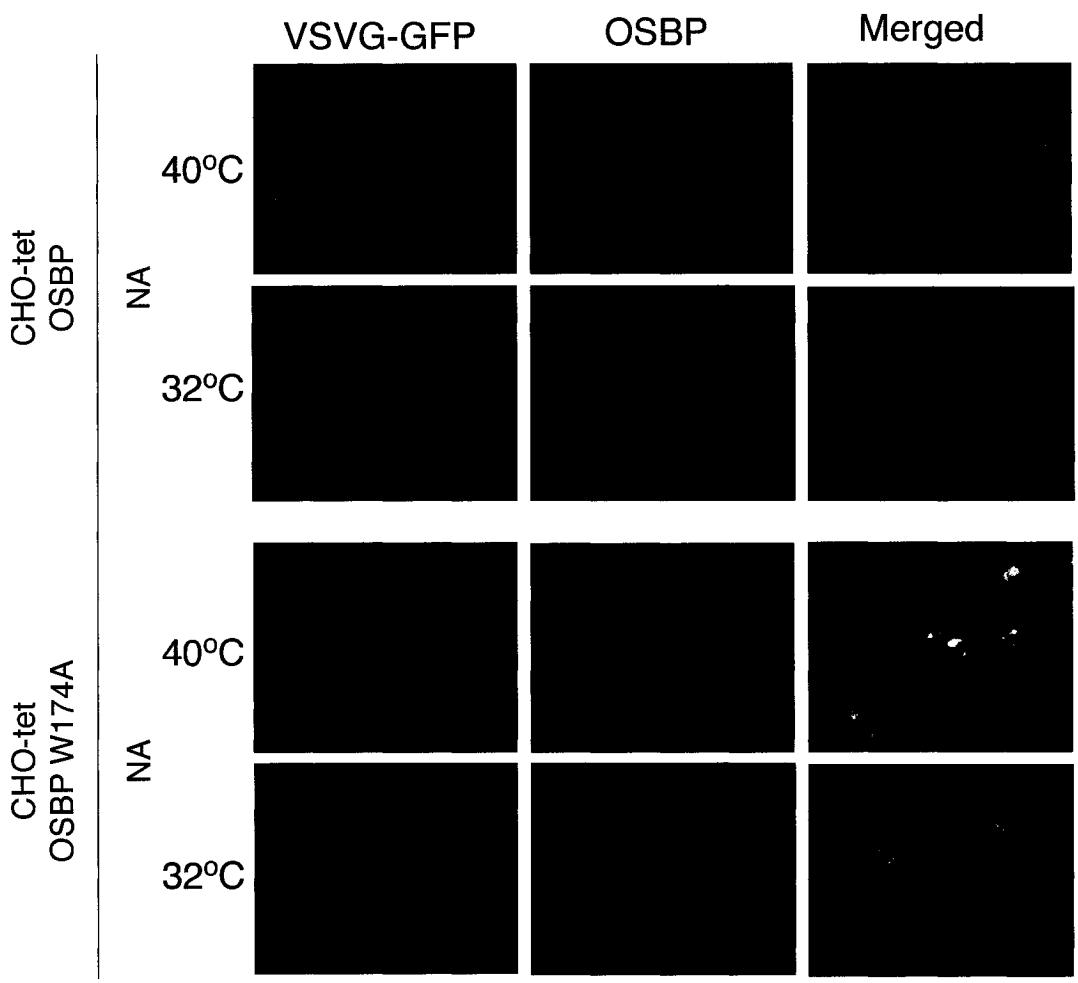
VSVG-GFP
OSBP
Merged
CHO-tet OSBP
NA
40°C
32°C
CHO-tet OSBP W174A
NA
40°C
32°C

Figure 25

Figure 26. Defective trafficking of C_5-DMB-ceramide in CHO-tet-OSBP W174A cells. CHO-tet-OSBP and CHO-tet-OSBP W174A cells were cultured as described in the legend to Figure 23. Cells were loaded with C_5-DMB-ceramide at 4°C (Section 3.2.10) and either fixed immediately or following incubation at 37°C for 1h (Section 3.2.6). The lower panels represent a 2.5X enlargement of induced and uninduced CHO-tet-OSBP W174A cells after 1 h incubation at 37°C. Photographs were taken immediately with an Axiovert 200M fluorescence microscope equipped with a 100X objective and an Axiocam HRC image capture system. Abbreviations: *NA*, no addition; *DOX*, doxycycline.

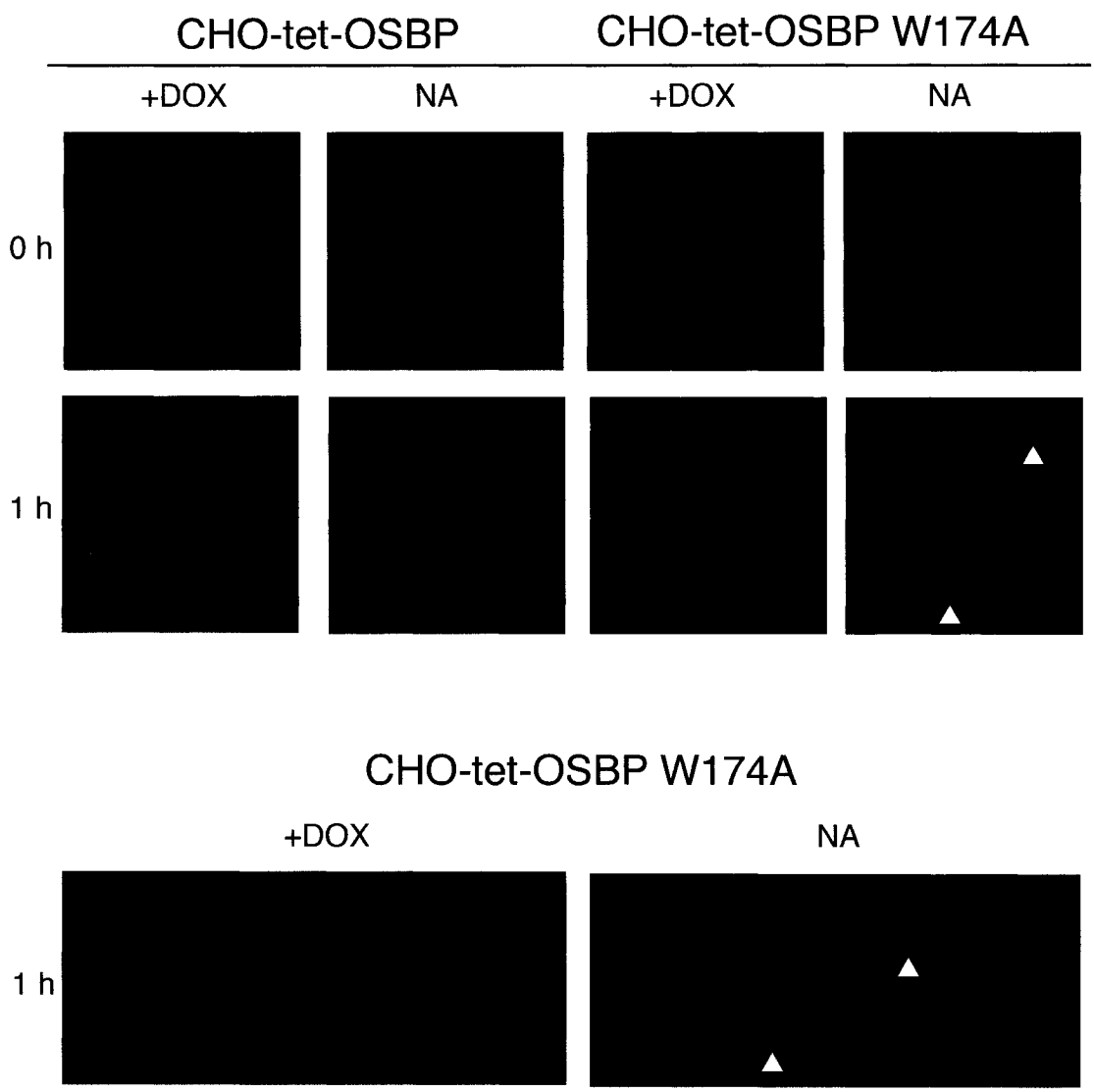
CHO-tet-OSBP
CHO-tet-OSBP W174A
+DOX
NA
+DOX
NA
0 h
1 h
CHO-tet-OSBP W174A
+DOX
NA
1 h

Figure 26

was initially localized to the ER, and was transported to the Golgi apparatus when the cells were shifted to 37°C. In induced CHO-tet-OSBP W174A cells, C_5-DMB-ceramide was initially localized to the ER, although not prominently to the ER-derived structures. After shifting the cells to 37°C, C_5-DMB-ceramide accumulated in the ER-derived structures as indicated by the arrows in Figure 26. As well, transport to the Golgi apparatus was inhibited, as indicated by reduced or disorganized C_5-DMB-ceramide staining of the Golgi apparatus at the transport permissive temperature when compared to cells overexpressing wildtype OSBP. This finding is in agreement with an observed decrease in SM synthesis in induced CHO-tet-OSBP W174A cells compared to uninduced controls or induced CHO-tet-OSBP cells [143].

4.5.4 Lipid binding of OSBP and OSBP W174A PH domains

A possible explanation for the enhanced interaction of OSBP W174A with VAP-A is that disruption of the PH domain inhibits PI-4,5-P_2 or PI-4-P binding, thus allowing constitutive binding to VAP-A. To test this, the PH domain of OSBP W174A was characterized with respect to its ability to bind phospholipid vesicles (Fig. 27). GST fusions of the intact PH domain (GST-PH) or a PH domain with the W174A (GST-PH W174A) mutation were prepared and incubated with increasing concentrations of PC vesicles supplemented with 5 mol% of PS, PI, PI-4, or PI-4,5-P_2. Vesicles with bound fusion proteins were separated from unbound proteins by centrifugation and analyzed by SDS 10%-PAGE and Coomassie staining. Both fusion proteins bound quantitatively to PI-4-P and PI-4,5-P_2 containing vesicles at the lowest vesicle concentration tested, and bound only weakly to vesicles containing PS and PI. The binding of GST-PH and GST-

Figure 27. The W174A PH domain mutation does not affect PI-4-P or PI-4,5-P_2 binding. GST, GST-PH or GST-PH W174A (2.5 mM) was incubated with 0.25 - 5.0 mM PC vesicles containing 5 mol% of the indicated phospholipid for 5 min at 20°C (Section 3.2.15). Samples were subjected to centrifugation for 15 min at 400,000*g* and equivalent volumes of supernatant and pellet fractions were resolved on SDS 12%-PAGE gels. Proteins were detected by Coomassie Blue staining. Experiment was repeated three times with similar results. Abbreviation used: *sup*, supernatant.

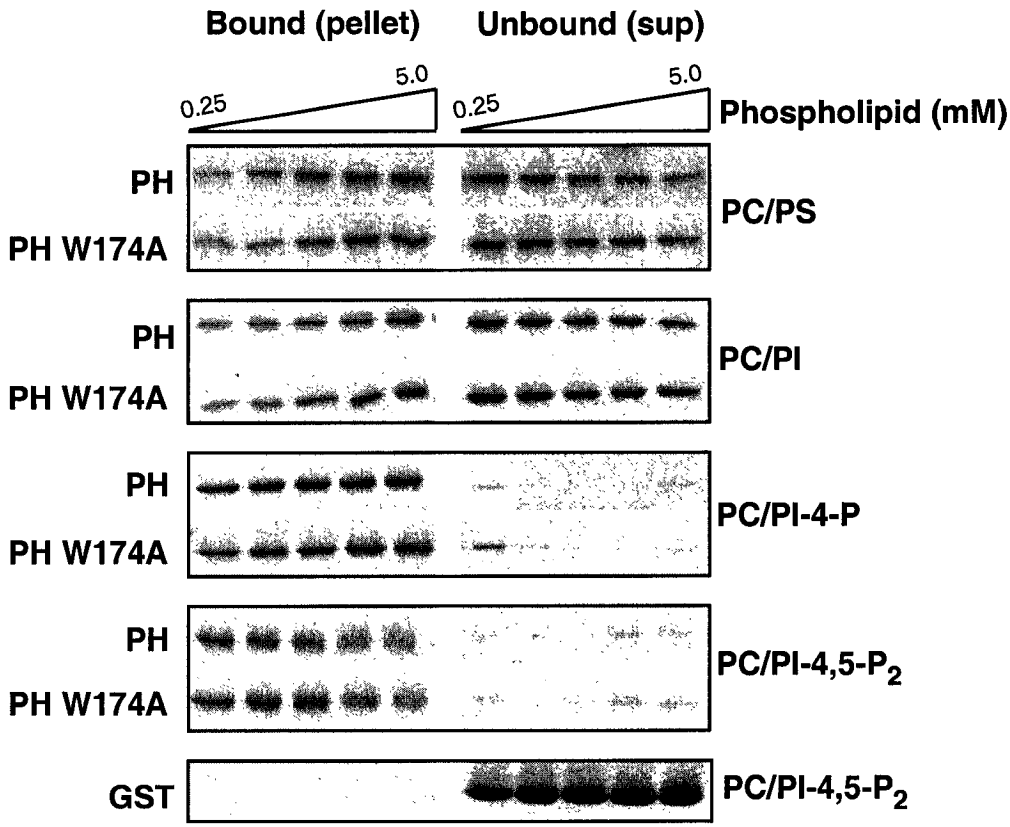
Bound (pellet)
Unbound (sup)
0.25
5.0
0.25
5.0
Phospholipid (mM)
PH
PH W174A
PC/PS
PH
PH W174A
PC/PI
PH
PH W174A
PC/PI-4-P
PH
PH W174A
PC/PI-4,5-P2
GST
PC/PI-4,5-P2

Figure 27

PH W174A to PI-4 and PI-4,5-P_2 was specific, as indicated by the lack of binding of purified GST to PI-4,5-P_2 containing vesicles. Thus the W174A mutation did not appear to affect the binding of OSBP to phosphorylated phosphatidylinositols, at least in the context of the isolated PH domain.

4.6 Role of ORP9 in organellar structure and cell viability

4.6.1 Effects of inducible overexpression of ORP9

In order to characterize the roles of ORP9L and ORP9S, their inducible overexpression in CHO-tet-ORP9S and CHO-tet-ORP9L cell lines was studied with respect to effects on growth rate, organellar morphology, and OSBP expression and phosphorylation. Inducible cell lines were developed because transient expression of the ORP9S cDNA was toxic, making the development of a constitutively overexpressing cell line impossible. As well, transient transfection of the ORP9L cDNA resulted in expression that was approximately equal to that of the endogenous protein. The effect of inducible ORP9S or ORP9L overexpression on growth rate of the CHO-tet cells is shown in Figure 28. The rate of cell growth was compared between induced and uninduced cells by harvesting cells at 12, 24, 48 or 72 h post-induction and measuring TX-100-soluble protein content per dish. By light microscopy, most ORP9S cells were dead or dying at 48 h post induction. This translated into a dramatic reduction in cell number compared to uninduced controls. ORP9L overexpression reduced cell growth rate to a lesser extent than ORP9S and did not appear to affect cell viability. The addition of doxycycline to untransformed CHO-tet-on cells had no effect on cell growth (data not shown).

Figure 28. Expression of ORP9S or ORP9L inhibits cell growth. CHO-tet-ORP9S or ORP9L cells were cultured in Medium A for 24 h before inducing expression with 2 μg/ml doxycycline. Uninduced controls received fresh medium A without doxycycline. Cells were harvested at 0, 12, 24, 48 or 72 h post-induction and were lysed in PBS containing 0.5% TX-100, 2 mM EDTA, 2 mM EGTA and protease inhibitor cocktail (Section 3.2.8). Protein content was determined by a modified μLowry assay (Section 3.2.7) and represents the TX-100-soluble protein per one 60 mm dish. Results are the average of duplicate determinants and are from a representative experiment that was repeated three times with similar results. ■ ORP9S uninduced, □ ORP9S induced, ● ORP9L uninduced, O ORP9L induced. Abbreviations: *NA*, no addition; *DOX*, doxycycline.

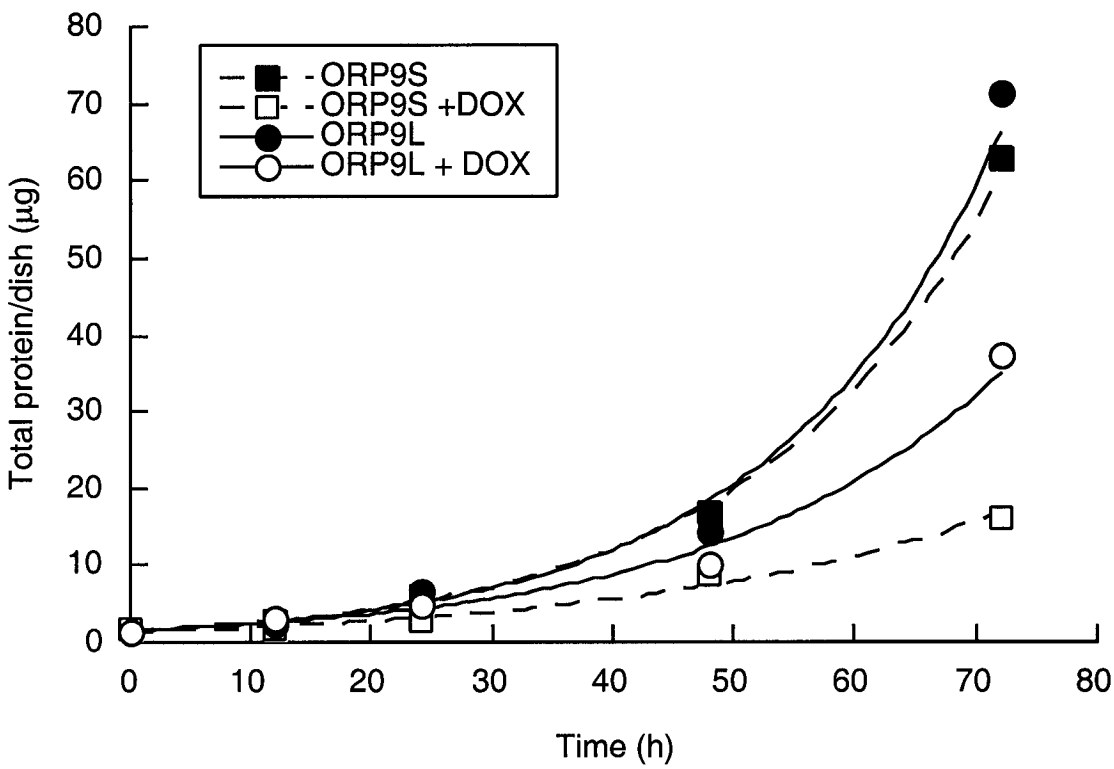
80
70
60
50
40
30
20
10
0
Total protein/dish (µg)
- ORP9S
- ORP9S +DOX
ORP9L
ORP9L + DOX
0
10
20
30
40
50
60
70
80
Time (h)

Figure 28

In an effort to determine how ORP9S was compromising cell viability and growth, cleavage of poly(ADP-ribose) polymerase (PARP), a substrate for caspase 3 and a commonly used indicator of apoptosis, was assessed in induced CHO-tet-ORP9S cells (Fig. 29A). PARP cleavage was not evident in CHO-tet-ORP9S cells induced for 16 or 24 h, demonstrating that cell death is by a non-apoptotic mechanism. PARP cleavage was also not seen in cells induced for 48 or 72 h (data not shown). PARP cleavage was evident to a similar extent in both induced and uninduced CHO-tet-ORP9S cells by treatment with 20 μg/ml chelerythrine for 2 h (Fig. 29A), demonstrating that the apoptotic pathway is functional in CHO-tet-ORP9S cells.

It is possible that ORP9S itself mimics a caspase cleavage product of ORP9L and induces an apoptototic pathway that does not involve PARP cleavage. In order to determine if ORP9L is a caspase substrate, CHO-K1 and HEK 293 cells were treated with chelerythrine to induce apoptosis and cell lysates were analyzed for ORP9L and OSBP cleavage products (Fig. 29B). Endogenous ORP9L was not cleaved in response to the induction of apoptosis in CHO-K1 or HEK cells, further evidence that the effects of ORP9S and ORP9L on cell viability and growth do not involve caspase-mediated apoptosis. A small amount of OSBP was proteolyzed in CHO-K1 and HEK cells treated with chelerythrine, generating a band of approximately 50 kDa (Fig. 29B, bands marked with *). It is possible that the caspase that cleaves OSBP is poorly activated by chelerythrine treatment and OSBP could be cleaved more efficiently in response to another apoptotic agent. The 50 kDA cleavage product of OSBP is not seen in the samples treated with staurosporin because this drug failed to induce apoptosis in CHO-K1 and HEK 293 cells as determined by PARP cleavage (data not shown). The identity

Figure 29. Reduced growth and viability of CHO-tet-ORP9S cells is not due to induction of apoptosis. *(A)* CHO-tet-ORP9S cells were cultured in Medium A for 24 h before inducing ORP9S expression with 2 μg/ml doxycycline for 16 or 24 h as shown. A control set of dishes was treated with 20 μg/ml chelerythrine for 2 h to induce apoptosis. Samples were lysed on ice for 15 min in a high salt Tris buffer (10 mM Tris-HCl, pH 7.4, 1% Triton X-100, 500 mM NaCl, 2 mM EDTA, 1 mM DTT, 0.1 mM phenylmethylsulfonyl fluoride and protease inhibitor cocktail) and subjected to centrifugation at 16,000*g* for 15 min at 4°C to remove Triton X-100-insoluble material. Proteins (7.5 μg) were separated on SDS 10%-PAGE and immunoblotted with a PARP polyclonal antibody. *(B)* CHO-K1 and HEK 293 cells were cultured in Medium C and Medium E, respectively, for 48 h. Cells were treated with 1 μM staurosporin or 10 μM chelerythrine for 2 h. Samples were lysed in PBS containing 0.5% TX-100 (Section 3.2.8) and proteins (7.5 μg) were separated by SDS 10%-PAGE and immunoblotted with the ORP9 and pan-ORP polyclonal antibodies. Abbreviations: *NA*, no addition; *DOX*, doxycycline; *Chel*, chelerythrine; *Sto*, staurosporin.

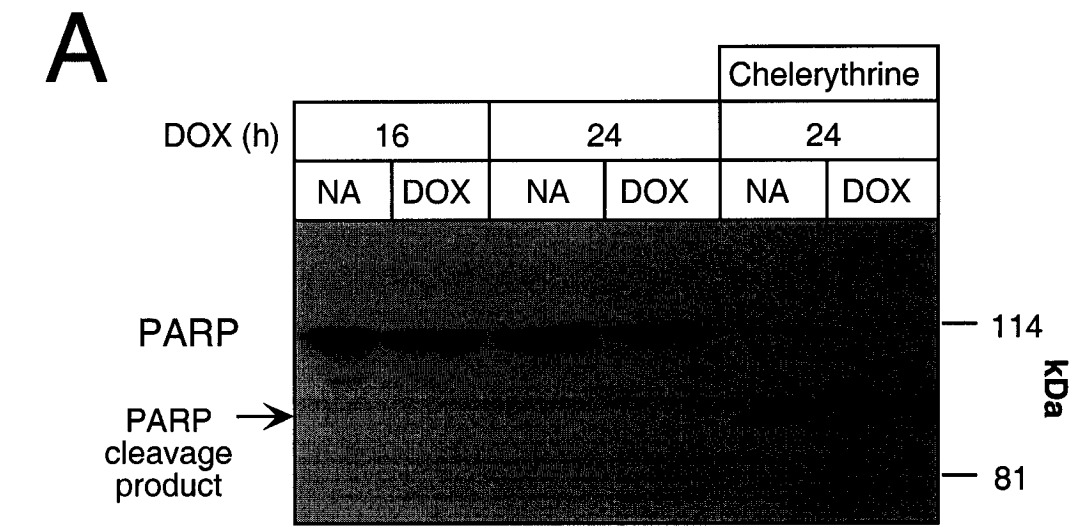
A
Chelerythrine
DOX (h)
16
24
24
NA
DOX
NA
DOX
NA
DOX
PARP
PARP cleavage product
114
kDa
81

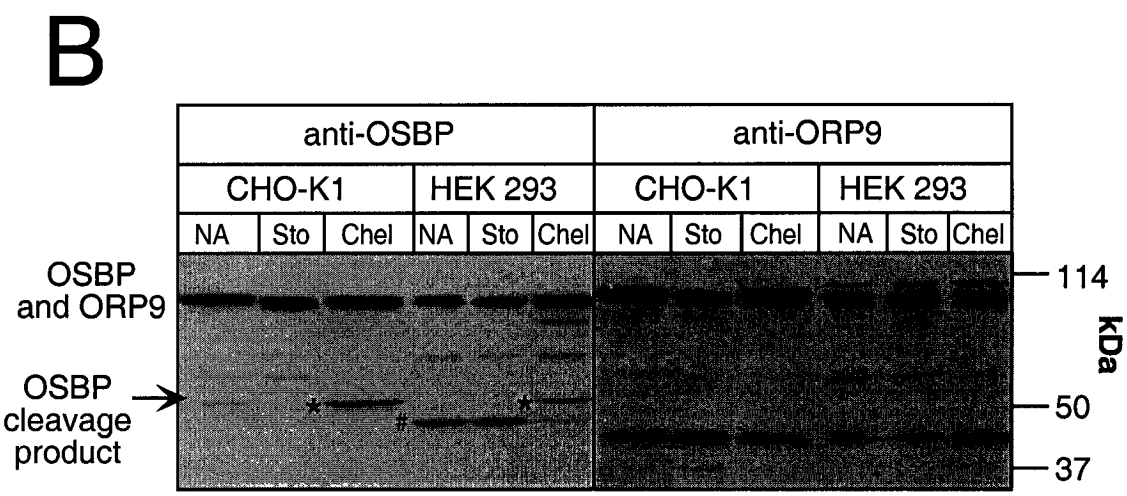
B
anti-OSBP
anti-ORP9
CHO-K1
HEK 293
CHO-K1
HEK 293
NA
Sto
Chel
NA
Sto
Chel
NA
Sto
Chel
NA
Sto
Chel
OSBP and ORP9
OSBP cleavage product
*
#
*
114
kDa
50
37

Figure 29

of the 47 kDa protein in HEK 293 cells (Fig. 29B, bands marked with #) is not known, but could be another ORP, as the immunoblot was probed with the pan-ORP polyclonal antibody 170.

4.6.2 Cellular localization of ORP9S and ORP9L

Since both ORP9S and ORP9 interacted with VAP-A, and seem to do so more strongly than OSBP, we determined if their overexpression would affect the ER in a manner similar to OSBP W174A. Co-immunofluorescence studies were performed in CHO-tet-ORP9S and ORP9L cells to assess the site of ORP9 expression and effects on organellar structure. We initially examined localization of endogenous ORP9 in uninduced CHO-tet-ORP9L cells (Fig. 30). Endogenous ORP9L was localized to two compartments: typical Golgi apparatus localization at one pole of the nucleus and a punctate pattern throughout the body of the cell. This diffuse staining in the body of the cell did not overlap with PDI, an ER marker (Fig 30A). Rather, this localization pattern is similar to that of endogenous OSBP, which is found in a cytosolic/vesicular compartment [33]. ORP9 immunostaining near the nucleus co-localized with FITC-lentil lectin, a commonly used Golgi apparatus marker (Fig. 30B). To confirm that ORP9L was on the Golgi apparatus, cells were treated with BFA, a fungal metabolite which causes the Golgi apparatus to be absorbed into the ER [110-112]. Both endogenous ORP9 and lentil lectin were relocalized to the ER in response to BFA treatment, confirming the Golgi localization of ORP9. In addition to the ER localization of lentil lectin, a significant amount was found on the PM due to the high cell density. The localization of ORP9 was also disrupted by nocodazole (Fig. 31), a drug that fragments the Golgi apparatus by

Figure 30. Endogenous ORP9 is localized to the Golgi apparatus. Uninduced CHO-tet-ORP9L cells were cultured on glass coverslips in medium A for 48 h. *(A)* Cells were fixed, permeabilized and processed for immunofluorescence using the ORP9 polyclonal antibody in conjunction with Alexa-fluor GAR-488 (green) and a PDI monoclonal antibody in conjunction with Alexa– fluor GAM-555 (red) (Section 3.2.6). *(B)* Cells were treated with 2 μg/ml BFA for 30 min before processing for immunofluorescence (Section 3.2.6) using the ORP9 polyclonal antibody in conjunction with Alexa-fluor GAR-555 (red). FITC-lentil lectin (green) was used to detect the Golgi apparatus. Cells were photographed using a Zeiss Axiovert 100M Laser Scanning Confocal Microscope 510 with a 100X objective. Images are single 0.2 μm slices. Abbreviation used: *NA*, no addition.

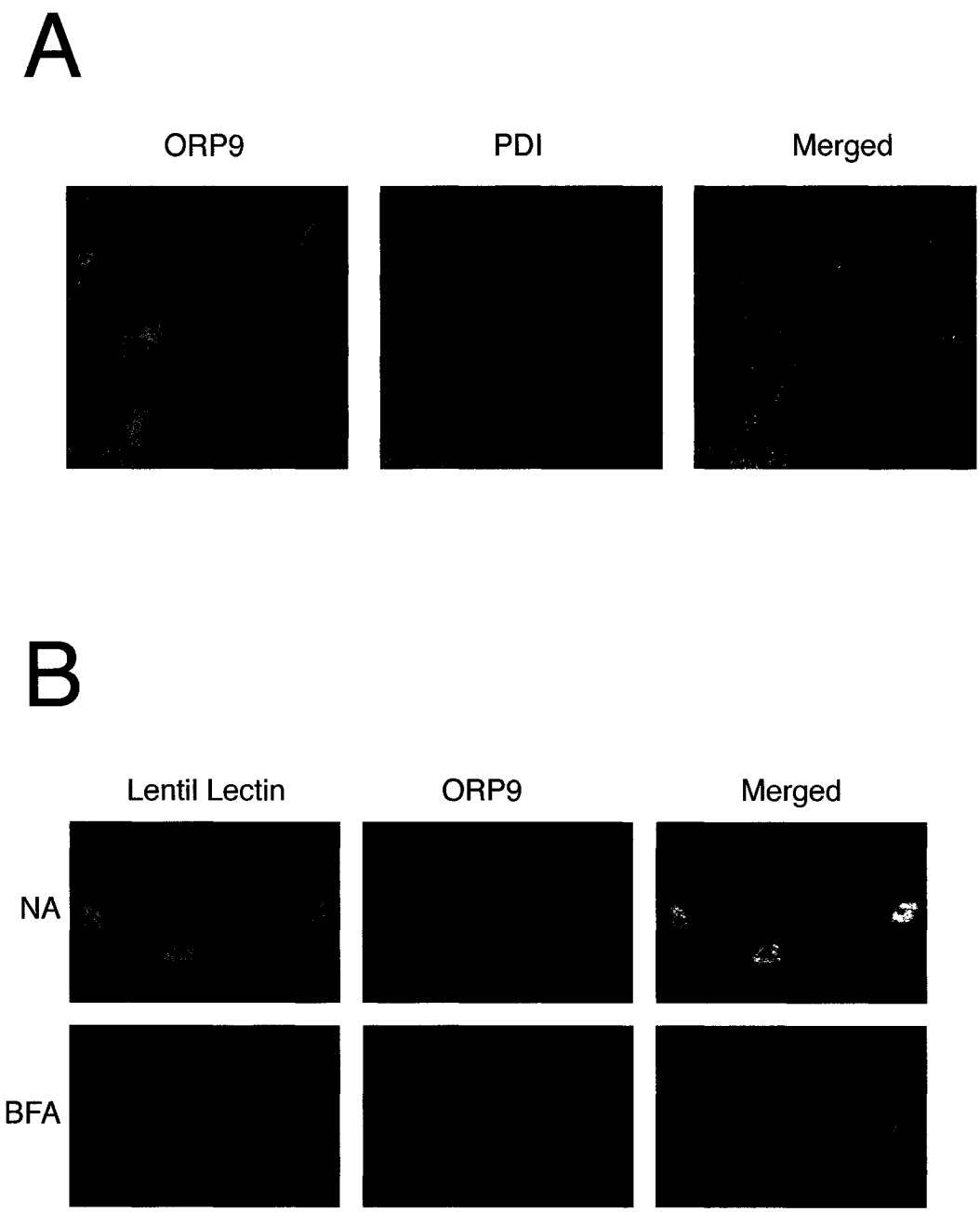

Figure 30

Figure 31. Nocodazole treatment disrupts ORP9 localization. Uninduced CHO-tet-ORP9L cells were cultured on glass coverslips in Medium A for 48 h, treated with 2 μg/ml nocodazole for 1h, fixed, permeabilized and processed for immunofluorescence using the ORP9 polyclonal antibody in conjunction with Alex-fluor GAR-555 (red) and a tubulin monoclonal antibody in conjunction with Alex-fluor GAM-488 (green) (Section 3.2.6). Cells were photographed using a Zeiss Axiovert 100M Laser Scanning Confocal Microscope 510 with a 100X objective. Images are single 0.2 μm slices. Abbreviations: *NA*, no addition; *noc*, nocodazole.

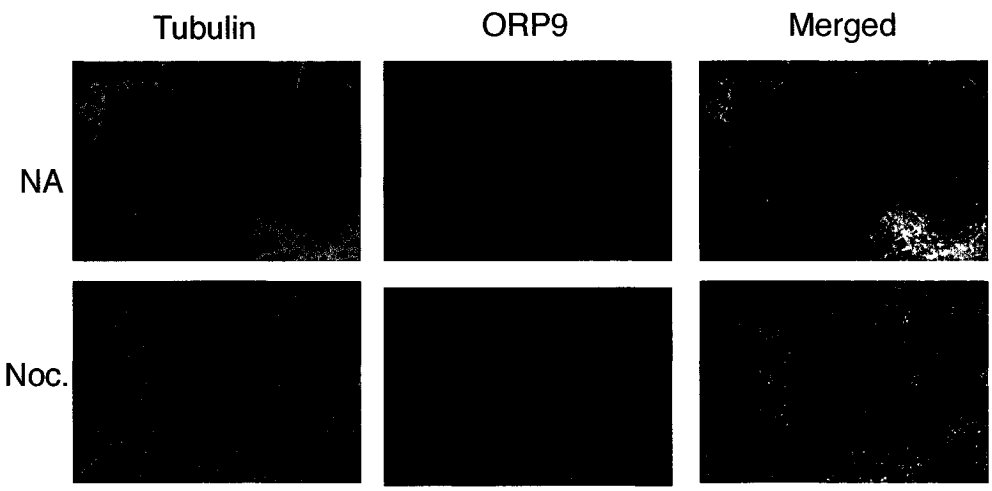

Figure 31

disrupting the microtubule network, thereby further confirming the localization of ORP9 to the Golgi apparatus.

To determine the morphological effects of ORP9S overexpression, co-immunofluorescence with several organellar markers was performed (Fig. 32). Induction of ORP9S in CHO-tet-ORP9S cells by the addition of doxycycline caused the formation of small inclusions that were reminiscent of the structures induced by OSBP W174A (see Fig. 24), although the ORP9S structures were smaller and no tubules were evident. ORP9S localized partially to these inclusions, but was primarily cytosolic and distributed throughout the cell. In addition to ORP9S, VAP and calnexin (a membrane-bound ER protein) were found in the inclusions. However, PDI was not, suggesting that the inclusions are derived from the ER membrane and do not include lumenal proteins. p58 also localized to the ER-derived inclusions with VAP and ORP9S, indicating that the ERGIC is mislocalized by ORP9S overexpression. The Golgi apparatus was not altered as shown by normal giantin localization, nor was the microtubule network affected. Thus, ORP9S overexpression altered the ER and ERGIC but not compartments further along the secretory pathway.

The morphological effects of ORP9L overexpression were investigated in the same manner. Like ORP9S, overexpressed ORP9L itself was primarily cytosolic and localized throughout the cell (Fig. 33). However, induction of ORP9L expression caused the formation of large vesicles throughout the cell, most of which were close to the nucleus. VAP and calnexin strongly localized to the outer rim of the vesicles, indicating that they are ER membrane-derived. PDI also localized weakly to the surface of the ER-derived vesicles. The localization of VAP was disrupted to a much greater extent than

Figure 32. Co-localization of organellar markers with ORP9S. CHO-tet-ORP9S cells were cultured on glass coverslips in Medium A for 24 h before inducing expression with 2 μg/ml doxycycline for 48 h. Cells were fixed, permeabilized and processed for immunofluorescence. Primary antibodies (indicated in the figure) were used in conjunction with Alexa-fluor conjugated secondary antibodies (Section 3.2.6). Cells were photographed using a Zeiss Axiovert 100M Laser Scanning Confocal Microscope 510 with a 100X objective. Images are single 0.2 μm slices.

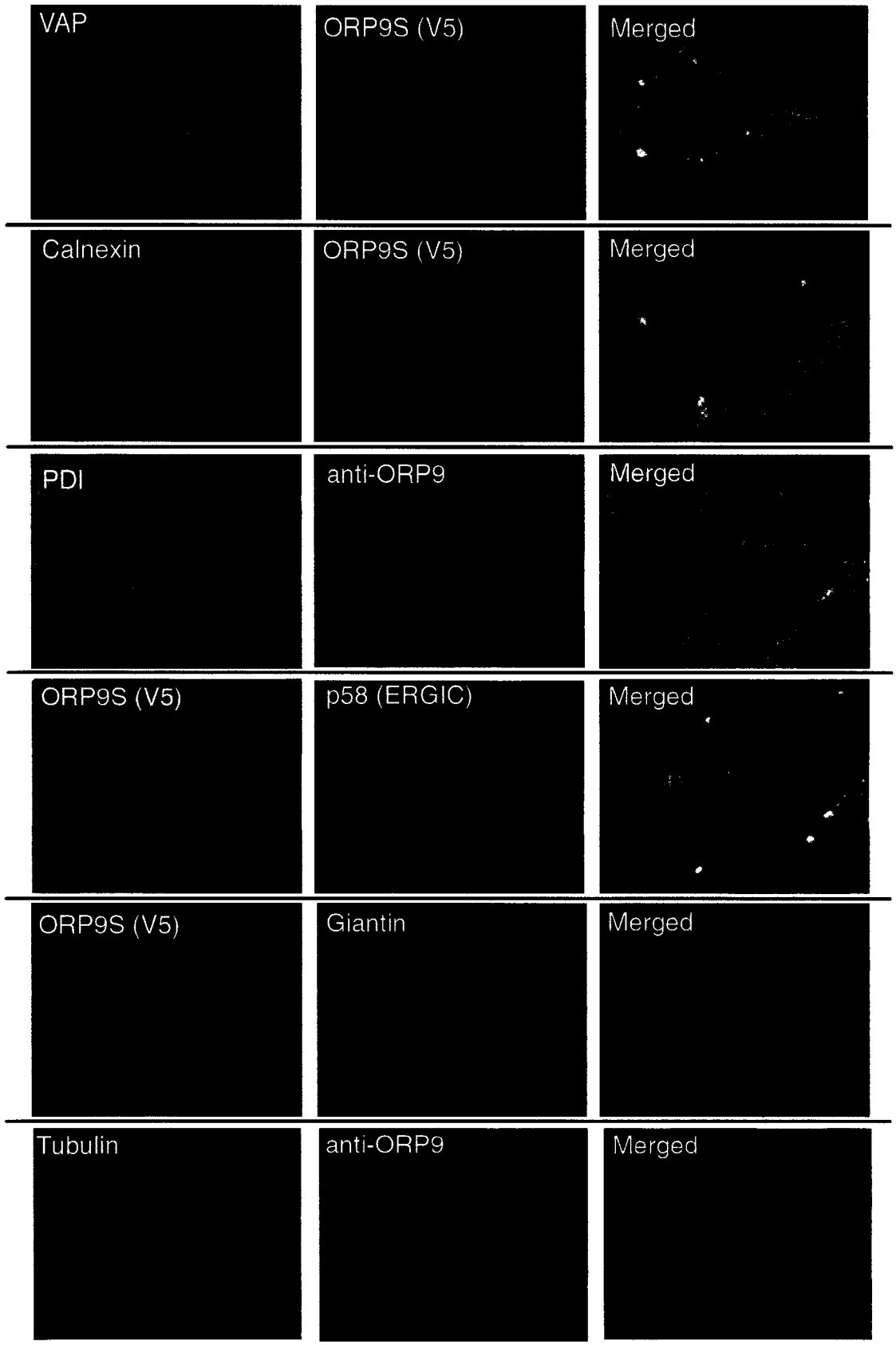
VAP
ORP9S (V5)
Merged
Calnexin
ORP9S (V5)
Merged
PDI
anti-ORP9
Merged
ORP9S (V5)
p58 (ERGIC)
Merged
ORP9S (V5)
Giantin
Merged
Tubulin
anti-ORP9
Merged

Figure 32

Figure 33. Co-localization of organellar markers with ORP9L. CHO-tet-ORP9L cells were cultured on glass coverslips in Medium A for 24 h before inducing with 2 μg/ml doxycycline for 48 h. Cells were fixed, permeabilized and processed for immunofluorescence. Primary antibodies (indicated in the figure) were used in conjunction with Alexa-fluor conjugated secondary antibodies (Section 3.2.6). Cells were photographed using a Zeiss Axiovert 100M Laser Scanning Confocal Microscope 510 with a 100X objective. Images are single 0.2 μm slices.

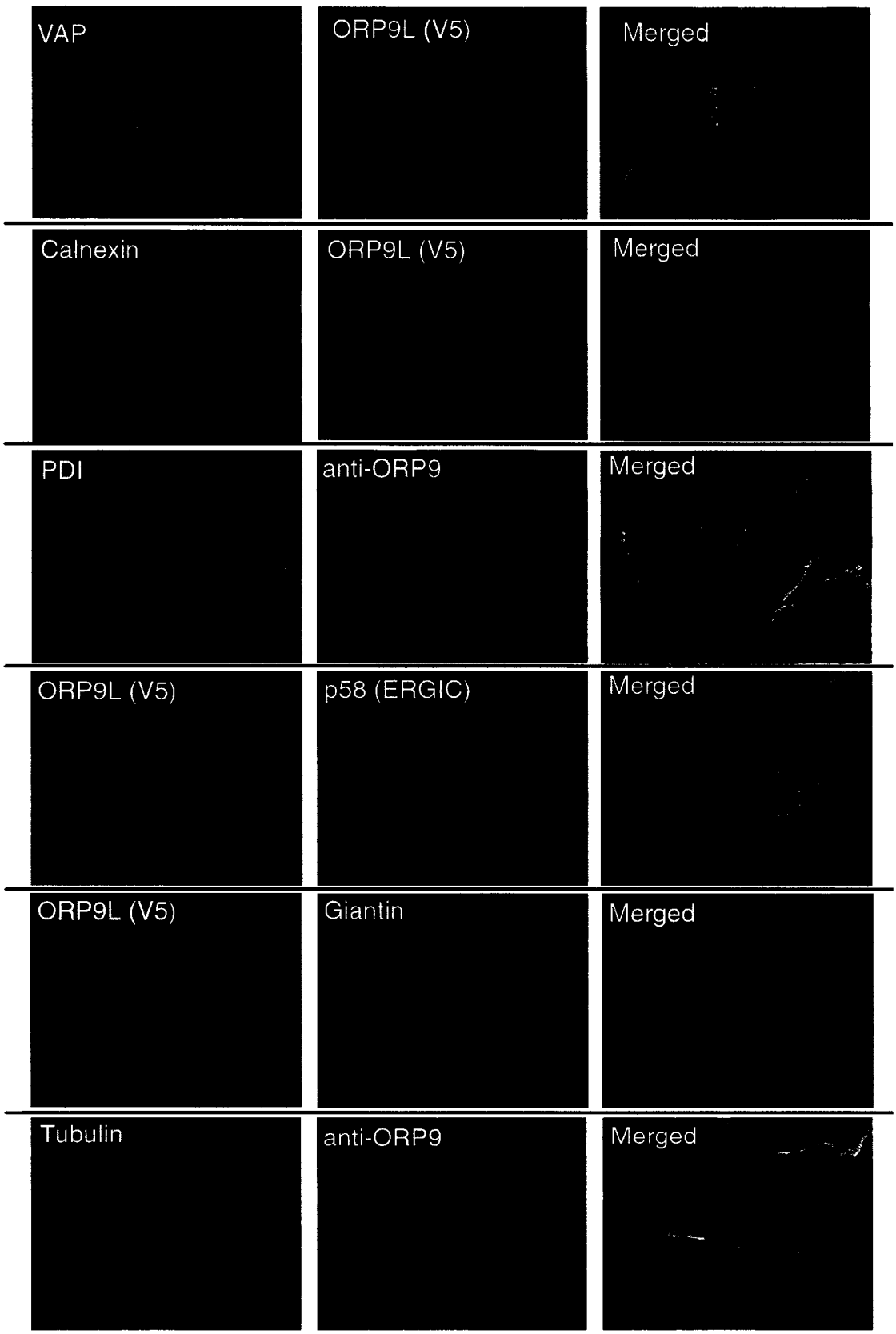
VAP
ORP9L (V5)
Merged
Calnexin
ORP9L (V5)
Merged
PDI
anti-ORP9
Merged
ORP9L (V5)
p58 (ERGIC)
Merged
ORP9L (V5)
Giantin
Merged
Tubulin
anti-ORP9
Merged

Figure 33

either calnexin or PDI. p58 also localized to the ER-derived vesicles, indicating that the ERGIC compartment is mislocalized by the overexpression of ORP9L. Similar to cells in which ORP9S expression was induced, ORP9L did not alter the structure of the Golgi apparatus or the microtubule network as assessed by giantin or tubulin immunostaining, respectively. Therefore, similar to ORP9S overexpressing cells, overexpression of ORP9L altered the ER and ERGIC but not compartments further along the secretory pathway.

Although it was clear that ORP9L overexpression caused the formation of ER-derived vesicles, the high concentration of ORP9L in the cytosol made it was difficult to determine the extent of ORP9L localization to their suface. In order to assess this, ORP9S and ORP9L expressing cells were permeabilized with saponin to remove cytosolic proteins prior to fixation (Fig. 34). The majority of cytosolic ORP9S was lost in cells pretreated with saponin, but the ER-membrane derived inclusions were retained. ORP9S also remained on the nuclear envelope, a localization that cannot be detected in non-saponin treated cells due to the presence of ORP9S in the cytosol. In saponin treated cells ORP9L was lost from the cytosol but remained on the surface of the vesicles.

4.6.3 Expression of ORP9 induces multinucleation

Although neither ORP9S not ORP9L localized to the nucleus, in the course of the experiments described above we noted that a large number of ORP9S or ORP9L overexpressing cells were multinucleated or had multi-lobed nucleii. Some of the ORP9 interacting proteins identified by yeast two-hybrid analysis (Section 4.1.3, Table 2) also suggested a role in nuclear-localized pathways. Int6/eIF3e and PA28β are components of

Figure 34. Overexpressed ORP9S and ORP9L are both cytosolic and membrane-associated. CHO-tet-ORP9S and CHO-tet-ORP9L cells were cultured on glass coverslips in Medium A for 24 h before inducing with 2 μg/ml doxycycline for 24 h. Cells were washed with cold PBS and either fixed immediately or pretreated with 0.5% (w/v) saponin for 1 min on ice. Cells were then processed for immunofluorescence (Section 3.2.6) using monoclonal antibody V5 in conjunction with Alexa-fluor 488 (green) to detect overexpressed ORP9S and ORP9L. Cells were photographed using a Zeiss Axiovert 100M Laser Scanning Confocal Microscope 510 with a 100X objective. Images are single 0.2 μm slices. Microscope settings were identical between images. Abbreviations: *NA*, no addition; *DOX*, doxycycline.

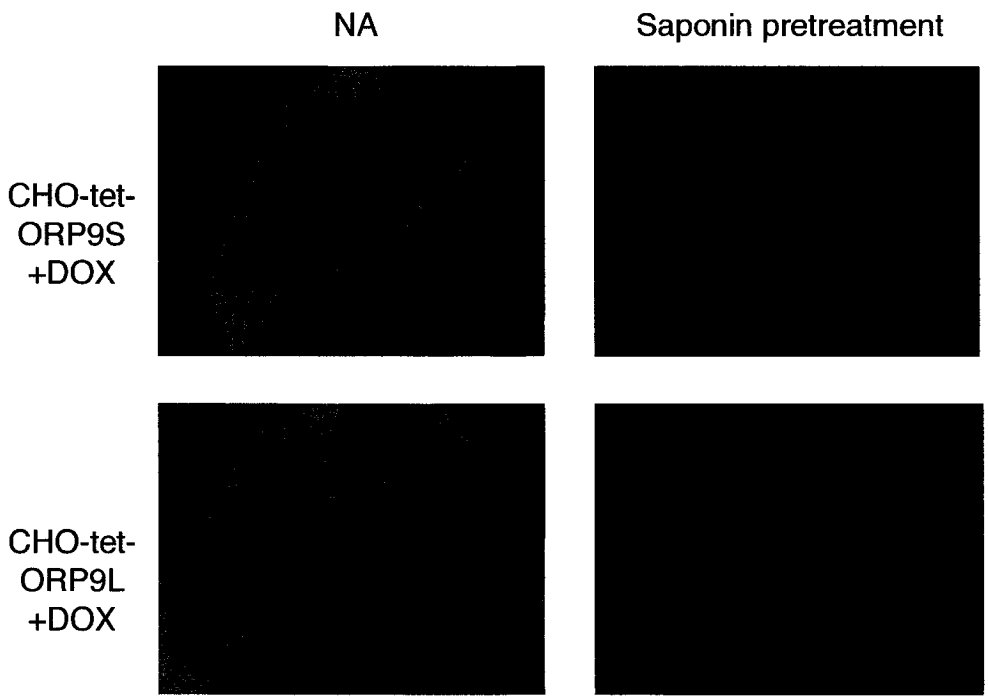

Figure 34

the proteasome, a complex involved in protein degradation that is involved in cell cycle control and nuclear division through cyclin degradation [167,170]. As well, importin-α is involved in nuclear import [164]. To quantify the extent of multinucleation, approximately 200 ORP9S or ORP9L overexpressing cells were counted and scored for multinucleation and compared to a similar number of uninduced CHO-tet-ORP9S and ORP9L cells. By this method nearly 50% of CHO-tet-ORP9S or ORP9L expressing cells were multinucleated or had multi-lobed nucleii, compared to only 3-6% of non-induced cells.

Although induced CHO-tet-ORP9S and ORP9L cells were multinucleated or had multi-lobed nucleii, localization of the nuclear pore complex and lamin A/C was not altered (Fig. 35), indicating that the nucleus was still structurally intact. As well, propidium iodide staining did not show DNA condensation or aggregation (data not shown).

4.6.4 Effect of ORP9S and ORP9L overexpression on OSBP expression and phosphorylation

Since OSBP and VAP-A interact in CHO-K1 cells, we investigated whether overexpression of other VAP-A binding proteins, ORP9S or ORP9L, affected OSBP expression and phosphorylation state (Fig. 36). Overexpression of ORP9S or ORP9L caused a decrease in OSBP phosphorylation and expression that was evident even before maximal induction of ORP9S or ORP9L had been reached. In the case of ORP9S overexpressing cells, the expression of both OSBP and ORP9S was reduced by 48 and 72 h. Expression of VAP-A and VAP-B was not altered, demonstrating that this was not a

Figure 35. Localization of nuclear markers in ORP9S and ORP9L overexpressing cells. CHO-tet-ORP9S and ORP9L cells were grown on glass coverslips in Medium A for 24 h before inducing with 2 μg/ml doxycycline for 48 h. Cells were fixed with formaldehyde for detection of the nuclear pore complex or with methanol/acetone for the detection of lamin A/C (Section 3.2.6). Primary antibodies (indicated in the figure) were used in conjunction with Alex-fluor conjugated secondary antibodies. Cells were photographed using a Zeiss Axiovert 100M Laser Scanning Confocal Microscope 510 with a 100X objective. Images are single 0.2 μm slices. Abbreviation: *NPC,* nuclear pore complex.

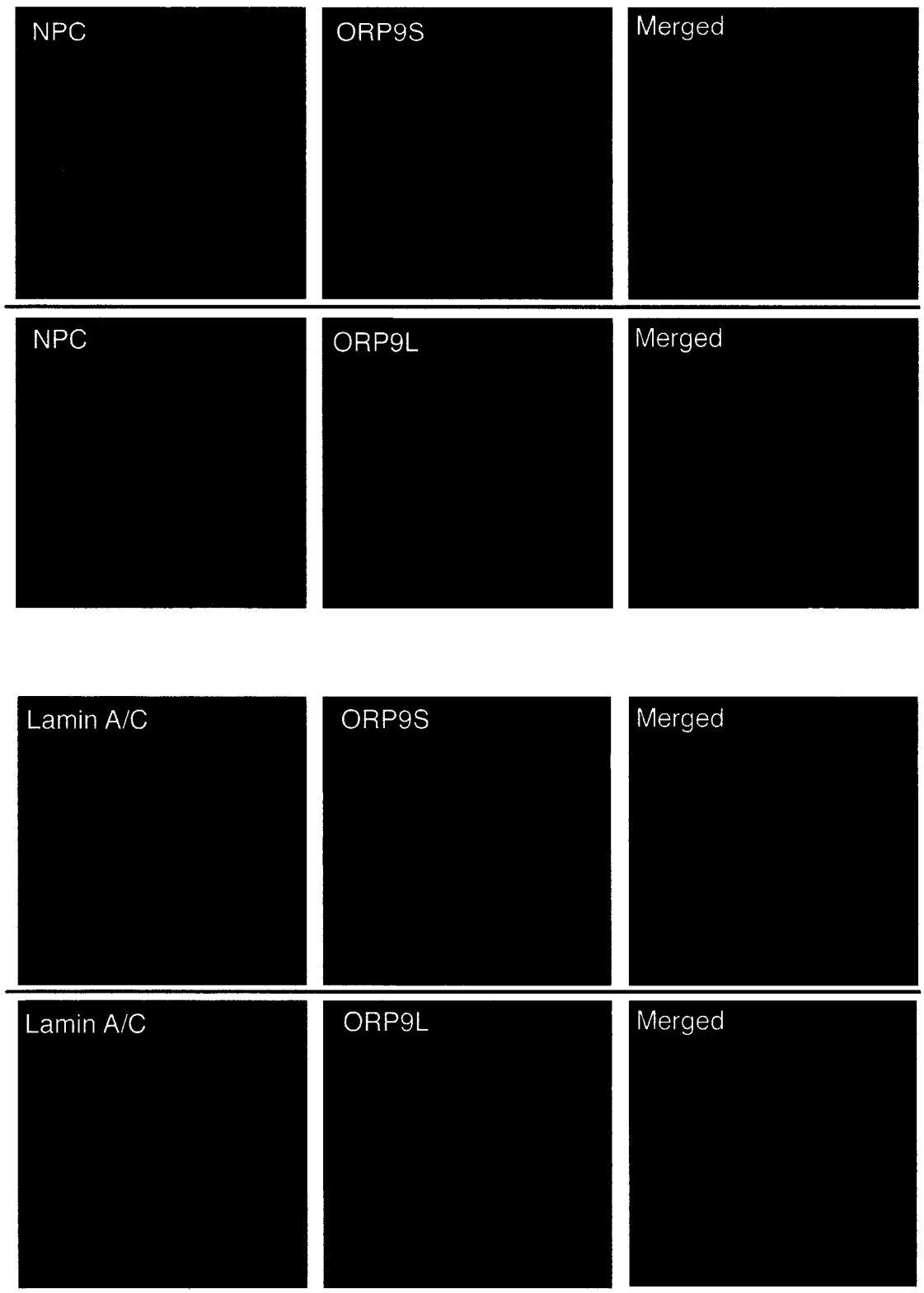
NPC
ORP9S
Merged
NPC
ORP9L
Merged
Lamin A/C
ORP9S
Merged
Lamin A/C
ORP9L
Merged

Figure 35

Figure 36. Overexpression of ORP9S or ORP9L decreased OSBP phosphorylation and expression. CHO-tet-ORP9S and ORP9L cells were cultured in Medium A for 24 h before inducing expression with 2 μg/ml doxycycline for 12, 24 or 48 h. Cells were harvested and lysed (Section 3.2.8). Proteins (10 μg) were separated by SDS 8%-PAGE (ORP9 and OSBP) or SDS 10%-PAGE (VAP) and immunoblotted with pan ORP polyclonal antibody 170 or the VAP polyclonal antibody. Abbreviations: *NA*, no addition; *DOX*, doxycycline.

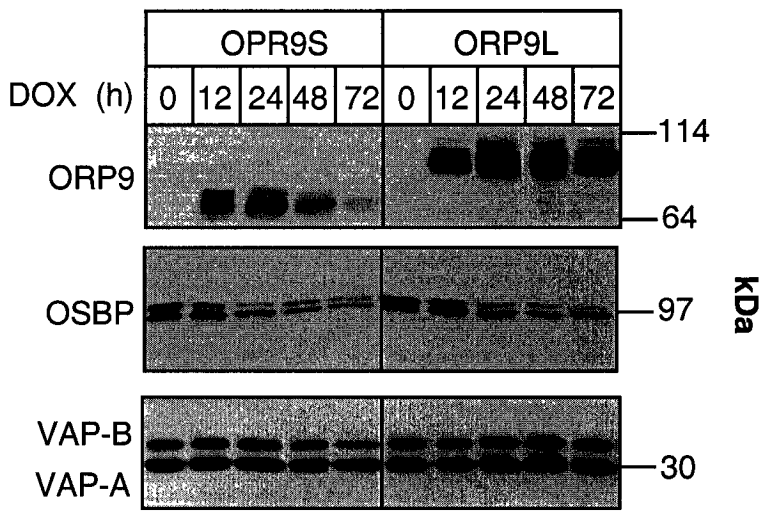
OPR9S
ORP9L
DOX (h)
0
12
24
48
72
0
12
24
48
72
ORP9
114
64
OSBP
97
kDa
VAP-B
VAP-A
30

Figure 36

global effect on protein expression or viability. This suggests that overexpression of the ORP9 variants saturates the VAP-A binding sites that OSBP would normally occupy, thus leading to its displacement from VAP-A and subsequent degradation due to mislocalization.

5 Discussion

OSBP has been implicated in the regulation of cholesterol and sphingolipid homeostasis by virtue of its oxysterol binding activity and changes in localization and phosphorylation in response to alterations in cholesterol transport [19,27,28,109]. The PH domain and ligand-binding region of OSBP mediate its effects on cholesterol and sphingolipid homeostasis by regulating Golgi-localization [21,33]. OSBP is also localized to the ER via its interaction with VAP-A, and the dual localization of OSBP and other ORP family members further suggests that they coordinate transport events between the ER and Golgi apparatus or other organelles. While the role(s) of the other ORP family members has not been well defined, regulation of vesicle biogenesis, lipid transport and cholesterol synthesis have emerged as common themes.

Results presented here define a protein-protein interaction network between VAP-A and the ORP family implicated in cholesterol and lipid trafficking through regulation of trafficking pathways (Fig. 37). On a functional level, we have demonstrated that OSBP interacts with VAP-A to regulate a pre-transport step in ER to Golgi apparatus trafficking. This is consistent with prior observations that overexpression of OSBP or its PH domain caused enhanced trafficking of ceramide from the ER to the Golgi apparatus [80], or disruption of the Golgi apparatus and anterograde traffic of VSVG, respectively [25]. We also showed that overexpression of a second VAP-A binding partner, either ORP9S or ORP9L, caused dramatic changes in ER structure, as well as mislocalization of an ERGIC marker, indicating that they may regulate transport between these compartments. Our identification of five ORPs that interact with VAP-A suggests that the

Figure 37. Protein-protein interactions between VAP-A and the ORP family. Interacting proteins identified in the course of this study are shown. A heavy line indicates interactions that were confirmed by co-immunoprecipitation and characterized *in vivo*. Thin lines indicate interactions that have been observed by GST pull-down analysis. Dashed lines indicate interactions with partial cDNAs cloned by yeast two-hybrid analysis.

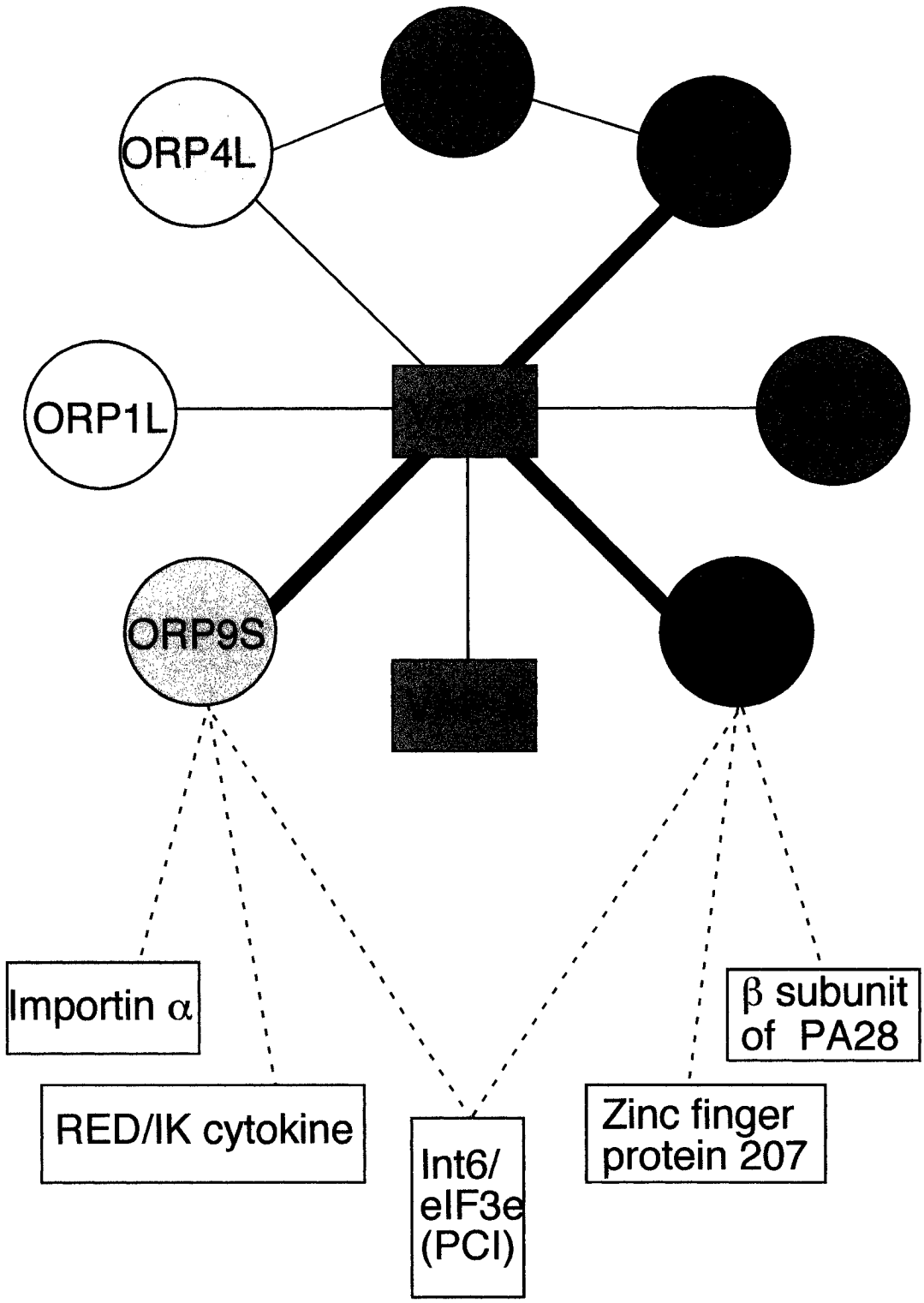
ORP4L
ORP1L
ORP9S
Importin α
RED/IK cytokine
Int6/
eIF3e
(PCI)
Zinc finger
protein 207
β subunit
of PA28

Figure 37

aforementioned effects on ER structure and export could be a common theme among members of the ORP family.

5.1 A protein-protein interaction network between VAP-A and the ORP family

Although VAP-A, an ER-localized type II integral membrane protein, was partially TX-100 insoluble, and potentially implicated in cholesterol regulation through its interaction with OSBP, extensive studies showed that it was not associated with DIGs/caveolae (Fig. 19). However, interaction with the cytoskeleton could explain the partial TX-100 insolubility. In support of this, the mouse orthologue of VAP-A was shown to co-localize with tubulin by electron microscopy [155] and DVAP-33A, a *Drosophila* orthologue of VAP-A, is proposed to provide the membrane attachment site for microtubules on the PM of boutons, contact points between nerves and muscles in fruit fly larvae [154]. Microtubule organization within the bouton is disrupted in DVAP-33A mutants, implicating it in the organization and/or maintenance of microtubule architecture. This work suggests a role for DVAP-33A in the stabilization of protein:membrane interactions and suggests a model whereby VAP-A could regulate vesicle attachment or transport along microtubules. We were unable to demonstrate an interaction between human VAP-A and tubulin using a similar technique as discussed in the DVAP-33A study. However, the use of TX-100 in our study could have dissociated the VAP-A complexes required for interaction with tubulin, or VAP-A could have been removed from its native lipid environment, thus altering its affinity for tubulin.

Analysis of OSBP mutants by yeast two-hybrid and GST pull-down analysis allowed the identification of a VAP-A binding region between amino acids 351 and 431

(Fig. 9). This region of OSBP overlaps with the N-terminus of the ligand-binding region and OHD. Sequence comparison of the VAP-binding region among ORP family members indicated two conserved sub-regions; one toward the N-terminal that is conserved in a subset of ORP family members (amino acids 360-364 of OSBP, in ORPs 1, 2, 3, 4, 6, 7 and 9) and another near the C-terminus that is conserved in all ORPs (amino acids 421-431 of OSBP) (Fig. 38). Supporting our results, a recent report further defined the VAP-A binding region to a small motif designated 'FFAT' (two phenylalanines in an acidic tract), which corresponds to the N-terminal conserved region (amino acids 360-364 of OSBP) [26]. This motif was shown to regulate the ER localization of several yeast proteins that were previously shown to interact with Scs2p, the yeast orthologue of VAP-A, in a large scale study identifying yeast protein complexes [132]. Based on conservation of this motif, OSBP and ORPs 1, 2, 3, 4, 6, 7 and 9 are predicted to be VAP-A binding proteins. Our data showed that OSBP and ORPs 1L, 3(1d), 4L, 9S and 9L are VAP-A binding proteins (Figs. 8, 10-12, 14), supporting the identification of the FATT motif as an Scs2p/VAP-A binding domain. Analysis of the partial ORP9 cDNA cloned by yeast two-hybrid analysis (Fig. 6) localized the VAP-A binding activity to a region of ORP9 that contained both the 80 amino acid region that we identified as well as the FFAT motif. We did not test the interaction of ORPs 6 and 7 with VAP-A, and the binding of ORP2 to VAP-A was inconclusive due to interference from GST antibodies in the GST-VAP-A pull-down assays.

The VAP-A binding region of OSBP is contained in the ligand-binding region. Sequence comparison of OSBP and ORP4L, both of which bind 25OH, to ORP4S, which does not, suggests that the region between residues 300 and 365 of OSBP is necessary for

Figure 38. Alignment of VAP-A binding regions of the ORP family. An alignment of the predicted VAP-A binding region for OSBP and ORPs based on yeast two-hybrid and GST pull-down analysis. Numbers at the top refer to amino acids in the OSBP sequence. The two regions identified as having high identity between ORP family members are boxed, and the FFAT motif is indicated. Sequences were aligned using MacVector (version 6.5.3) and a Blosum 30 algorithm with an open gap penalty of 10 and an extend gap penalty of 0.1.

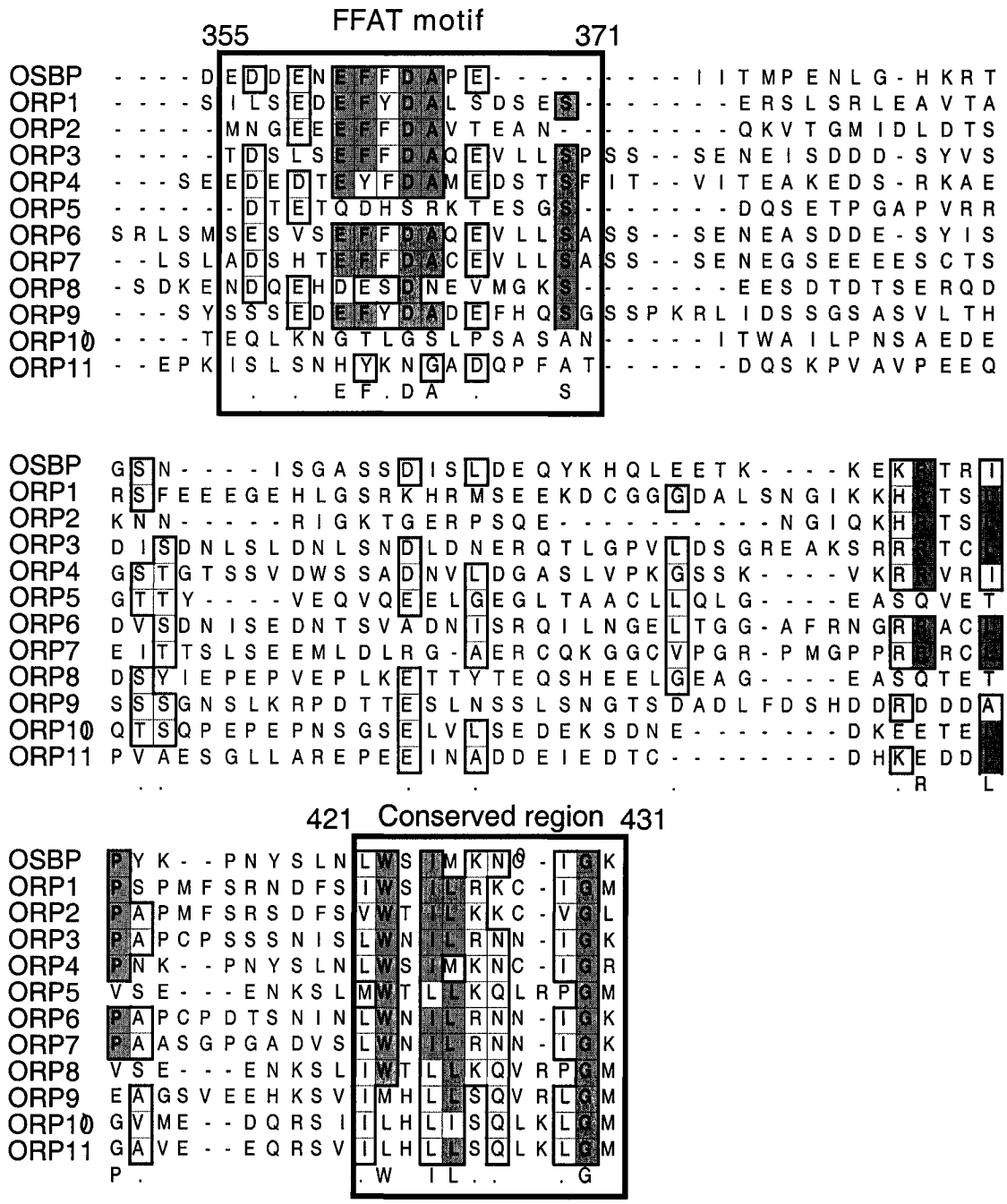
FFAT motif
355
371
OSBP
ORP1
ORP2
ORP3
ORP4
ORP5
ORP6
ORP7
ORP8
ORP9
ORP10
ORP11
421
Conserved region
431

Figure 38

oxysterol binding [1,33]. This region contains part of the VAP binding region and the FFAT motif. However, an OSBP truncation mutant containing residues 1-454 did not bind oxysterols [33], indicating that residues 300-365 are not sufficient for oxysterol binding. Truncation of OSBP closer to the N-terminal (OSBP 1-442) did not inhibit binding to VAP-A (Fig. 8), thus oxysterol-binding activity does not seem to be required for interaction with VAP-A. This is supported by the observations that VAP localization is not altered by 25OH treatment (Fig. 17) and inclusion of 25OH in co-immunoprecipitation experiments did not alter the stability of the VAP-A/OSBP complex (data not shown). Additionally, ORP3(1d) and ORP9L did not bind 25OH (Wang and Ridgway, unpublished results), but bound VAP-A in GST pull-down assays. These data suggest that the VAP-A and 25OH binding sites are mutually exclusive, but partially overlapping. Future experiments are needed to define the boundaries of the oxysterol-binding region and to define the relationship between VAP-A and oxysterol binding.

The FFAT motif was also identified in Osh1p, Osh2p and Osh3p, three PH domain containing yeast orthologues of the ORP family that share a high degree of similarity with OSBP and ORP4 (Table 1) [8,26]. In addition to the Osh and ORP families, the FFAT motif is found in several proteins involved in lipid metabolism including Opi1p, a negative regulator of inositol metabolism in yeast [182], protein tyrosine kinase (PYK)2 N-terminal domain-interacting receptors (NIR)1, 2 and 3, human orthologues of a *Drosophila* phospholipid transfer protein, rdgB [183], and Goodpasture's antigen binding protein (GPBP), a predicted phospholipid binding protein [184]. In addition, the FFAT motif is found in Rab11 binding protein (Rab11BP), a small G protein implicated in vesicle recycling from the early endosomes to recycling

endosomes [185]. Rab11, its binding partner, has been implicated in cholesterol and SM trafficking in the endosomal system [186].

The FFAT motif regulated the ER localization of truncated versions of Osh1p, Osh2p and OSBP [26], supporting our conclusion that VAP-A regulates ER localization of the ORP proteins. A yeast protein complex isolated using Scs2p as bait contained Osh1p and Osh2p as well as Opi1p and Stt4p, a PM localized PI-4 kinase [132]. These data suggest a functional link between the regulation of inositol or phosphorylated PI metabolism and Scs2p and its binding partners. This conclusion is supported by earlier studies showing that deletion of *SCS2* caused inositol auxotrophy at temperatures over 34°C, a defect that was suppressed by the overexpression of Ino1p (inositol-1 phosphatase), an essential enzyme in inositol biosynthesis [150]. Since Scs2p binds Opi1p [26,132], loss of Scs2p could lead to the inappropriate suppression of inositol biosynthesis. As would be expected, overexpression of wildtype Scs2p reversed the auxotrophy [150]. However, overexpression of a mutant Scs2p lacking the N-terminal VAP consensus domain was unable to rescue the auxotrophy, demonstrating that this domain is central to the function of Scs2p. As well, yeast lacking Osh1p are defective for tryptophan uptake. Overexpression of wildtype Osh1p reversed this defect but overexpression of an Osh1p construct in which the FFAT motif was mutated did not [26], further supporting the functional significance of the interaction of FFAT motif-containing proteins with Scs2p.

In addition to identifying the region of OSBP involved in binding to VAP-A, the region(s) of VAP-A involved in its interaction with the ORP family was investigated. Analysis of VAP-A mutants (Figure 9) by yeast two-hybrid analysis revealed differences

in the binding of ORP9 and OSBP by VAP-A (Table 3). Deletion of the VAP consensus domain had no effect on dimerization of VAP-A, but inhibited its interaction with both OSBP and ORP9. Deletion of the coiled-coil or transmembrane domains had no effect on ORP9 binding, but inhibited binding to OSBP. A possible explanation is that, like the ORP9 variants, OSBP interacts with VAP-A via the consensus domain, but only in the context of a membrane localized protein. More extensive mutational analysis of VAP-A is required to resolve this issue.

Collectively, evidence from studies in yeast supports our identification of a VAP-A and ORP family network of proteins that is involved in the regulation of sterol and lipid synthesis. However, unlike studies in mammalian cells that have implicated VAP-A in vesicle transport, deletion of *SCS2* did not affect secretion [150]. A poorly characterized homologue of Scs2p, Scs22p, has been identified that may fulfill this role [158,187]. Deletion of *SCS22* caused a mild inositol auxotrophy at 37°C and enhanced the inositol auxotrophy of yeast lacking Scs2p at 34°C, indicating a role in the same pathway. Scs22p lacks the coiled-coil and transmembrane domains, making it structurally similar to the major sperm protein (MSP), a VAP orthologue found in *C. elegans* that forms a cytosolic filament network that translocates vesicles to the PM and contributes to sperm pseudopodial movement [152,188]. A model can be predicted in which Scs22p regulates trafficking, while Scs2p regulates membrane localization. In the mammalian orthologues, these roles may be combined in both VAP-A and VAP-B.

The role of VAP-B, which heterodimerizes with VAP-A [153], with respect to the ORP family has not been investigated. It is possible that the endogenous ligand of some of the ORPs is VAP-B rather than VAP-A, and that the interaction detected in GST

pull-down assays is indirect and due to the interaction of the ORP with endogenous VAP-B, which is able to heterodimerize with GST-VAP-A. Indeed, VAP-B was co-immunoprecipitated by OSBP monoclonal antibody 11H9 (Fig. 12), as well as by V5 monoclonal and ORP9 polyclonal antibodies (Fig. 14), suggesting a functional interaction of VAP-B with the ORP family. The VAP polyclonal antibody used here recognizes both VAP-A and VAP-B. Thus the contribution of VAP-B to the co-immunoprecipitation of OSBP and the ORP9 variants is unclear. Isoform specific antibodies or yeast two-hybrid analysis of the interaction of VAP-B with OSBP and the ORP family is required to address this issue.

5.2 VAP-A and OSBP regulate a pre-transport step in ceramide and VSVG trafficking

The discovery that OSBP interacts with VAP-A, and the subsequent identification of a network of several VAP-A binding ORPs, supports the conclusion that the ORP family interacts with the vesicle trafficking machinery in order to perform its role(s). Support for a role of VAP-A and its homologue, VAP-B, in vesicle trafficking pathways have been demonstrated in several different systems. Microinjection of VAP-A antibodies into 3T3-L1 adipocytes or the overexpression of VAP-A in L6 myoblasts inhibited insulin-dependent glucose transporter 4 (GLUT4) trafficking to the PM, presumably by interacting with VAMP-2 and preventing its interaction with target SNAREs [159]. Co-overexpression of VAMP-2 restored trafficking in L6 myoblasts, implying that the ratio of VAP-A and VAMP-2 is important in this trafficking pathway [159]. As well, VAP-B has been implicated in COPI vesicle transport within the Golgi

apparatus, and between the ERGIC and the ER [161]. In that study, addition of a VAP-B antibody to an *in vitro* assay examining transport between purified donor and acceptor Golgi membranes from CHO cells inhibited transport of VSVG through the Golgi apparatus. Since this inhibition was due to the accumulation of coated COPI vesicles, VAP-B is implicated in vesicle uncoating and fusion rather than formation. The addition of soluble recombinant VAP-B reversed the inhibition. In *S. cerevisiae,* vesicle uncoating is stimulated by ARF-GAP, which, through its interaction with Arf1p, may have genetic and functional interactions with OSBP and Osh4/Kes1p [138]. Collectively, these data show that VAP-A and VAP-B are involved in transport within the Golgi apparatus and between the Golgi apparatus and the ER. As a consequence of their interaction with VAP-A, OSBP, ORP1L, ORP3(1d), ORP4L, ORP9S and ORP9L are predicted regulators of vesicle transport in an ER/Golgi apparatus trafficking pathway.

Although there were previous indications that OSBP affected sterol and sphingolipid metabolism via regulation of transport [80,106], the work presented in this thesis is the first to identify the proteins involved with OSBP in this process. Mutations in the PH domain of OSBP lead to its constitutive association with VAP-A (Fig. 12), resulting in altered ER structure (Figs. 23,24) as well as aberrant compartmentation and export of VSVG-GFP and ceramide, respectively (Figs. 25, 26). However, the PH domain of OSBP was not required for the interaction of OSBP and GST-VAP-A *in vitro* (Fig. 8), and thus is not directly involved in the localization of OSBP to the ER through its association with VAP-A. A possible explanation is that the extent of OSBP localization to the ER and Golgi apparatus is mediated by the relative contribution of the PH domain and VAP-A binding region (Fig. 39). In this model, the disruption of the PH

Figure 39. Translocation of the ORP family between the ER and Golgi apparatus. Schematic model showing the predicted translocation of OSBP or ORP family members to the ER via the interaction with VAP-A, or to the Golgi apparatus via the interaction of the PH domain with a phosphorylated PI and an undetermined binding partner (X).

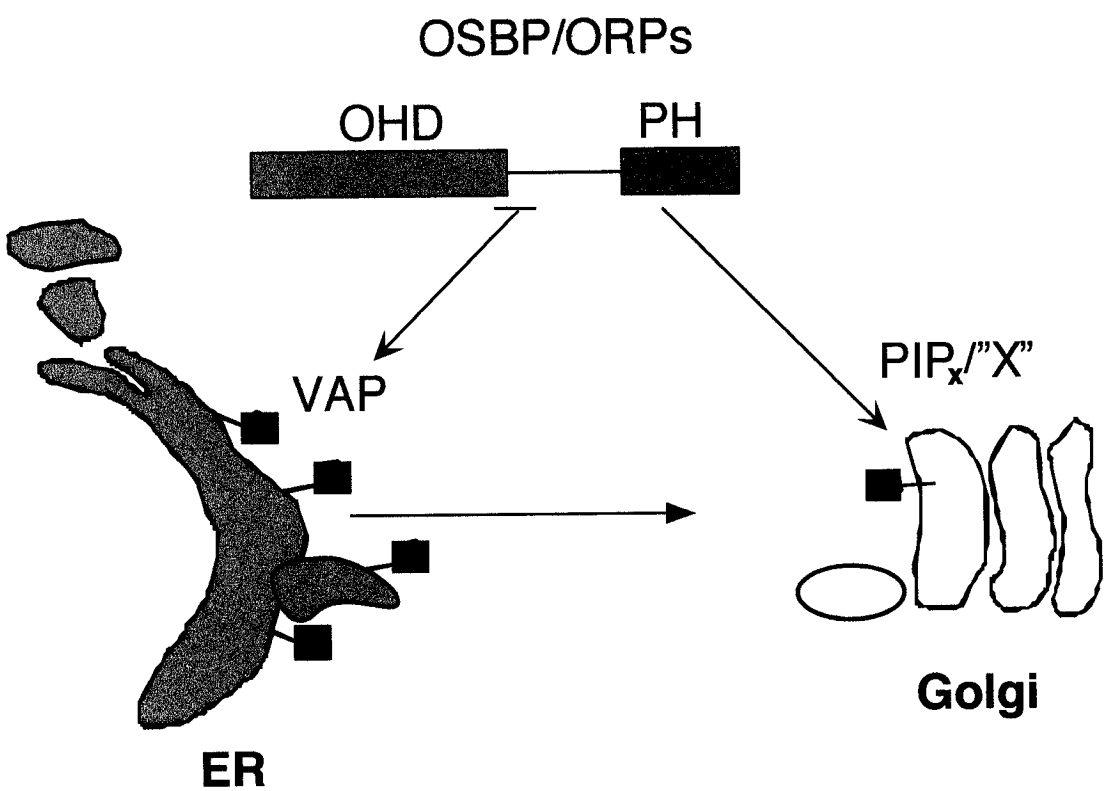

ER/ERGIC morphology
Lipid and protein export

Figure 39

or VAP-A binding domain would be predicted to lead to constitutive localization to the ER or Golgi apparatus, respectively. In support of this, the isolated OSBP-PH domain localizes to the Golgi apparatus *in vivo* and to purified Golgi membranes *in vitro* [25], and a segment of OSBP encoding amino acids 188-425 was ER-localized in COS cells [26]. Although the FFAT motif was shown to regulate ER-localization of truncated versions of Opi1p, Osh1p, and Osh2p, none of these proteins are constitutively ER-associated, indicating that Scs2p-mediated localization is not a dominant signal. Deletion or overexpression of Scs2p altered the subcellular localization of these proteins, confirming that Scs2p plays a role in localization, but its effects on targeting are integrated with other signals. In support of this, endogenous OSBP is localized to what appears to be a cytoplasmic/vesicular compartment rather than predominantly to the ER or Golgi apparatus. OSBP could translocate between these three compartments, and ER- or Golgi-localization may only occur in response to specific stimuli, such as 25OH or sterol transport. A stimulus promoting constitutive ER localization has not yet been identified.

The OSBP W174A mutation did not affect binding to PI-4,5-P_2 (Fig. 27). This argues against a model wherein the activity of each domain affects cellular localization. Instead, this suggests that a second activity associated with the PH domain is altered by the W174A mutation or deletion of the C-terminal half of the PH domain, thus allowing the interaction of OSBP with VAP-A to become dominant. Potential candidates include previously identified protein partners for the OSBP PH domain such as RACK1, the $\beta\gamma$ subunit of heterotrimeric G-proteins and tubulin [68,78,79]. The finding that ER-derived structures formed in response to induction of OSBP W174A were involved in trafficking

of C_5-DMB-ceramide from the ER to the Golgi was not unexpected, since OSBP and oxysterols had previously been shown to regulate ceramide trafficking from the ER to the Golgi apparatus for conversion to SM [80,106]. Since this pathway was stimulated by overexpression of OSBP but suppressed by OSBP W174A, the OSBP W174A mutant appears to act as a dominant inhibitor [80,143]. Ceramide is synthesized on the cytosolic surface of the ER by the condensation of L-serine and palmitoyl-CoA to form 3-ketodihydrosphinogosine, which is then *N*-acylated and desaturated to form ceramide [189-192]. Ceramide is then transported to the lumenal or cytosolic surface of the Golgi for conversion to SM by SM synthase, or to glucosylceramide by ceramide glucosyltransferase, respectively [107,193-196]. The mechanisms that regulate the topology and transport of ceramide to the Golgi apparatus are controversial. Transport to the lumenal surface is ATP- and cytosol-dependent, whereas transport to the cytosolic surface is ATP-independent (or partially independent) [197,198]. Protein transport is normal in cell lines that are defective for ATP-dependent ceramide transport, indicating the existence of a ceramide-specific transport pathway.

Like ceramide and other lipids, proteins must be transported from the ER to the Golgi apparatus prior to secretion or delivery to other cellular compartments. COPII vesicles mediate anterograde protein traffic from the ER to the Golgi apparatus, while COPI vesicles mediate both retrograde transport and transport within the Golgi stack [199-205]. COPII vesicle formation is initiated by the recruitment of Sar1, a small GTPase, to the ER membrane, while the subsequent recruitment of two heterodimeric complexes, Sec23/Sec24 and Sec13/Sec31, drives vesicle formation and contributes to cargo selection [199,206-208]. After leaving the ER, COPII vesicles uncoat and fuse to

form vesicular-tubular clusters which comprise the ERGIC. Preformed COPI complexes are then recruited to the ERGIC to promote the retrograde transport of escaped ER proteins, as well as further anterograde transport to the Golgi apparatus [209,210].

It has been assumed that all proteins share a common transport pathway, and therefore that protein sorting does not occur until after arrival at the Golgi apparatus. However, recent evidence from yeast suggests that this may not be the case, as GPI anchored proteins are transported to the Golgi apparatus separately from other secretory proteins [211]. Although this potentially has wide implications in the regulation of ER export, the mechanisms regulating this process are as yet unclear.

Since transport of ceramide and protein from the ER to the Golgi involves different pathways, it is unclear why C_5-DMB-ceramide and VSVG-GFP would occupy the same compartment in induced CHO-tet-OSBP W174A cells. A potential explanation is that the primary effect of OSBP W174A is on ceramide transport and unfolded VSVG-GFP localized to the ER-derived structures non-specifically. In support of this, unfolded VSVG-GFP was found in the undistorted regions of the ER and exited the ER-derived structures normally at the permissive temperature. This was not the case for C_5-DMB-ceramide, which was retained in the structures and appeared to have delayed transport to the Golgi apparatus. Defective transport of ceramide to the Golgi is supported by an observed decrease in SM synthesis in OSBP W174A expressing cells.

The appearance and accumulation of misfolded VSVG-GFP and C_5-DMB-ceramide in the ER-derived structures suggests a role in an ER export or protein maturation pathway. Since localization of Sec31 and p58, markers of the transitional ER and ERGIC, respectively, was not altered by OSBP W174A expression (Fig. 24), OSBP

and VAP-A are more likely to regulate an early step in export. The presence of misfolded VSVG-GFP and co-localization with GRP74/BiP and GRP94 indicates the ER-derived structures are a protein folding compartment. While the localization of VSVG-GFP to the ER-derived structures could be non-specific and simply due to proliferation or expansion of this abnormal compartment, evidence from yeast studies indicates otherwise. A relationship between *SCS2*, phospholipid regulation and the unfolded protein response (UPR) was demonstrated by suppression of the inositol auxotrophy of a *hac1Δ* strain by overexpression of Scs2p. [158]. Hac1p mRNA is spliced by Ire1p, a bifunctional ER-localized kinase/endoribonuclease, in response to the accumulation of unfolded proteins in the ER [212-215]. Hac1p is proposed to have two roles: (i) increase transcription of protein chaperones [216] and (ii) increase phospholipid synthesis by antagonizing the activity of Opi1p, which negatively regulates the transcription of several genes involved in phospholipid biosynthesis [217]. Therefore, it is possible that Scs2p alters lipid synthesis or export during a stress response such that increased phospholipid synthesis in response to Hac1p is unnecessary. We suggest that overexpression of Scs2p suppresses the inositol auxotrophy of the *hac1Δ* strain by increasing localization of Opi1p to the ER, thus preventing it from entering the nucleus. Thus the Hac1p and Scs2p pathways converge on repression of Opi1p activity in order to positively regulate phospholipid synthesis. A model can be predicted in which the same changes that activate Ire1p also activate Scs2p, causing it to bind more Opi1p and preventing its nuclear localization and inhibition of phospholipid synthesis.

5.3 ORP9 variants alter ER structure

Like ORP1 and ORP4 [1,3], two ORP9 variants are expressed as a result of alternate promoter start sites and splicing (Wang and Ridgway unpublished results). Endogenous ORP9L, which is the only form detectable by Western blotting in CHO-K1 and HEK 293 cells (Fig. 29), was localized primarily to the Golgi apparatus in uninduced CHO-tet-ORP9L cells (Fig. 30). Like OSBP and Osh1p, Golgi apparatus localization of ORP9L is probably mediated via its PH domain, although this has not been confirmed. However, the sequence of OSBP and ORP9L PH domains are quite similar, suggesting that they may bind similar targets. Both ORP9 variants also contain the FFAT motif (although the second phenylalanine is mutated to tyrosine), which is predicted to regulate their localization to the ER through interaction with VAP-A. Since ORP9S does not have a PH domain, the FFAT motif may be the dominant localization signal.

The subcellular localization of overexpressed ORP9S and ORP9L was quite different from that of endogenous ORP9L (Figs. 30, 32,33). Although both ORP9 variants were primarily cytosolic when overexpressed, they both caused the formation of ER-derived membranous structures with VAP and ORP9 on the surface. Neither ORP9S nor ORP9L appeared to co-localize with regions of the ER other than the abnormal structures. Since the ER localization of the ORP9 variants is mediated via VAP-A, these structures probably represent coalesced VAP-A/ORP9 complexes that, in the case of ORP9L, contain most or all of the VAP-A in the cell. Although endogenous ORP9L is Golgi-localized (Fig. 30A), immunostaining of the Golgi apparatus by the polyclonal ORP9 antibody in ORP9L overexpressing cells could not be detected. Since overexpression of ORP9L did not alter the structure of the Golgi apparatus (Fig. 33),

Golgi-localization of overexpressed ORP9L may have been obscured by abundant cytoplasmic expression. However, ORP9L was not detected in the Golgi apparatus of cells pre-treated with saponin. This could either indicate that the localization of ORP9L to the Golgi apparatus was sensitive to saponin treatment, or that overexpression of ORP9L caused metabolic change(s) such that localization to the Golgi apparatus was inhibited. This also suggests that ORP9L binding to the Golgi apparatus is weak or the site is of low abundance and saturated by overexpression of ORP9L. Overexpressed ORP9S was also not detected in the Golgi apparatus, but this was not unexpected due to the lack of a PH domain. VAP-A binding sites are probably also saturated by the overexpression of ORP9S and ORP9L leading to extensive cytoplasmic localization. These data suggest that, like OSBP, the ORP9 variants are dynamic receptors that localize to the Golgi apparatus or the ER via the VAP-A binding domain or PH domain.

Apart from the effects on the ERGIC, the morphological changes caused by overexpression of the ORP9 variants were similar to those caused by overexpression of OSBP W174A (Figs. 24, 32,33). The interaction between VAP-A and both of the ORP9 variants appeared more stable than the interaction between VAP-A and OSBP (compare Figs. 12 and 14). Thus, increasing the stability of the VAP-A/ORP complex, either by introducing a stabilizing mutation or by overexpression of a stronger binding partner, results in structural changes in the ER. The lack of ER structure alteration seen with OSBP overexpression could be due to relatively lower expression levels, however. In support of this OSBP was overexpressed approximately 6- to 8-fold compared to approximately 100-fold overexpression of ORP9L (Fig. 13, [143]). Theoretically, if a number of ORPs, as well as other FFAT motif-containing proteins, localize to the ER

through their interaction with VAP-A, then an excess of one partner would displace the others and disrupt their downstream signalling and regulatory pathways. Overexpression of VAP-A did not alter ER structure or interfere with ceramide or VSVG-GFP export (Figs. 18, 21, 22), demonstrating that it is not a limiting component of these pathways. Therefore, the alterations in ER structure are most likely due to the saturation of VAP-A by the overexpression of one of its binding partners, or to the displacement of endogenous binding partners. How this leads to alterations in ER structure is unclear.

OSBP expression was decreased in ORP9S or ORP9L overexpressing cells (Fig. 36), potentially due to its displacement from VAP-A by the ORP9 variants. As the subcellular localization of OSBP is central to its function [21,27,28], preventing its interaction with VAP-A may lead to its degradation. Conversely, overexpression of ORP9S or ORP9L may activate an independent pathway leading to inhibition of OSBP expression. Since expression of VAP-A and VAP-B was not altered by overexpression of the ORP9 variants, this is not a global effect on protein expression.

Overexpression of the ORP9 variants also caused OSBP to become dephosphorylated, as shown by the increase in the lower band of the OSBP doublet on SDS-PAGE (Fig. 36). Dephosphorylation of OSBP occurred before the decrease in OSBP expression, suggesting that the pathway(s) resulting in OSBP dephosphorylation were activated prior to reduced expression (Fig. 36). The reverse of these experiments was also true. Overexpression of VAP-A caused increased phosphorylation of OSBP, as well as an increase in the amount of membrane-associated OSBP, potentially due to enhanced localization of OSBP to the ER (Fig. 16). Therefore, the decreased

phosphorylation of OSBP in ORP9S and ORP9L overexpressing cells (Fig. 36) indicates that reduced ER localization may cause OSBP dephosphorylation.

In addition to effects on OSBP phosphorylation and expression, overexpression of the ORP9 variants caused an overall decrease in cell growth rate. ORP9L slowed growth rates compared to uninduced controls, while ORP9S expressing cells were more severely affected (Figs. 13, 28). Endogenous ORP9S was not detectable in CHO-K1, HEK 293 or uninduced CHO-tet-on cells (Figs. 13, 29), but the protein can be detected in human liver (Wang and Ridgway, unpublished data). The lack of endogenous ORP9S expression may indicate that ORP9S has cell-specific functions and is toxic when inappropriately expressed. Conversely, ORP9S may only be expressed at a certain point of the cell cycle or developmental stage, and its enforced expression at inappropriate times may be toxic. Since overexpression of ORP9L was not as toxic as that of ORP9S, the PH domain is predicted to alter ORP9L localization and mitigate toxic effects of overexpression. Substantially more ORP9L was membrane associated than ORP9S (Fig. 34). However, both ORP9S and ORP9L interact with VAP-A at the ER, and the interactions seemed to be equally stable as assessed by co-immunoprecipitation (Fig. 14).

We have demonstrated that the ORP9 variants interact with VAP-A in the ER, but their function(s) at this site is unknown. However, cDNAs cloned by yeast two-hybrid analysis using these proteins as bait have provided some clues. Five cDNAs were isolated (Table 2), and although the only structural difference between ORP9S and ORP9L is the PH domain, only Int6/eIF3e interacted with both variants. Int6/eIF3e was identified both as a component of translation initiation factor 3 [167] and the proteasome [168]. The two roles are not mutually exclusive, as translation and degradation are often

linked in order to facilitate degradation of misfolded or incorrectly translated proteins [218]. ORP9S and ORP9L both interacted specifically with the PCI domain of Int6/eIF3e, a domain also found in several components of the proteasome and the related COP9 signalosome [219]. A link to proteasomal degradation can also be inferred from the interaction of ORP9L with the β subunit of PA28, a proteasome activator [170]. Although PA28 does play a general role in proteasome activation, it does so in the context of antigen generation for presentation on MHC class I molecules [220]. Interestingly, RED/IK cytokine, which was identified as an ORP9S binding protein, is involved in the downregulation of antigen presentation via HLAII molecules [165,166], and cathepsin B, which is a lysosomal cysteine protease proposed to play a role in the processing of antigens in the immune response has a FFAT motif [26,221]. The significance of these interactions has yet to be defined, but they hint at a role for the ORP9 variants in proteasomal-mediated degradation.

6 Conclusions and future directions

This study is the first to identify interactions of ORP proteins with the ER-localized protein VAP-A and demonstrate a role in regulation of ER-based pathways. Based on prior evidence from our lab and others, data from studies in *S. cerevisiae* and the work presented in this thesis, this network of proteins is predicted to regulate cholesterol and sphingolipid metabolism through effects on ER structure and export. The interaction of VAP-A with components of the vesicle trafficking and UPR pathways suggests that the ORP family exerts its effects through similar routes and affects diverse cellular processes. Members of the ORP family are predicted to be lipid or sterol sensors that regulate trafficking or transduce signals by translocating between cellular compartments. Their localization to distinct compartments is regulated by the integration of targeting signals such as the N-terminal PH domain, the C-terminal OHD and the VAP-A binding motif, as well as by oxysterol binding and regulation of phosphorylation.

Future work to investigate the functions of other members of the ORP family and their binding partners will help to elucidate the role of this protein network. The network of proteins identified in this study may regulate one common pathway or several interconnected ones. This work has only begun to define the role of this family and many issues need to be addressed:

(i) Investigation of the role of VAP-B, as well as the role of the VAP consensus domain in interaction with ORPs and other proteins.

(ii) Functional analysis of ER-localization of the ORP family, as well as characterization of ORP9 interacting proteins and the identification of other ORP binding partners, will help to determine if VAP-A and the ORP family regulate one central or several interconnected pathways.

(iii) The OHD is conserved among all family members, yet no function as been ascribed to this domain. Identification of protein partners or lipid ligands for this domain may help determine a function common to all ORPs.

(iv) A SCAP/SREBP transport complex isolated from CHO cells contained both VAP-A and VAP-B [222], thus providing evidence of a direct role for OSBP or other members of the ORP family in the regulation of cholesterol synthesis. Determining how VAP-A and OSBP (or other ORPs) regulate SCAP/SREBP activity may determine a mechanistic role in sterol regulation.

7 Appendix I

PCR primers

Primer #	Lab Designation	Sequence (5' –3')
ON1	TH1	CGGCATATGGCGGCGACGGAGCTGAGA
ON2	OSBP11	CGGGATCCGGGCCACTTCAGAAAATGTC
ON3	OSBP12	GGCGGCCCATGGCGGCGACGGAGCTG
ON4	OSBP15(Nde1)	GGGCATATGAGTGATGAGGAT
ON5	VAP33EcoR1(pGEX)	GGGAATTCACTCTACAAGATGAATTTCCC
ON6	VAP33BamH1(pGEX)	GGGGATCCCCATGGCGAAGCACGAGCAG
ON7	VAP33-EcoR1-5'	GGAATTCGCCACCATGGCGAAGCACGAGC
ON8	VAP33-BamH1-3'	GGGATCCACTCTACAAGATGAATTTCCC
ON9	VAP33ΔTMD-BamH1	GGGATCCCTTAAGGACTGGTGACATTATCTC
ON10	VAPΔTMD(Not1)	GGCGGCCGCCTTAAGGACTGGTGACATTATCTC
ON11	pAS1/ORP4 Nde1	CATATGAGCGCTTCCACG
ON12	pAS1/ORP4 Sal1	GGATCCTCAGAAGATGTTGGG
ON13	ORP4 5' Nco1	CCCATGGCGCTTCCACGTCC
ON14	ORP9-5' Nco1	TACCATGGTAGAATCAATTAAACAC
ON15	ORP9 3' Xma1	CAGGGCCCAACCTAATGCTTGGC
ON16	eIF3e-Nco1	CCCATGGCGGAGTACGACTTGAC
ON17	eIF3e-Nde1	CCATATGGCGGAGTACGACTTGAC
ON18	eIF3e-BamH1	GGATCCTCAGTAGAAGCCAGAATC
ON19	Int6-PCI	CCCATGGACTTTGATGGGGCTCAG

Mutagenic primers

Primer #	Lab Designation	Mutation	Sequence (5'-3')
ON20	OSBP-SDM-1	OSBP Δ261-296	CGAAAAGATCAAACAGGTCCA GTATGAGAGAGACCAGC
ON21	OSBP-SDM-2	OSBP Δ262-278	GCAACGAAAAGATCAAACAGT GCAGAGATTTCCTCGTGC
ON22	OSBP-SDM-3	OSBP Δ279-296	GCCATGATCAATGCTTGCCAGT ATGAGAGAGACCAGC
ON23	OSBP-SDM-4	OSBP L306, 313A	GCGCATTCGAGCAGAAGAGACC CTCGAGCAGGCAGCAAAGCAGC
ON24	OSBP-SDM-6A	OSBP Δ288-296	GATTTCCTCGTGCTAGCTCAGAC CCAGTATGAGAGAGACCAGCGC
ON25	OSBP-SDM-7A	OSBP Δ209-305	TGGCAGAAGTCGCTGCAGTATCT GGAAGAGACCCTCGAGCAGCTG
ON26	OSBP-SDM-8B	OSBP L306Q	GACCAGCGCATTCGACAGGAA GAGACCCTCGAG
ON27	OSBP-SDM-10	OSBP Δ306-315	CCAGCGCATTCGACAGCACAAC CACC
ON28	OSBP-VAP-Int	OSBP Δ432-435	GAACTGCATTGGGAAAATCCCC ATGCCGGTG
ON29	11293-p4	OSBP W174A	GAGCGGCAGCGCGCGGTGACA GCCCTG
ON30	VAP33 Δ43-49		CGGATAGAAAAGTGTGTTTCCG CCGGTACTGTGTG
ON31	VAP33 Δ161-241		CACAGTGTTTCACTTTAAGATA CCGAAACAAGG
ON32	VAP33 ΔTMD		GATAATGTCACCAGTCCTTAAC CTTCACTTCTTG
ON33	ORP9L-5'-Nco1		GGCGGCTCCCCCATGGCGTCCA TCATGG

8 Literature Cited

1. Wang C, JeBailey, L., Ridgway, N.D.: **Oxysterol Binding Protien (OSBP)-related protein 4 binds 25-hydroxycholesterol and interacts with vimentin intermediate filaments.** *Biochem Journal* 2002, **361**:461-472.

2. Lehto M, Olkkonen VM: **The OSBP-related proteins: a novel protein family involved in vesicle transport, cellular lipid metabolism, and cell signalling.** *Biochim Biophys Acta* 2003, **1631**:1-11.

3. Johansson M, Bocher V, Lehto M, Chinetti G, Kuismanen E, Ehnholm C, Staels B, Olkkonen VM: **The Two Variants of Oxysterol Binding Protein-related Protein-1 Display Different Tissue Expression Patterns, Have Different Intracellular Localization, and Are Functionally Distinct.** *Mol Biol Cell* 2003, **14**:903-915.

4. Jaworski CJ, Moreira E, Li A, Lee R, Rodriguez IR: **A family of 12 human genes containing oxysterol-binding domains.** *Genomics* 2001, **78**:185-196.

5. Collier FM, Gregorio-King CC, Apostolopoulos J, Walder K, Kirkland MA: **ORP3 Splice Variants and Their Expression in Human Tissues and Hematopoietic Cells.** *DNA Cell Biol* 2003, **22**:1-9.

6. Lehto M, Laitinen S, Chinetti G, Johansson M, Ehnholm C, Staels B, Ikonen E, Olkkonen VM: **The OSBP-related protein family in humans.** *J Lipid Res* 2001, **42**:1203-1213.

7. Laitinen S, Olkkonen VM, Ehnholm C, Ikonen E: **Family of human oxysterol binding protein (OSBP) homologues. A novel member implicated in brain sterol metabolism.** *J Lipid Res* 1999, **40**:2204-2211.

8. Beh CT, Cool L, Phillips J, Rine J: **Overlapping functions of the yeast oxysterol-binding protein homologues.** *Genetics* 2001, **157**:1117-1140.

9. Jiang B, Brown JL, Sheraton J, Fortin N, Bussey H: **A new family of yeast genes implicated in ergosterol synthesis is related to the human oxysterol binding protein.** *Yeast* 1994, **10**:341-353.

10. Sugawara K, Morita K, Ueno N, Shibuya H: **BIP, a BRAM-interacting protein involved in TGF-beta signalling, regulates body length in Caenorhabditis elegans**. *Genes Cells* 2001, **6**:599-606.

11. Anniss AM, Apostolopoulos J, Dworkin S, Purton LE, Sparrow RL: **An oxysterol-binding protein family identified in the mouse**. *DNA Cell Biol* 2002, **21**:571-580.

12. Hull CM, Johnson AD: **Identification of a mating type-like locus in the asexual pathogenic yeast Candida albicans**. *Science* 1999, **285**:1271-1275.

13. Fukuzawa M, Williams JG: **OSBPa, a predicted oxysterol binding protein of Dictyostelium, is required for regulated entry into culmination**. *FEBS Lett* 2002, **527**:37-42.

14. Alphey L, Jimenez J, Glover D: **A Drosophila homologue of oxysterol binding protein (OSBP)-- implications for the role of OSBP**. *Biochim Biophys Acta* 1998, **1395**:159-164.

15. Moreira EF, Jaworski C, Li A, Rodriguez IR: **Molecular and biochemical characterization of a novel oxysterol-binding protein (OSBP2) highly expressed in retina**. *J Biol Chem* 2001, **276**:18570-18578.

16. Galaud JP, Laval V, Carriere M, Barre A, Canut H, Rouge P, Pont-Lezica R: **Osmotic stress activated expression of an Arabidopsis plasma membrane-associated protein: sequence and predicted secondary structure**. *Biochim Biophys Acta* 1997, **1341**:79-86.

17. Dawson PA, Ridgway ND, Slaughter CA, Brown MS, Goldstein JL: **cDNA cloning and expression of oxysterol-binding protein, an oligomer with a potential leucine zipper**. *J Biol Chem* 1989, **264**:16798-16803.

18. Mayer K, Schuller C, Wambutt R, Murphy G, Volckaert G, Pohl T, Dusterhoft A, Stiekema W, Entian KD, Terryn N, et al.: **Sequence and analysis of chromosome 4 of the plant Arabidopsis thaliana**. *Nature* 1999, **402**:769-777.

19. Kandutsch AA, Chen HW, Shown EP: **Binding of 25-hydroxycholesterol and cholesterol to different cytoplasmic proteins**. *Proc Natl Acad Sci U S A* 1977, **74**:2500-2503.

20. Dawson PA, Van der Westhuyzen DR, Goldstein JL, Brown MS: **Purification of oxysterol binding protein from hamster liver cytosol.** *J Biol Chem* 1989, **264**:9046-9052.

21. Lagace TA, Byers DM, Cook HW, Ridgway ND: **Altered regulation of cholesterol and cholesteryl ester synthesis in Chinese-hamster ovary cells overexpressing the oxysterol-binding protein is dependent on the pleckstrin homology domain.** *Biochem J* 1997, **326**:205-213.

22. Ridgway ND, Lagace TA, Cook HW, Byers DM: **Differential effects of sphingomyelin hydrolysis and cholesterol transport on oxysterol-binding protein phosphorylation and Golgi localization.** *J Biol Chem* 1998, **273**:31621-31628.

23. Laitinen S, Lehto M, Lehtonen S, Hyvarinen K, Heino S, Lehtonen E, Ehnholm C, Ikonen E, Olkkonen VM: **ORP2, a homolog of oxysterol binding protein, regulates cellular cholesterol metabolism.** *J Lipid Res* 2002, **43**:245-255.

24. Levine TP, Munro S: **Dual targeting of Osh1p, a yeast homologue of oxysterol-binding protein, to both the Golgi and the nucleus-vacuole junction.** *Mol Biol Cell* 2001, **12**:1633-1644.

25. Levine TP, Munro S: **The pleckstrin homology domain of oxysterol-binding protein recognises a determinant specific to Golgi membranes.** *Curr Biol* 1998, **8**:729-739.

26. Loewen CJ, Roy A, Levine TP: **A conserved ER targeting motif in three families of lipid binding proteins and in Opi1p binds VAP.** *Embo J* 2003, **22**:2025-2035.

27. Storey MK, Byers DM, Cook HW, Ridgway ND: **Cholesterol regulates oxysterol binding protein (OSBP) phosphorylation and Golgi localization in Chinese hamster ovary cells: correlation with stimulation of sphingomyelin synthesis by 25-hydroxycholesterol.** *Biochem J* 1998, **336**:247-256.

28. Mohammadi A, Perry RJ, Storey MK, Cook HW, Byers DM, Ridgway ND: **Golgi localization and phosphorylation of oxysterol binding protein in Niemann-Pick C and U18666A-treated cells.** *J Lipid Res* 2001, **42**:1062-1071.

29. Taylor FR, Saucier SE, Shown EP, Parish EJ, Kandutsch AA: **Correlation between oxysterol binding to a cytosolic binding protein and potency in the repression of hydroxymethylglutaryl coenzyme A reductase.** *J Biol Chem* 1984, **259**:12382-12387.

30. Taylor FR, Shown EP, Thompson EB, Kandutsch AA: **Purification, subunit structure, and DNA binding properties of the mouse oxysterol receptor.** *J Biol Chem* 1989, **264**:18433-18439.

31. Levanon D, Hsieh CL, Francke U, Dawson PA, Ridgway ND, Brown MS, Goldstein JL: **cDNA cloning of human oxysterol-binding protein and localization of the gene to human chromosome 11 and mouse chromosome 19.** *Genomics* 1990, **7**:65-74.

32. Vogel US, Dixon RA, Schaber MD, Diehl RE, Marshall MS, Scolnick EM, Sigal IS, Gibbs JB: **Cloning of bovine GAP and its interaction with oncogenic ras p21.** *Nature* 1988, **335**:90-93.

33. Ridgway ND, Dawson PA, Ho YK, Brown MS, Goldstein JL: **Translocation of oxysterol binding protein to Golgi apparatus triggered by ligand binding.** *J Cell Biol* 1992, **116**:307-319.

34. Klarlund JK, Guilherme A, Holik JJ, Virbasius JV, Chawla A, Czech MP: **Signaling by phosphoinositide-3,4,5-trisphosphate through proteins containing pleckstrin and Sec7 homology domains.** *Science* 1997, **275**:1927-1930.

35. Lemmon MA, Ferguson KM: **Signal-dependent membrane targeting by pleckstrin homology (PH) domains.** *Biochem J* 2000, **350 Pt 1**:1-18.

36. Lemmon MA: **Phosphoinositide recognition domains.** *Traffic* 2003, **4**:201-213.

37. Gibson TJ, Hyvonen M, Musacchio A, Saraste M, Birney E: **PH domain: the first anniversary.** *Trends Biochem Sci* 1994, **19**:349-353.

38. Lemmon MA, Ferguson KM, Schlessinger J: **PH domains: diverse sequences with a common fold recruit signaling molecules to the cell surface.** *Cell* 1996, **85**:621-624.

39. Downing AK, Driscoll PC, Gout I, Salim K, Zvelebil MJ, Waterfield MD: **Three-dimensional solution structure of the pleckstrin homology domain from dynamin**. *Curr Biol* 1994, **4**:884-891.

40. Ferguson KM, Lemmon MA, Schlessinger J, Sigler PB: **Crystal structure at 2.2 A resolution of the pleckstrin homology domain from human dynamin**. *Cell* 1994, **79**:199-209.

41. Ferguson KM, Lemmon MA, Schlessinger J, Sigler PB: **Structure of the high affinity complex of inositol trisphosphate with a phospholipase C pleckstrin homology domain**. *Cell* 1995, **83**:1037-1046.

42. Fushman D, Cahill S, Lemmon MA, Schlessinger J, Cowburn D: **Solution structure of pleckstrin homology domain of dynamin by heteronuclear NMR spectroscopy**. *Proc Natl Acad Sci U S A* 1995, **92**:816-820.

43. Macias MJ, Musacchio A, Ponstingl H, Nilges M, Saraste M, Oschkinat H: **Structure of the pleckstrin homology domain from beta-spectrin**. *Nature* 1994, **369**:675-677.

44. Yoon HS, Hajduk PJ, Petros AM, Olejniczak ET, Meadows RP, Fesik SW: **Solution structure of a pleckstrin-homology domain**. *Nature* 1994, **369**:672-675.

45. Shaw G: **The pleckstrin homology domain: an intriguing multifunctional protein module**. *Bioessays* 1996, **18**:35-46.

46. Mayer BJ, Ren R, Clark KL, Baltimore D: **A putative modular domain present in diverse signaling proteins**. *Cell* 1993, **73**:629-630.

47. Haslam RJ, Koide HB, Hemmings BA: **Pleckstrin domain homology**. *Nature* 1993, **363**:309-310.

48. Musacchio A, Gibson T, Rice P, Thompson J, Saraste M: **The PH domain: a common piece in the structural patchwork of signalling proteins**. *Trends Biochem Sci* 1993, **18**:343-348.

49. Blomberg N, Baraldi E, Nilges M, Saraste M: **The PH superfold: a structural scaffold for multiple functions**. *Trends Biochem Sci* 1999, **24**:441-445.

50. Bottomley MJ, Salim K, Panayotou G: **Phospholipid-binding protein domains.** *Biochim Biophys Acta* 1998, **1436**:165-183.

51. Harlan JE, Hajduk PJ, Yoon HS, Fesik SW: **Pleckstrin homology domains bind to phosphatidylinositol-4,5- bisphosphate.** *Nature* 1994, **371**:168-170.

52. Harlan JE, Yoon HS, Hajduk PJ, Fesik SW: **Structural characterization of the interaction between a pleckstrin homology domain and phosphatidylinositol 4,5-bisphosphate.** *Biochemistry* 1995, **34**:9859-9864.

53. Rebecchi MJ, Scarlata S: **Pleckstrin homology domains: a common fold with diverse functions.** *Annu Rev Biophys Biomol Struct* 1998, **27**:503-528.

54. Lemmon MA, Ferguson KM, Abrams CS: **Pleckstrin homology domains and the cytoskeleton.** *FEBS Lett* 2002, **513**:71-76.

55. Maffucci T, Falasca M: **Specificity in pleckstrin homology (PH) domain membrane targeting: a role for a phosphoinositide-protein co-operative mechanism.** *FEBS Lett* 2001, **506**:173-179.

56. Fruman DA, Rameh LE, Cantley LC: **Phosphoinositide binding domains: embracing 3-phosphate.** *Cell* 1999, **97**:817-820.

57. Rameh LE, Cantley LC: **The role of phosphoinositide 3-kinase lipid products in cell function.** *J Biol Chem* 1999, **274**:8347-8350.

58. Vanhaesebroeck B, Waterfield MD: **Signaling by distinct classes of phosphoinositide 3-kinases.** *Exp Cell Res* 1999, **253**:239-254.

59. Vanhaesebroeck B, Jones GE, Allen WE, Zicha D, Hooshmand-Rad R, Sawyer C, Wells C, Waterfield MD, Ridley AJ: **Distinct PI(3)Ks mediate mitogenic signalling and cell migration in macrophages.** *Nat Cell Biol* 1999, **1**:69-71.

60. Leevers SJ, Vanhaesebroeck B, Waterfield MD: **Signalling through phosphoinositide 3-kinases: the lipids take centre stage.** *Curr Opin Cell Biol* 1999, **11**:219-225.

61. Vanhaesebroeck B, Higashi K, Raven C, Welham M, Anderson S, Brennan P, Ward SG, Waterfield MD: **Autophosphorylation of p110delta phosphoinositide 3-kinase: a new paradigm for the regulation of lipid kinases in vitro and in vivo.** *Embo J* 1999, **18**:1292-1302.

62. Cullen PJ, Chardin P: **Membrane targeting: what a difference a G makes.** *Curr Biol* 2000, **10**:R876-878.

63. Stauffer TP, Ahn S, Meyer T: **Receptor-induced transient reduction in plasma membrane PtdIns(4,5)P2 concentration monitored in living cells.** *Curr Biol* 1998, **8**:343-346.

64. Varnai P, Balla T: **Visualization of phosphoinositides that bind pleckstrin homology domains: calcium- and agonist-induced dynamic changes and relationship to myo-[3H]inositol-labeled phosphoinositide pools.** *J Cell Biol* 1998, **143**:501-510.

65. Sugars JM, Cellek S, Manifava M, Coadwell J, Ktistakis NT: **Hierarchy of membrane-targeting signals of phospholipase D1 involving lipid modification of a pleckstrin homology domain.** *J Biol Chem* 2002, **277**:29152-29161.

66. Burks DJ, Wang J, Towery H, Ishibashi O, Lowe D, Riedel H, White MF: **IRS pleckstrin homology domains bind to acidic motifs in proteins.** *J Biol Chem* 1998, **273**:31061-31067.

67. Wang DS, Shaw R, Hattori M, Arai H, Inoue K, Shaw G: **Binding of pleckstrin homology domains to WD40/beta-transducin repeat containing segments of the protein product of the Lis-1 gene.** *Biochem Biophys Res Commun* 1995, **209**:622-629.

68. Touhara K, Inglese J, Pitcher JA, Shaw G, Lefkowitz RJ: **Binding of G protein beta gamma-subunits to pleckstrin homology domains.** *J Biol Chem* 1994, **269**:10217-10220.

69. Tsukada S, Simon MI, Witte ON, Katz A: **Binding of beta gamma subunits of heterotrimeric G proteins to the PH domain of Bruton tyrosine kinase.** *Proc Natl Acad Sci U S A* 1994, **91**:11256-11260.

70. Baumeister MA, Martinu L, Rossman KL, Sondek J, Lemmon MA, Chou MM: **Loss of phosphatidylinositol 3-phosphate binding by the C-terminal Tiam-1**

pleckstrin homology domain prevents in vivo Rac1 activation without affecting membrane targeting. *J Biol Chem* 2003, **278**:11457-11464.

71. Levine TP, Munro S: **Targeting of Golgi-Specific Pleckstrin Homology Domains Involves Both PtdIns 4-Kinase-Dependent and -Independent Components.** *Curr Biol* 2002, **12**:695-704.

72. Donaldson JG, Jackson CL: **Regulators and effectors of the ARF GTPases.** *Curr Opin Cell Biol* 2000, **12**:475-482.

73. Orci L, Palmer DJ, Amherdt M, Rothman JE: **Coated vesicle assembly in the Golgi requires only coatomer and ARF proteins from the cytosol.** *Nature* 1993, **364**:732-734.

74. Watari H, Blanchette-Mackie EJ, Dwyer NK, Watari M, Neufeld EB, Patel S, Pentchev PG, Strauss JF, 3rd: **Mutations in the leucine zipper motif and sterol-sensing domain inactivate the Niemann-Pick C1 glycoprotein.** *J Biol Chem* 1999, **274**:21861-21866.

75. Neufeld EB, Wastney M, Patel S, Suresh S, Cooney AM, Dwyer NK, Roff CF, Ohno K, Morris JA, Carstea ED, et al.: **The Niemann-Pick C1 protein resides in a vesicular compartment linked to retrograde transport of multiple lysosomal cargo.** *J Biol Chem* 1999, **274**:9627-9635.

76. Carstea ED, Morris JA, Coleman KG, Loftus SK, Zhang D, Cummings C, Gu J, Rosenfeld MA, Pavan WJ, Krizman DB, et al.: **Niemann-Pick C1 disease gene: homology to mediators of cholesterol homeostasis.** *Science* 1997, **277**:228-231.

77. Pitcher JA, Touhara K, Payne ES, Lefkowitz RJ: **Pleckstrin homology domain-mediated membrane association and activation of the beta-adrenergic receptor kinase requires coordinate interaction with G beta gamma subunits and lipid.** *J Biol Chem* 1995, **270**:11707-11710.

78. Rodriguez MM, Ron D, Touhara K, Chen CH, Mochly-Rosen D: **RACK1, a protein kinase C anchoring protein, coordinates the binding of activated protein kinase C and select pleckstrin homology domains in vitro.** *Biochemistry* 1999, **38**:13787-13794.

79. Yao L, Janmey P, Frigeri LG, Han W, Fujita J, Kawakami Y, Apgar JR, Kawakami T: **Pleckstrin homology domains interact with filamentous actin.** *J Biol Chem* 1999, **274**:19752-19761.

80. Lagace TA, Byers DM, Cook HW, Ridgway ND: **Chinese hamster ovary cells overexpressing the oxysterol binding protein (OSBP) display enhanced synthesis of sphingomyelin in response to 25-hydroxycholesterol.** *J Lipid Res* 1999, **40**:109-116.

81. Ridgway ND: **Interactions between metabolism and intracellular distribution of cholesterol and sphingomyelin.** *Biochim Biophys Acta* 2000, **1484**:129-141.

82. Brown DA, London E: **Structure and origin of ordered lipid domains in biological membranes.** *J Membr Biol* 1998, **164**:103-114.

83. Anderson RG: **The caveolae membrane system.** *Annu Rev Biochem* 1998, **67**:199-225.

84. Simons K, Ikonen E: **Functional rafts in cell membranes.** *Nature* 1997, **387**:569-572.

85. Rietveld A, Simons K: **The differential miscibility of lipids as the basis for the formation of functional membrane rafts.** *Biochim Biophys Acta* 1998, **1376**:467-479.

86. Kolesnick RN: **Sphingomyelin and derivatives as cellular signals.** *Prog Lipid Res* 1991, **30**:1-38.

87. Lange Y, Swaisgood MH, Ramos BV, Steck TL: **Plasma membranes contain half the phospholipid and 90% of the cholesterol and sphingomyelin in cultured human fibroblasts.** *J Biol Chem* 1989, **264**:3786-3793.

88. Lange Y, Ye J, Chin J: **The fate of cholesterol exiting lysosomes.** *J Biol Chem* 1997, **272**:17018-17022.

89. Patton S: **Correlative relationship of cholesterol and sphingomyelin in cell membranes.** *J Theor Biol* 1970, **29**:489-491.

90. Brown DA, Rose JK: **Sorting of GPI-anchored proteins to glycolipid-enriched membrane subdomains during transport to the apical cell surface.** *Cell* 1992, **68**:533-544.

91. Underwood KW, Jacobs NL, Howley A, Liscum L: **Evidence for a cholesterol transport pathway from lysosomes to endoplasmic reticulum that is independent of the plasma membrane.** *J Biol Chem* 1998, **273**:4266-4274.

92. Neufeld EB, Cooney AM, Pitha J, Dawidowicz EA, Dwyer NK, Pentchev PG, Blanchette-Mackie EJ: **Intracellular trafficking of cholesterol monitored with a cyclodextrin.** *J Biol Chem* 1996, **271**:21604-21613.

93. Cruz JC, Sugii S, Yu C, Chang TY: **Role of Niemann-Pick type C1 protein in intracellular trafficking of low density lipoprotein-derived cholesterol.** *J Biol Chem* 2000, **275**:4013-4021.

94. Kaplan MR, Simoni RD: **Transport of cholesterol from the endoplasmic reticulum to the plasma membrane.** *J Cell Biol* 1985, **101**:446-453.

95. Brown MS, Goldstein JL: **The SREBP pathway: regulation of cholesterol metabolism by proteolysis of a membrane-bound transcription factor.** *Cell* 1997, **89**:331-340.

96. DeBose-Boyd RA, Brown MS, Li WP, Nohturfft A, Goldstein JL, Espenshade PJ: **Transport-dependent proteolysis of SREBP: relocation of site-1 protease from Golgi to ER obviates the need for SREBP transport to Golgi.** *Cell* 1999, **99**:703-712.

97. Slotte JP, Bierman EL: **Depletion of plasma-membrane sphingomyelin rapidly alters the distribution of cholesterol between plasma membranes and intracellular cholesterol pools in cultured fibroblasts.** *Biochem J* 1988, **250**:653-658.

98. Gatt S, Bierman EL: **Sphingomyelin suppresses the binding and utilization of low density lipoproteins by skin fibroblasts.** *J Biol Chem* 1980, **255**:3371-3376.

99. Kudchodkar BJ, Albers JJ, Bierman EL: **Effect of positively charged sphingomyelin liposomes on cholesterol metabolism of cells in culture.** *Atherosclerosis* 1983, **46**:353-367.

100. Slotte JP, Hedstrom G, Rannstrom S, Ekman S: **Effects of sphingomyelin degradation on cell cholesterol oxidizability and steady-state distribution between the cell surface and the cell interior.** *Biochim Biophys Acta* 1989, **985**:90-96.

101. Gupta AK, Rudney H: **Plasma membrane sphingomyelin and the regulation of HMG-CoA reductase activity and cholesterol biosynthesis in cell cultures.** *J Lipid Res* 1991, **32**:125-136.

102. Schoonjans K, Brendel C, Mangelsdorf D, Auwerx J: **Sterols and gene expression: control of affluence.** *Biochim Biophys Acta* 2000, **1529**:114-125.

103. Kandutsch AA, Chen HW: **Inhibition of sterol synthesis in cultured mouse cells by 7alpha- hydroxycholesterol, 7beta-hydroxycholesterol, and 7-ketocholesterol.** *J Biol Chem* 1973, **248**:8408-8417.

104. Janowski BA, Willy PJ, Devi TR, Falck JR, Mangelsdorf DJ: **An oxysterol signalling pathway mediated by the nuclear receptor LXR alpha.** *Nature* 1996, **383**:728-731.

105. Peet DJ, Janowski BA, Mangelsdorf DJ: **The LXRs: a new class of oxysterol receptors.** *Curr Opin Genet Dev* 1998, **8**:571-575.

106. Ridgway ND: **25-Hydroxycholesterol stimulates sphingomyelin synthesis in Chinese hamster ovary cells.** *J Lipid Res* 1995, **36**:1345-1358.

107. Futerman AH, Stieger B, Hubbard AL, Pagano RE: **Sphingomyelin synthesis in rat liver occurs predominantly at the cis and medial cisternae of the Golgi apparatus.** *J Biol Chem* 1990, **265**:8650-8657.

108. Jeckel D, Karrenbauer A, Birk R, Schmidt RR, Wieland F: **Sphingomyelin is synthesized in the cis Golgi.** *FEBS Lett* 1990, **261**:155-157.

109. Ridgway ND, Badiani K, Byers DM, Cook HW: **Inhibition of phosphorylation of the oxysterol binding protein by brefeldin A.** *Biochim Biophys Acta* 1998, **1390**:37-51.

110. Helms JB, Rothman JE: **Inhibition by brefeldin A of a Golgi membrane enzyme that catalyses exchange of guanine nucleotide bound to ARF.** *Nature* 1992, **360**:352-354.

111. Donaldson JG, Lippincott-Schwartz J, Bloom GS, Kreis TE, Klausner RD: **Dissociation of a 110-kD peripheral membrane protein from the Golgi apparatus is an early event in brefeldin A action.** *J Cell Biol* 1990, **111**:2295-2306.

112. Klausner RD, Donaldson JG, Lippincott-Schwartz J: **Brefeldin A: insights into the control of membrane traffic and organelle structure.** *J Cell Biol* 1992, **116**:1071-1080.

113. Gross SD, Anderson RA: **Casein kinase I: spatial organization and positioning of a multifunctional protein kinase family.** *Cell Signal* 1998, **10**:699-711.

114. Chalfant CE, Kishikawa K, Mumby MC, Kamibayashi C, Bielawska A, Hannun YA: **Long chain ceramides activate protein phosphatase-1 and protein phosphatase-2A. Activation is stereospecific and regulated by phosphatidic acid.** *J Biol Chem* 1999, **274**:20313-20317.

115. Dobrowsky RT, Kamibayashi C, Mumby MC, Hannun YA: **Ceramide activates heterotrimeric protein phosphatase 2A.** *J Biol Chem* 1993, **268**:15523-15530.

116. Galadari S, Kishikawa K, Kamibayashi C, Mumby MC, Hannun YA: **Purification and characterization of ceramide-activated protein phosphatases.** *Biochemistry* 1998, **37**:11232-11238.

117. Kishikawa K, Chalfant CE, Perry DK, Bielawska A, Hannun YA: **Phosphatidic acid is a potent and selective inhibitor of protein phosphatase 1 and an inhibitor of ceramide-mediated responses.** *J Biol Chem* 1999, **274**:21335-21341.

118. Xu Y, Liu Y, Ridgway ND, McMaster CR: **Novel members of the human oxysterol-binding protein family bind phospholipids and regulate vesicle transport.** *J Biol Chem* 2001, **276**:18407-18414.

119. Sedgwick SG, Smerdon SJ: **The ankyrin repeat: a diversity of interactions on a common structural framework.** *Trends Biochem Sci* 1999, **24**:311-316.

120. Fang M, Kearns BG, Gedvilaite A, Kagiwada S, Kearns M, Fung MK, Bankaitis VA: **Kes1p shares homology with human oxysterol binding protein and participates in a novel regulatory pathway for yeast Golgi-derived transport vesicle biogenesis.** *Embo J* 1996, **15**:6447-6459.

121. Repa JJ, Mangelsdorf DJ: **The role of orphan nuclear receptors in the regulation of cholesterol homeostasis.** *Annu Rev Cell Dev Biol* 2000, **16**:459-481.

122. Ou J, Tu H, Shan B, Luk A, DeBose-Boyd RA, Bashmakov Y, Goldstein JL, Brown MS: **Unsaturated fatty acids inhibit transcription of the sterol regulatory element-binding protein-1c (SREBP-1c) gene by antagonizing ligand-dependent activation of the LXR.** *Proc Natl Acad Sci U S A* 2001, **98**:6027-6032.

123. Song C, Hiipakka RA, Liao S: **Auto-oxidized cholesterol sulfates are antagonistic ligands of liver X receptors: implications for the development and treatment of atherosclerosis.** *Steroids* 2001, **66**:473-479.

124. Lawn RM, Wade DP, Garvin MR, Wang X, Schwartz K, Porter JG, Seilhamer JJ, Vaughan AM, Oram JF: **The Tangier disease gene product ABC1 controls the cellular apolipoprotein-mediated lipid removal pathway.** *J Clin Invest* 1999, **104**:R25-31.

125. Gregorio-King CC, Collier GR, McMillan JS, Waugh CM, McLeod JL, Collier FM, Kirkland MA: **ORP-3, a human oxysterol-binding protein gene differentially expressed in hematopoietic cells.** *Blood* 2001, **98**:2279-2281.

126. Fournier MV, Guimaraes da Costa F, Paschoal ME, Ronco LV, Carvalho MG, Pardee AB: **Identification of a gene encoding a human oxysterol-binding protein- homologue: a potential general molecular marker for blood dissemination of solid tumors.** *Cancer Res* 1999, **59**:3748-3753.

127. Paramio JM, Jorcano JL: **Beyond structure: do intermediate filaments modulate cell signalling?** *Bioessays* 2002, **24**:836-844.

128. Gillard BK, Thurmon LT, Harrell RG, Capetanaki Y, Saito M, Yu RK, Marcus DM: **Biosynthesis of glycosphingolipids is reduced in the absence of a vimentin intermediate filament network.** *J Cell Sci* 1994, **107**:3545-3555.

129. Gillard BK, Clement R, Colucci-Guyon E, Babinet C, Schwarzmann G, Taki T, Kasama T, Marcus DM: **Decreased synthesis of glycosphingolipids in cells lacking vimentin intermediate filaments.** *Exp Cell Res* 1998, **242**:561-572.

130. Sarria AJ, Panini SR, Evans RM: **A functional role for vimentin intermediate filaments in the metabolism of lipoprotein-derived cholesterol in human SW-13 cells.** *J Biol Chem* 1992, **267**:19455-19463.

131. Kohlwein SD, Eder S, Oh CS, Martin CE, Gable K, Bacikova D, Dunn T: **Tsc13p is required for fatty acid elongation and localizes to a novel structure at the nuclear-vacuolar interface in Saccharomyces cerevisiae.** *Mol Cell Biol* 2001, **21**:109-125.

132. Gavin AC, Bosche M, Krause R, Grandi P, Marzioch M, Bauer A, Schultz J, Rick JM, Michon AM, Cruciat CM, et al.: **Functional organization of the yeast proteome by systematic analysis of protein complexes.** *Nature* 2002, **415**:141-147.

133. Park YU, Hwang O, Kim J: **Two-hybrid cloning and characterization of OSH3, a yeast oxysterol- binding protein homolog.** *Biochem Biophys Res Commun* 2002, **293**:733-740.

134. Song Y, Kim S, Kim J: **ROK1, a high-copy-number plasmid suppressor of kem1, encodes a putative ATP-dependent RNA helicase in Saccharomyces cerevisiae.** *Gene* 1995, **166**:151-154.

135. Kim J, Ljungdahl PO, Fink GR: **kem mutations affect nuclear fusion in Saccharomyces cerevisiae.** *Genetics* 1990, **126**:799-812.

136. Interthal H, Bellocq C, Bahler J, Bashkirov VI, Edelstein S, Heyer WD: **A role of Sep1 (= Kem1, Xrn1) as a microtubule-associated protein in Saccharomyces cerevisiae.** *Embo J* 1995, **14**:1057-1066.

137. White JM, Rose MD: **Yeast mating: getting close to membrane merger.** *Curr Biol* 2001, **11**:R16-20.

138. Li X, Rivas MP, Fang M, Marchena J, Mehrotra B, Chaudhary A, Feng L, Prestwich GD, Bankaitis VA: **Analysis of oxysterol binding protein homologue Kes1p function in regulation of Sec14p-dependent protein transport from the yeast Golgi complex.** *J Cell Biol* 2002, **157**:63-77.

139. Kearns BG, McGee TP, Mayinger P, Gedvilaite A, Phillips SE, Kagiwada S, Bankaitis VA: **Essential role for diacylglycerol in protein transport from the yeast Golgi complex.** *Nature* 1997, **387**:101-105.

140. Cleves AE, McGee TP, Whitters EA, Champion KM, Aitken JR, Dowhan W, Goebl M, Bankaitis VA: **Mutations in the CDP-choline pathway for phospholipid biosynthesis bypass the requirement for an essential phospholipid transfer protein.** *Cell* 1991, **64**:789-800.

141. Wilcox LJ, Balderes DA, Wharton B, Tinkelenberg AH, Rao G, Sturley SL: **Transcriptional profiling identifies two members of the ATP-binding cassette transporter superfamily required for sterol uptake in yeast.** *J Biol Chem* 2002, **277**:32466-32472.

142. **Genome sequence of the nematode C. elegans: a platform for investigating biology. The C. elegans Sequencing Consortium.** *Science* 1998, **282**:2012-2018.

143. Wyles JP, McMaster CR, Ridgway ND: **Vesicle-associated Membrane Protein-associated Protein-A (VAP-A) Interacts with the Oxysterol-binding Protein to Modify Export from the Endoplasmic Reticulum.** *J Biol Chem* 2002, **277**:29908-29918.

144. Sambrook J, Russell DW: *Molecular Cloning: A Laboratory Manual* edn 3rd Ed; 2001.

145. Esser V, Limbird LE, Brown MS, Goldstein JL, Russell DW: **Mutational analysis of the ligand binding domain of the low density lipoprotein receptor.** *J Biol Chem* 1988, **263**:13282-13290.

146. Smith DB, Johnson KS: **Single-step purification of polypeptides expressed in Escherichia coli as fusions with glutathione S-transferase.** *Gene* 1988, **67**:31-40.

147. Peterson GL: **A simplification of the protein assay method of Lowry et al. which is more generally applicable.** *Anal Biochem* 1977, **83**:346-356.

148. Pagano RE, Martin OC, Kang HC, Haugland RP: **A novel fluorescent ceramide analogue for studying membrane traffic in animal cells: accumulation at the**

Golgi apparatus results in altered spectral properties of the sphingolipid precursor. *J Cell Biol* 1991, **113**:1267-1279.

149. Presley JF, Cole NB, Schroer TA, Hirschberg K, Zaal KJ, Lippincott-Schwartz J: **ER-to-Golgi transport visualized in living cells**. *Nature* 1997, **389**:81-85.

150. Kagiwada S, Hosaka K, Murata M, Nikawa J, Takatsuki A: **The Saccharomyces cerevisiae SCS2 gene product, a homolog of a synaptobrevin-associated protein, is an integral membrane protein of the endoplasmic reticulum and is required for inositol metabolism**. *J Bacteriol* 1998, **180**:1700-1708.

151. Lapierre LA, Tuma PL, Navarre J, Goldenring JR, Anderson JM: **VAP-33 localizes to both an intracellular vesicle population and with occludin at the tight junction**. *J Cell Sci* 1999, **112**:3723-3732.

152. Laurent F, Labesse G, de Wit P: **Molecular cloning and partial characterization of a plant VAP33 homologue with a major sperm protein domain**. *Biochem Biophys Res Commun* 2000, **270**:286-292.

153. Nishimura Y, Hayashi M, Inada H, Tanaka T: **Molecular cloning and characterization of mammalian homologues of vesicle-associated membrane protein-associated (VAMP-associated) proteins**. *Biochem Biophys Res Commun* 1999, **254**:21-26.

154. Pennetta G, Hiesinger P, Fabian-Fine R, Meinertzhagen I, Bellen H: **Drosophila VAP-33A directs bouton formation at neuromuscular junctions in a dosage-dependent manner**. *Neuron* 2002, **35**:291-306.

155. Skehel PA, Fabian-Fine R, Kandel ER: **Mouse VAP33 is associated with the endoplasmic reticulum and microtubules**. *Proc Natl Acad Sci U S A* 2000, **97**:1101-1106.

156. Weir ML, Klip A, Trimble WS: **Identification of a human homologue of the vesicle-associated membrane protein (VAMP)-associated protein of 33 kDa (VAP-33): a broadly expressed protein that binds to VAMP**. *Biochem J* 1998, **333**:247-251.

157. Klass MR, Kinsley S, Lopez LC: **Isolation and characterization of a sperm-specific gene family in the nematode Caenorhabditis elegans**. *Mol Cell Biol* 1984, **4**:529-537.

158. Nikawa J, Murakami A, Esumi E, Hosaka K: **Cloning and sequence of the SCS2 gene, which can suppress the defect of INO1 expression in an inositol auxotrophic mutant of Saccharomyces cerevisiae.** *J Biochem (Tokyo)* 1995, **118**:39-45.

159. Foster LJ, Weir ML, Lim DY, Liu Z, Trimble WS, Klip A: **A functional role for VAP-33 in insulin-stimulated GLUT4 traffic.** *Traffic* 2000, **1**:512-521.

160. Weir ML, Xie H, Klip A, Trimble WS: **VAP-A binds promiscuously to both v- and tSNAREs.** *Biochem Biophys Res Commun* 2001, **286**:616-621.

161. Soussan L, Burakov D, Daniels MP, Toister-Achituv M, Porat A, Yarden Y, Elazar Z: **ERG30, a VAP-33-related protein, functions in protein transport mediated by COPI vesicles.** *J Cell Biol* 1999, **146**:301-311.

162. Skehel PA, Martin KC, Kandel ER, Bartsch D: **A VAMP-binding protein from Aplysia required for neurotransmitter release.** *Science* 1995, **269**:1580-1583.

163. Skehel PA, Armitage BA, Bartsch D, Hu Y, Kaang BK, Siegelbaum SA, Kandel ER, Martin KC: **Proteins functioning in synaptic transmission at the sensory to motor synapse of Aplysia.** *Neuropharmacology* 1995, **34**:1379-1385.

164. Gorlich D, Kraft R, Kostka S, Vogel F, Hartmann E, Laskey RA, Mattaj IW, Izaurraide E: **Importin provides a link between nuclear protein import and U snRNA export.** *Cell* 1996, **87**:21-32.

165. Krief P, Augery-Bourget Y, Plaisance S, Merck MF, Assier E, Tanchou V, Billard M, Boucheix C, Jasmin C, Azzarone B: **A new cytokine (IK) down-regulating HLA class II: monoclonal antibodies, cloning and chromosome localization.** *Oncogene* 1994, **9**:3449-3456.

166. Assier E, Bouzinba-Segard H, Stolzenberg MC, Stephens R, Bardos J, Freemont P, Charron D, Trowsdale J, Rich T: **Isolation, sequencing and expression of RED, a novel human gene encoding an acidic-basic dipeptide repeat.** *Gene* 1999, **230**:145-154.

167. Asano K, Merrick WC, Hershey JW: **The translation initiation factor eIF3-p48 subunit is encoded by int-6, a site of frequent integration by the mouse mammary tumor virus genome.** *J Biol Chem* 1997, **272**:23477-23480.

168. Diella F, Levi G, Callahan R: **Characterization of the INT6 mammary tumor gene product.** *DNA Cell Biol* 1997, **16**:839-847.

169. Pahl PM, Hodges YK, Meltesen L, Perryman MB, Horwitz KB, Horwitz LD: **ZNF207, a ubiquitously expressed zinc finger gene on chromosome 6p21.3.** *Genomics* 1998, **53**:410-412.

170. Song X, von Kampen J, Slaughter CA, DeMartino GN: **Relative functions of the alpha and beta subunits of the proteasome activator, PA28.** *J Biol Chem* 1997, **272**:27994-28000.

171. Yen HC, Gordon C, Chang EC: **Schizosaccharomyces pombe Int6 and Ras homologs regulate cell division and mitotic fidelity via the proteasome.** *Cell* 2003, **112**:207-217.

172. Bech-Otschir D, Seeger M, Dubiel W: **The COP9 signalosome: at the interface between signal transduction and ubiquitin-dependent proteolysis.** *J Cell Sci* 2002, **115**:467-473.

173. van Meer G, Holthuis JC: **Sphingolipid transport in eukaryotic cells.** *Biochim Biophys Acta* 2000, **1486**:145-170.

174. de Silva A, Braakman I, Helenius A: **Posttranslational folding of vesicular stomatitis virus G protein in the ER: involvement of noncovalent and covalent complexes.** *J Cell Biol* 1993, **120**:647-655.

175. Hammond C, Helenius A: **Folding of VSV G protein: sequential interaction with BiP and calnexin.** *Science* 1994, **266**:456-458.

176. Alvarez C, Garcia-Mata R, Hauri HP, Sztul E: **The p115-interactive proteins GM130 and giantin participate in endoplasmic reticulum-Golgi traffic.** *J Biol Chem* 2001, **276**:2693-2700.

177. Duden R, Griffiths G, Frank R, Argos P, Kreis TE: **Beta-COP, a 110 kd protein associated with non-clathrin-coated vesicles and the Golgi complex, shows homology to beta-adaptin.** *Cell* 1991, **64**:649-665.

178. Poon PP, Wang X, Rotman M, Huber I, Cukierman E, Cassel D, Singer RA, Johnston GC: **Saccharomyces cerevisiae Gcs1 is an ADP-ribosylation factor GTPase-activating protein.** *Proc Natl Acad Sci U S A* 1996, **93**:10074-10077.

179. Lahtinen U, Dahllof B, Saraste J: **Characterization of a 58 kDa cis-Golgi protein in pancreatic exocrine cells.** *J Cell Sci* 1992, **103 (Pt 2)**:321-333.

180. Aridor M, Weissman J, Bannykh S, Nuoffer C, Balch WE: **Cargo selection by the COPII budding machinery during export from the ER.** *J Cell Biol* 1998, **141**:61-70.

181. Navarro D, Qadri I, Pereira L: **A mutation in the ectodomain of herpes simplex virus 1 glycoprotein B causes defective processing and retention in the endoplasmic reticulum.** *Virology* 1991, **184**:253-264.

182. Greenberg ML, Reiner B, Henry SA: **Regulatory mutations of inositol biosynthesis in yeast: isolation of inositol-excreting mutants.** *Genetics* 1982, **100**:19-33.

183. Lev S, Hernandez J, Martinez R, Chen A, Plowman G, Schlessinger J: **Identification of a novel family of targets of PYK2 related to Drosophila retinal degeneration B (rdgB) protein.** *Mol Cell Biol* 1999, **19**:2278-2288.

184. Ponting CP, Aravind L: **START: a lipid-binding domain in StAR, HD-ZIP and signalling proteins.** *Trends Biochem Sci* 1999, **24**:130-132.

185. Zeng J, Ren M, Gravotta D, De Lemos-Chiarandini C, Lui M, Erdjument-Bromage H, Tempst P, Xu G, Shen TH, Morimoto T, et al.: **Identification of a putative effector protein for rab11 that participates in transferrin recycling.** *Proc Natl Acad Sci U S A* 1999, **96**:2840-2845.

186. Holtta-Vuori M, Tanhuanpaa K, Mobius W, Somerharju P, Ikonen E: **Modulation of cellular cholesterol transport and homeostasis by Rab11.** *Mol Biol Cell* 2002, **13**:3107-3122.

187. Giaever G, Chu AM, Ni L, Connelly C, Riles L, Veronneau S, Dow S, Lucau-Danila A, Anderson K, Andre B, et al.: **Functional profiling of the Saccharomyces cerevisiae genome.** *Nature* 2002, **418**:387-391.

188. Italiano JE, Jr., Roberts TM, Stewart M, Fontana CA: **Reconstitution in vitro of the motile apparatus from the amoeboid sperm of Ascaris shows that filament assembly and bundling move membranes.** *Cell* 1996, **84**:105-114.

189. Merrill AH, Jr., Jones DD: **An update of the enzymology and regulation of sphingomyelin metabolism.** *Biochim Biophys Acta* 1990, **1044**:1-12.

190. Hirschberg K, Rodger J, Futerman AH: **The long-chain sphingoid base of sphingolipids is acylated at the cytosolic surface of the endoplasmic reticulum in rat liver.** *Biochem J* 1993, **290 (Pt 3)**:751-757.

191. Mandon EC, Ehses I, Rother J, van Echten G, Sandhoff K: **Subcellular localization and membrane topology of serine palmitoyltransferase, 3-dehydrosphinganine reductase, and sphinganine N-acyltransferase in mouse liver.** *J Biol Chem* 1992, **267**:11144-11148.

192. Michel C, van Echten-Deckert G: **Conversion of dihydroceramide to ceramide occurs at the cytosolic face of the endoplasmic reticulum.** *FEBS Lett* 1997, **416**:153-155.

193. Coste H, Martel MB, Got R: **Topology of glucosylceramide synthesis in Golgi membranes from porcine submaxillary glands.** *Biochim Biophys Acta* 1986, **858**:6-12.

194. Futerman AH, Pagano RE: **Determination of the intracellular sites and topology of glucosylceramide synthesis in rat liver.** *Biochem J* 1991, **280 (Pt 2)**:295-302.

195. Jeckel D, Karrenbauer A, Burger KN, van Meer G, Wieland F: **Glucosylceramide is synthesized at the cytosolic surface of various Golgi subfractions.** *J Cell Biol* 1992, **117**:259-267.

196. Trinchera M, Fabbri M, Ghidoni R: **Topography of glycosyltransferases involved in the initial glycosylations of gangliosides.** *J Biol Chem* 1991, **266**:20907-20912.

197. Funakoshi T, Yasuda S, Fukasawa M, Nishijima M, Hanada K: **Reconstitution of ATP- and cytosol-dependent transport of de novo synthesized ceramide to the site of sphingomyelin synthesis in semi-intact cells.** *J Biol Chem* 2000, **275**:29938-29945.

198. Fukasawa M, Nishijima M, Hanada K: **Genetic evidence for ATP-dependent endoplasmic reticulum-to-Golgi apparatus trafficking of ceramide for sphingomyelin synthesis in Chinese hamster ovary cells.** *J Cell Biol* 1999, **144**:673-685.

199. Barlowe C, Orci L, Yeung T, Hosobuchi M, Hamamoto S, Salama N, Rexach MF, Ravazzola M, Amherdt M, Schekman R: **COPII: a membrane coat formed by Sec proteins that drive vesicle budding from the endoplasmic reticulum.** *Cell* 1994, **77**:895-907.

200. Campbell JL, Schekman R: **Selective packaging of cargo molecules into endoplasmic reticulum-derived COPII vesicles.** *Proc Natl Acad Sci U S A* 1997, **94**:837-842.

201. Malhotra V, Serafini T, Orci L, Shepherd JC, Rothman JE: **Purification of a novel class of coated vesicles mediating biosynthetic protein transport through the Golgi stack.** *Cell* 1989, **58**:329-336.

202. Orci L, Stamnes M, Ravazzola M, Amherdt M, Perrelet A, Sollner TH, Rothman JE: **Bidirectional transport by distinct populations of COPI-coated vesicles.** *Cell* 1997, **90**:335-349.

203. Ostermann J, Orci L, Tani K, Amherdt M, Ravazzola M, Elazar Z, Rothman JE: **Stepwise assembly of functionally active transport vesicles.** *Cell* 1993, **75**:1015-1025.

204. Cosson P, Letourneur F: **Coatomer interaction with di-lysine endoplasmic reticulum retention motifs.** *Science* 1994, **263**:1629-1631.

205. Letourneur F, Gaynor EC, Hennecke S, Demolliere C, Duden R, Emr SD, Riezman H, Cosson P: **Coatomer is essential for retrieval of dilysine-tagged proteins to the endoplasmic reticulum.** *Cell* 1994, **79**:1199-1207.

206. Oka T, Nakano A: **Inhibition of GTP hydrolysis by Sar1p causes accumulation of vesicles that are a functional intermediate of the ER-to-Golgi transport in yeast.** *J Cell Biol* 1994, **124**:425-434.

207. Yoshihisa T, Barlowe C, Schekman R: **Requirement for a GTPase-activating protein in vesicle budding from the endoplasmic reticulum.** *Science* 1993, **259**:1466-1468.

208. Matsuoka K, Orci L, Amherdt M, Bednarek SY, Hamamoto S, Schekman R, Yeung T: **COPII-coated vesicle formation reconstituted with purified coat proteins and chemically defined liposomes**. *Cell* 1998, **93**:263-275.

209. Aridor M, Bannykh SI, Rowe T, Balch WE: **Sequential coupling between COPII and COPI vesicle coats in endoplasmic reticulum to Golgi transport**. *J Cell Biol* 1995, **131**:875-893.

210. Scales SJ, Pepperkok R, Kreis TE: **Visualization of ER-to-Golgi transport in living cells reveals a sequential mode of action for COPII and COPI**. *Cell* 1997, **90**:1137-1148.

211. Muniz M, Morsomme P, Riezman H: **Protein sorting upon exit from the endoplasmic reticulum**. *Cell* 2001, **104**:313-320.

212. Cox JS, Shamu CE, Walter P: **Transcriptional induction of genes encoding endoplasmic reticulum resident proteins requires a transmembrane protein kinase**. *Cell* 1993, **73**:1197-1206.

213. Mori K, Ma W, Gething MJ, Sambrook J: **A transmembrane protein with a cdc2+/CDC28-related kinase activity is required for signaling from the ER to the nucleus**. *Cell* 1993, **74**:743-756.

214. Nikawa J, Yamashita S: **IRE1 encodes a putative protein kinase containing a membrane-spanning domain and is required for inositol phototrophy in Saccharomyces cerevisiae**. *Mol Microbiol* 1992, **6**:1441-1446.

215. Sidrauski C, Walter P: **The transmembrane kinase Ire1p is a site-specific endonuclease that initiates mRNA splicing in the unfolded protein response**. *Cell* 1997, **90**:1031-1039.

216. Cox JS, Walter P: **A novel mechanism for regulating activity of a transcription factor that controls the unfolded protein response**. *Cell* 1996, **87**:391-404.

217. Cox JS, Chapman RE, Walter P: **The unfolded protein response coordinates the production of endoplasmic reticulum protein and endoplasmic reticulum membrane**. *Mol Biol Cell* 1997, **8**:1805-1814.

218. von Arnim AG, Chamovitz DA: **Protein Homeostasis: A Degrading Role for Int6/eIF3e**. *Curr Biol* 2003, **13**:R323-325.

219. Hofmann K, Bucher P: **The PCI domain: a common theme in three multiprotein complexes**. *Trends Biochem Sci* 1998, **23**:204-205.

220. Groettrup M, Soza A, Eggers M, Kuehn L, Dick TP, Schild H, Rammensee HG, Koszinowski UH, Kloetzel PM: **A role for the proteasome regulator PA28alpha in antigen presentation**. *Nature* 1996, **381**:166-168.

221. Zhang T, Maekawa Y, Hanba J, Dainichi T, Nashed BF, Hisaeda H, Sakai T, Asao T, Himeno K, Good RA, et al.: **Lysosomal cathepsin B plays an important role in antigen processing, while cathepsin D is involved in degradation of the invariant chain inovalbumin-immunized mice**. *Immunology* 2000, **100**:13-20.

222. Yang T, Espenshade PJ, Wright ME, Yabe D, Gong Y, Aebersold R, Goldstein JL, Brown MS: **Crucial step in cholesterol homeostasis: sterols promote binding of SCAP to INSIG-1, a membrane protein that facilitates retention of SREBPs in ER**. *Cell* 2002, **110**:489-500.